

IMPROVING SUSTAINABILITY IN PROTECTIVE COATING SYSTEMS

A Dissertation  
Submitted to the Graduate Faculty  
of the  
North Dakota State University  
of Agriculture and Applied Science

By

Alison Marie Rohly

In Partial Fulfillment of the Requirements  
for the Degree of  
DOCTOR OF PHILOSOPHY

Major Department:  
Coatings and Polymeric Materials

January 2019

Fargo, North Dakota

North Dakota State University  
Graduate School

---

**Title**

IMPROVING SUSTAINABILITY IN PROTECTIVE COATING  
SYSTEMS

---

**By**

Alison Marie Rohly

---

The Supervisory Committee certifies that this *disquisition* complies with North Dakota State University's regulations and meets the accepted standards for the degree of

**DOCTOR OF PHILOSOPHY**

SUPERVISORY COMMITTEE:

Dean C. Webster

---

Chair

Stuart G. Croll

---

Dante Battocchi

---

Andrew Croll

---

Approved:

March 28<sup>th</sup>, 2019

---

Date

Dean C. Webster

---

Department Chair

## ABSTRACT

Sustainability has been a driving factor in the recent development of protective coating systems, from reducing volatile organic compounds (VOC's), integrating biomass for the replacement of petrochemicals, to reducing the number of synthetic or processing steps within a coating system. Incorporating changes to established technologies requires research initiatives focused on matching or exceeding performance properties while maintaining or lowering costs. As a result, sustainable changes to protective coating systems have been under heavy investigation as market demands shift from petrochemicals to renewable materials.

This research focuses on the development of unique thermoset coating systems and sustainable improvements. The first study explores the hydrolytic stability between a silanol and an isocyanate, a frequently used reaction that has been relatively understudied. Incorporation of potential hydrolytically unstable silyl carbamates into polyurethane systems may decrease the crosslinking efficiency of the overall network, negatively impacting coating performance. As a result, investigation into the stability of silyl-carbamates may prevent further inefficiencies by eliminating use of this chemistry within polyurethane systems. The second study focuses on the development of alkoxy silane sol-gel consolidants for the protection of stone materials. Sustainable approaches to consolidant formulation include the reduction and elimination of solvent while improving consolidating properties through material selection. The last two studies focus on the incorporation of lignin-derived vanillin into epoxy thermosets and melamine formaldehydes, increasing the overall biobased content of each system.

## ACKNOWLEDGEMENTS

I am deeply grateful for the support and encouragement of my advisor, Dr. Dean Webster, throughout the course of pursuing my Ph.D. Dr. Webster has greatly enhanced my scientific knowledge and research experience with the opportunity to be a part of several diverse research projects. After a point of self-doubt, Dr. Webster commented “I have never once doubted your ability to obtain a Ph.D.”. His constant support and encouragement gave me the confidence to continue the path, and I am ever grateful for his mentorship.

I would secondly like to thank my committee members, Dr. Stuart Croll, Dr. Dante Battocchi, and Dr. Andrew Croll for their patience and support throughout my time in graduate school. Their expertise, advice and mentorship has played a key role in my success.

Many people within the CPM department were instrumental during my time in Fargo. I've formed lifelong friendships with many of the graduate students. I'd like to thank Teluka Galhenage, Madhura Pade, Arvin Yu, Eric Krall, Raul Setien, Jackson Benda, and AliReza Rahimi for their close friendship. Weekends would not be nearly as fun without them. I would also like to thank Joshua Bernier and Andrii Tiiara, my students, for contributing to some of the research within this dissertation. I'd also like to thank Heidi Docktor, Chunju Gu, James Bahr, Fred Haring, Greg Strommen, and Jayma Moore for their time and expertise with instrumentation trainings. Finally, Katherine Backen-Anderson and Janice Hanson deserve much thanks for answering my unending questions pertaining to everything.

I would not be in this position today without the unwavering love and support from my family. They have shaped me into the person I am today, and I am forever grateful for their constant affirmation and love.

To my best friend, Kara Jankord, you have sacrificed more time and energy driving to Fargo and ensuring my sanity than any person in this world. I love you to death and cannot imagine where I'd be today without your friendship. Thank you for all your love and support, and I look forward to more adventures with you in the near future.

Finally, I would like to thank my love, Jonah Karanja, for his enormous support and encouragement as I pursue my Ph.D. His patience and understanding in addition to his humor and love has been a constant source of strength and motivation. I could not have asked for a better life partner and look forward to the next chapter of our lives together.

## **DEDICATION**

To my role model, my mentor, my teacher, my counselor, my father.

Dad, I dedicate this dissertation to you.

## TABLE OF CONTENTS

ABSTRACT .....	iii
ACKNOWLEDGEMENTS .....	iv
DEDICATION .....	vi
LIST OF TABLES .....	xi
LIST OF FIGURES .....	xiii
LIST OF SCHEMES.....	xvi
CHAPTER 1. GENERAL INTRODUCTION .....	1
1.1. Sustainability .....	1
1.2. Stone conservation .....	3
1.2.1. Consolidant treatments .....	4
1.2.2. Alkoxysilanes .....	6
1.3. Lignin .....	8
1.3.1. Use of lignin in polymeric systems .....	9
1.3.2. Aromatic biomass from lignin.....	9
1.4. Conclusions .....	11
1.5. References .....	11
CHAPTER 2. FORMATION AND HYDROLYTIC STABILITY OF THE SILANOL- ISOCYANATE REACTION.....	21
2.1. Introduction .....	21
2.2. Experimental .....	26
2.2.1. Raw materials .....	26
2.2.2. Synthesis of silyl-carbamate linkages .....	27
2.2.3. Characterization of silyl-carbamate linkages .....	27
2.2.4. Computational calculations on silyl-carbamate linkage.....	28

2.3. Results and discussion.....	29
2.3.1. Silanol-isocyanate synthesis .....	29
2.3.2. Characterization of silyl-carbamate formation .....	30
2.3.3. Computational calculation correlations .....	39
2.4. Conclusions .....	42
2.5. References .....	43
<b>CHAPTER 3. ALKOXYSILANE SOL-GEL CONSOLIDANTS FOR CALCAREOUS STONE MATERIALS.....</b>	<b>47</b>
3.1. Introduction .....	47
3.2. Experimental .....	53
3.2.1. Raw materials .....	53
3.2.2. Methods .....	53
3.2.3. Mixture designs .....	58
3.2.4. Optimized formulations.....	65
3.2.5. POSS study.....	66
3.3. Results and discussion.....	68
3.3.1. Mixture designs .....	69
3.3.2. Formulation optimization .....	80
3.3.3. Optimized consolidant characterization and performance .....	80
3.3.4. POSS study.....	92
3.4. Conclusions .....	99
3.5. References .....	99
<b>CHAPTER 4. BIOBASED EPOXY THERMOSETS DERIVED FROM VANILLIN.....</b>	<b>105</b>
4.1. Introduction .....	105
4.2. Experimental .....	107
4.2.1. Raw materials .....	107



4.2.2. Characterization methods .....	108
4.2.3. Vanillin epoxy thermosets .....	109
4.2.4. Reductive amination of vanillin-Schiff base compounds.....	111
4.3. Results and discussion.....	113
4.3.1. Vanillin-epoxy thermosets.....	113
4.3.2. Reductive amination and crosslinking of vanillin-Schiff base compounds .....	125
4.4. Conclusion.....	133
4.5. References .....	134
<b>CHAPTER 5. BIOBASED MELAMINE-FORMALDEHYDE COATINGS FROM VANILLIN .....</b>	<b>145</b>
5.1. Introduction .....	145
5.2. Experimental .....	147
5.2.1. Raw materials .....	147
5.2.2. Methods .....	147
5.2.3. Acetoacetylation of polyols.....	149
5.2.4. Knoevenagel condensation and MF crosslinking.....	150
5.3. Results and discussion.....	151
5.3.1. Acetoacetylated polyols.....	151
5.3.2. Knoevenagel/MF crosslinking.....	155
5.4. Conclusion.....	162
5.5. References .....	163
<b>CHAPTER 6. OVERALL CONCLUSIONS.....</b>	<b>165</b>
6.1. Hydrolytic stability of the silanol-isocyanate.....	165
6.2. Alkoxysilane stone consolidants .....	165
6.3. Vanillin-epoxy thermosets .....	166
6.4. Vanillin-MF coatings .....	166

CHAPTER 7. FUTURE WORK .....	168
7.1. Hydrolytic stability of the silanol-isocyanate.....	168
7.2. Alkoxysilane stone consolidants .....	168
7.3. Vanillin-epoxy thermosets .....	168
7.4. Vanillin-MF coatings .....	169

## LIST OF TABLES

<u>Table</u>	<u>Page</u>
2.1. Potential reaction by-products for each isocyanate reaction.....	30
2.2. Results of reaction products from isocyanate-PDMS.....	38
2.3. Wiberg Bond Index values.....	39
2.4. Natural charges on carbamate atoms and absolute charge difference of Si-O and C-O bonds in carbamate linkage.....	40
2.5. Dipole (debye) values of carbamate structures.....	41
3.1. Stone consolidant property targets.....	59
3.2. Design A general formulation for TEOS-MTEOS-MTMOS in weight %.....	61
3.3. Design B formulations for GPTMS-POSS-SiO <sub>2</sub> in weight %.....	62
3.4. Design C formulations for GPTMS-PDMS-Ethanol in weight %.....	63
3.5. Design D formulations for GPTMS-PDSM-OTES-TEOS in weight %.....	64
3.6. Optimization: Target properties and importance.....	65
3.7. POSS consolidant formulations in weight %.....	68
3.8. Design C GPTMS-PDMS-Ethanol model significance and component p-values.....	76
3.9. GPTMS-PDMS-OTES-TEOS model significance and component gradient values.....	79
3.10. Optimized formulations 1-4 based on weight %.....	80
4.1. Vanillin-cyclohexylamine reductive amination formulations.....	112
4.2. Mass-to-charge ratio predictions vs actual values for Van-SB.....	115
4.3. Schiff base vs hydrolyzed product integration, EEW, and M <sub>n</sub> values.....	116
4.4. Temperature at 5% weight loss (T <sub>5%</sub> ) and glass transition temperature (T <sub>g</sub> ) of vanillin-epoxy thermosets.....	122
4.5. Gly-Van vs DGEBA epoxy thermosets for T <sub>5%</sub> and T <sub>g</sub> .....	124
4.6. HRMS m/z values for Van-SB products.....	128

4.7.	Epoxy equivalent weight of Gly-Red-Van-SB products and theoretical monomer, dimer and trimer EEW values for comparison .....	130
4.8.	Temperature at 5% weight loss (T5%) and glass transition temperature (Tg) of Gly-Red-Van-SB thermosets .....	132
5.1.	Coating characterization of Vanillin-MF and Joncryl coatings .....	157

## LIST OF FIGURES

<u>Figure</u>	<u>Page</u>
1.1. 12 Principles of Green Chemistry.....	2
1.2. Lignin depolymerization products .....	10
2.1. Product structures for bond stability calculations.....	28
2.2. Carbinol-isocyanate (left) and silanol-isocyanate (right) product appearance .....	29
2.3. Phenyl isocyanate and carbinol, silanol and urea comparison.....	31
2.4. FTIR for cyclohexyl isocyanate and carbinol, silanol and urea comparison .....	32
2.5. Hexyl isocyanate and carbinol, silanol and urea comparison .....	33
2.6. PhenylNCO and a.) silanol <sup>1</sup> H NMR b.) silanol <sup>13</sup> C NMR c.) carbinol <sup>1</sup> H NMR d.) carbinol <sup>13</sup> C NMR.....	35
2.7. CyclohexylNCO and a.) silanol <sup>1</sup> H NMR b.) silanol <sup>13</sup> C NMR c.) carbinol <sup>1</sup> H NMR d.) carbinol <sup>13</sup> C NMR.....	36
2.8. HexylNCO and a.) silanol <sup>1</sup> H NMR b.) silanol <sup>13</sup> C NMR c.) carbinol <sup>1</sup> H NMR d.) carbinol <sup>13</sup> C NMR.....	37
3.1. Structure-property relationship of alkoxy silane.....	48
3.2. Breathability of stone consolidants via POSS .....	52
3.3. a.) Consolidated filter paper samples and b.) BYK permeability cup S .....	56
3.4. XPS of cross-section of consolidated stone .....	57
3.5. Mixture Design A: TEOS-MTEOS-MTMOS .....	60
3.6. Mixture Design B: GPTMS-POSS-SiO <sub>2</sub> .....	61
3.7. a.) Phenyl-POSS and b.) Isooctyl-POSS.....	67
3.8. Gelation of TEOS-MTEOS-MTMOS formulations .....	69
3.9. Weight loss of Design A TEOS-MTEOS-MTMOS formulations.....	70
3.10. a.) Gelation and b.) opacity of GPTMS-POSS-SiO <sub>2</sub> formulations.....	71
3.11. % Weight loss profile of GPTMS-POSS-SiO <sub>2</sub> formulations a.) within first 5 hours and b.) contour plot of final weight loss values after 30 days .....	72

3.12.	Contact angle of GPTMS-POSS-SiO <sub>2</sub> .....	73
3.13.	a) Conservare vs Experimental films on steel panels b) transparent films in Al pans after 3 days c) Conservare after 14 days.....	75
3.14.	Contour plots of a.) weight loss and b.) % solids for GPTMS-PDMS-Ethanol.....	76
3.15.	Contour plots a.) opacity and b.) pencil hardness for GPTMS-PDMS-Ethanol.....	77
3.16.	Commercial and experimental consolidants a) film on Leneta paper and b) xerogel in Al pan.....	81
3.17.	Weight loss of experimental consolidants after a.) 6 hours b.) 400 hours.....	82
3.18.	% Solids of experimental and commercial consolidants.....	83
3.19.	Contact angle measurments a.) chart comparison b.) images.....	84
3.20.	Fluorescence microscopy of consolidation depth for commercial and experimental formulations.....	85
3.21.	SEM images of consolidated limestone and marble.....	86
3.22.	Color change ( $\Delta E$ ) of weathered consolidants on a.) limestone and b.) marble.....	87
3.23.	Water absorption of weathered consolidants after 1000 hours on a.) limestone and b.) marble.....	88
3.24.	SEM of consolidated filter paper a.) 1000x b.) 5000x.....	90
3.25.	Water vapor transmission rate of experimental and commercial consolidants.....	91
3.26.	Weight loss of POSS consolidants after a.) 6 hours b.) 400 hours.....	93
3.27.	Contact angle of POSS consolidants a.) images b.) values.....	94
3.28.	$\Delta E$ values of POSS consolidants over 1000 hours of accelerated weathering on a.) limestone and b.) marble.....	95
3.29.	$\Delta L$ , $\Delta a$ , $\Delta b$ values of POSS consolidants over 1000 hours of accelerated weathering on a.) limestone and b.) marble.....	97
3.30.	Water absorption of POSS consolidants over 1000 hours of accelerated weathering on a.) limestone and b.) marble.....	98
4.1.	a.) FTIR and b.) <sup>1</sup> H NMR of Van-SB products.....	115
4.2.	Gly-Van FTIR.....	118

4.3.	Gly-Van <sup>1</sup> H NMR .....	119
4.4.	Vanillin-epoxy thermosets .....	120
4.5.	DSC of Vanillin-epoxy thermosets for a.) triamines (Jeffamines) and b.) diamines.....	121
4.6.	Vanillin-cyclohexylamine reduction products a.) FTIR and b.) <sup>1</sup> H NMR.....	126
4.7.	<sup>1</sup> H NMR for Red-Van-SB with a.) butylamine and b.) cyclohexylamine .....	127
4.8.	HRMS of a.) Van-butylamine (Van-BA) and b.) Van-cyclohexylamine (Van-CA).....	128
4.9.	Gly-Red-Van-SB compounds of butylamine (left) and cyclohexylamine (right) .....	129
4.10.	<sup>1</sup> H NMR for Gly-Red-Van-SB with a.) butylamine and b.) cyclohexylamine.....	129
4.11.	a.) Gly-Red-Van-BA and b.) Gly-Red-Van-CA crosslinked with amines .....	131
5.1.	<sup>1</sup> H NMR of acetoacetylated glycerol .....	152
5.2.	<sup>1</sup> H NMR of acetoacetylated 1,3-propanediol.....	152
5.3.	<sup>1</sup> H NMR of acetoacetylated 1,4-butanediol .....	153
5.4.	<sup>1</sup> H NMR of acetoacetylated 1,5-pentanediol .....	153
5.5.	<sup>1</sup> H NMR of acetoacetylated 1,6-hexanediol .....	154
5.6.	Viscosity of acetoacetylated polyols.....	155
5.7.	a.) Wrinkling effect from MF content between 20-30% and b.) smooth coatings from MF content of 10-15% .....	156
5.8.	Wet film thickness vs dry film thickness of Joncryl 504 MF, 1,3-PD-TBAA MF, and Gly-TBAA MF.....	159
5.9.	Corrosion of MF coated panels from salt spray exposure .....	161

## LIST OF SCHEMES

<u>Scheme</u>	<u>Page</u>
2.1. Silanol-isocyanate reaction mechanism.....	25
2.2. Experimental approach for investigation of the silanol-isocyanate study .....	26
3.1. Sol-gel reaction: hydrolysis and condensation .....	49
4.1. Reductive amination of Schiff base .....	111
4.2. Crosslinked Vanillin-Schiff base epoxy thermosets via a.) Vanillin-SB, glycidylation and amine crosslinking and b.) vanillin glycidylation and amine crosslinking.....	114
5.1. 1.) Acetoacetylation of polyols 2.) Knoevenagel condensation of vanillin and 3.) MF crosslinking .....	147
5.2. One- Pot synthesis of Knoevenagel condensation and MF crosslinking.....	151



## CHAPTER 1. GENERAL INTRODUCTION

### 1.1. Sustainability

The National Environmental Policy Act of 1969 focused on sustainability, stating the need “to create and maintain conditions under which humans and nature can exist in productive harmony, that permit fulfilling the social, economic and other requirements of present and future generations.”<sup>1</sup> Consciously engaging in sustainability from a chemical approach may be understood from the 12 Principles of Green Chemistry, developed by Anastas and Warner for a sustainable approach to design, development and evaluation processes (Figure 1.1).<sup>2</sup>

The efforts put forward in this research incorporated principles of green chemistry, more specifically reducing solvent content, maximizing atom economy, increasing the use of renewable materials, lowering the toxicity of established technologies through biobased alternatives, and reducing synthetic steps where possible. The first study focused on maximizing atom economy by investigating a potentially hydrolytically unstable reaction between a silanol and isocyanate. Second, reduction in VOC content was achieved through the development of solvent-free alkoxysilane stone consolidants with superior performance properties than commercial consolidants. The final two studies focus on the utilization of biomass. With an increasing demand for reducing oil dependence, the use of biobased materials have been heavily investigated as either direct replacements or alternatives to petrochemicals. Specifically, lignin-derived vanillin was explored as a biobased alternative to diglycidyl ether of bisphenol A. Additionally, vanillin was incorporated to melamine-formaldehyde coating systems for increased biobased content.

1. Prevention	<ul style="list-style-type: none"> <li>• Waste elimination</li> </ul>
2. Atom Economy	<ul style="list-style-type: none"> <li>• Maximize product yield</li> </ul>
3. Less Hazardous Chemical Synthesis	<ul style="list-style-type: none"> <li>• Minimize toxic synthesis</li> </ul>
4. Designing Safer Chemicals	<ul style="list-style-type: none"> <li>• Reduce toxic compounds</li> </ul>
5. Safer Solvents and Auxiliaries	<ul style="list-style-type: none"> <li>• Decrease solvent use</li> </ul>
6. Design for Energy Efficiency	<ul style="list-style-type: none"> <li>• Lower energy inputs</li> </ul>
7. Use of Renewable Feedstocks	<ul style="list-style-type: none"> <li>• Increase biomass use</li> </ul>
8. Reduce Derivatives	<ul style="list-style-type: none"> <li>• Reduce synthetic steps (blocking, protecting)</li> </ul>
9. Catalysis	<ul style="list-style-type: none"> <li>• Increase atom economy with catalysts</li> </ul>
10. Design for Degradation	<ul style="list-style-type: none"> <li>• Design biodegradable systems</li> </ul>
11. Real-time Analysis for Pollution Prevention	<ul style="list-style-type: none"> <li>• Incorporate analytical tools for detection</li> </ul>
12. Inherently Safer Chemistry for Accident Prevention	<ul style="list-style-type: none"> <li>• Minimize accidents, explosions, fires, etc.</li> </ul>

**Figure 1.1. 12 Principles of Green Chemistry**

## 1.2. Stone conservation

Ancient stone artifacts and architecture naturally deteriorate over time due to several environmental factors, including wind, rain, humidity, temperature fluctuations, freeze/thaw cycles, salt growth, chemical attack, pollution and biodeterioration.<sup>3</sup> More severe and rapid forms of stone decay result from earthquakes, terrorism, floods, fires, and vandalism.<sup>4</sup> While full prevention of stone decay is difficult, addressing the slower deterioration from environmental factors is a major focus for conservationists. The three major environmental culprits for natural stone deterioration include air pollution, salt efflorescence and biodeterioration.<sup>5</sup> The prevalence of air pollution in urban cities is detrimental to calcium-carbonate based stone materials such as limestone, marble, and sandstone, as dissolution of the stone material results in gradual erosion of particles at the surface.<sup>6-8</sup> Additionally, salt efflorescence is another major damaging factor to stone materials. As water within the internal pores of the stone structure dries, crystalline salt deposits are left behind, generating stresses that are capable of overcoming the tensile strength of the stone.<sup>4, 9-13</sup> As a result, physical decay in the form of cracks or breaks within the material weakens the stone structure. From an aesthetic perspective, efflorescence leaves behind an undesirable white chalky appearance on the outside of the stone. Biodeterioration is another primary perpetrator in the degradation of stone materials.<sup>14</sup> Microorganisms are capable of growing on the surface of masonry materials as well as inside the pores and cracks, resulting in changes of appearance and chemical alterations of the stone surface.<sup>15</sup> Phototrophs such as algae and cyanobacteria have been identified as early settlers on masonry surfaces, facilitating the colonization of lichens and fungi through a nutrient-rich biofilm.<sup>16-18</sup> Algae and lichens secrete acidic substances that contribute to calcite dissolution, in addition to discoloration from the resulting biocrust formation.<sup>19</sup> In addition to microorganisms, biodeterioration occurs from

surrounding vegetative landscape such as tree overgrowth and root disruption, resulting in structural decay due to mechanical stress.<sup>20</sup>

Given the detrimental environmental factors for stone deterioration, effective stone consolidants are necessary for the conservation and protection of stone materials. A stone consolidant is a low-viscosity, transparent liquid that is applied by either brush, spray or immersion applications. The material is absorbed into the internal porous structure of the stone by capillary force, binding any loose granular particles in its path.<sup>4</sup> As a consolidant cures, it acts as a cohesive binder, reducing the porosity within the stone and increasing the structural integrity of the material. Consolidants have been widely used within the field of conservation for the prevention of decay from air pollution, salt efflorescence, and biodeterioration.

### **1.2.1. Consolidant treatments**

Many consolidant treatments for masonry materials have been explored by conservationists, including calcium hydroxide and barium hydroxide, acrylics, epoxies, and alkoxysilanes.<sup>4</sup> Calcium hydroxide solution, or lime, has been used extensively as one of the most simple stone consolidants.<sup>21</sup> Applied to a calcareous stone substrate, calcium hydroxide reacts with atmospheric carbon dioxide, restoring calcium carbonate back to the stone. However, Price et al. determined that deposition of lime only occurred within the first few millimeters, lowering the consolidant efficiency.<sup>22, 23</sup> Improvements in calcium hydroxide penetration have been explored using nano-lime, consisting of calcium hydroxide particles suspended in alcohol.<sup>24-29</sup> By replacing water with alcohol, higher loading of calcium hydroxide in addition to minimizing carbonation allows for deeper consolidation of the stone material. One of the downfalls, however, includes the use of solvents, raising VOC levels of the consolidant. Barium hydroxide has also been explored as a consolidating material, operating similarly to calcium

carbonate. However, the barium hydroxide is more soluble in water compared to calcium hydroxide, and the formation of barium carbonate is more resistant to acid rain calcium carbonate.<sup>22</sup> Primary applications of barium hydroxide consolidation treatments have been explored in wall paintings, however, the major challenges surrounding this treatment includes discoloration and undesirable texture.<sup>30-32</sup>

Although primarily used as adhesives within the field of conservation, epoxy resins have also been reported as potential consolidating materials.<sup>33, 34</sup> Cavalletti et al. successfully consolidated large granite columns using a cycloaliphatic epoxy (Eurostac EP2101), however, vacuum application was required due to the high viscosity of epoxy resins.<sup>35</sup> Ginell et al. detailed a method for reducing the yellowing effect upon ageing of epoxy resins by washing the consolidated surface with solvent to remove the surface layer, effectively preventing UV exposure of the epoxy.<sup>36</sup> However, the removal of the surface layer of epoxy leaves the exposed stone unconsolidated, defeating the purpose for consolidation in the first place. Given the high viscosity, tendency to yellow, and general brittleness of epoxy materials, the application as consolidating materials are impractical.

The use of acrylics as stone consolidants have been under investigation, imparting excellent adhesion properties that many other consolidating systems lack.<sup>4</sup> Paraloid B72, an acrylic resin based on poly(methyl methacrylate) (PMMA), is primarily used by conservationists as an adhesive for the restoration of glass and ceramic objects.<sup>37-41</sup> However, the use of B72 as a consolidant has been investigated in combination with alkoxysilanes by Wheeler et al., showing a weaker composite gel compared to the alkoxysilane alone.<sup>42</sup> The photodegradation of B72 when used as a stone consolidant was examined by Melo et al., and found to undergo significant chain scission upon UV irradiation.<sup>43</sup> Given the high rigidity and poor weatherability of acrylic

resins, applications as stone consolidants are not practical, and other chemistries should be explored.

### **1.2.2. Alkoxysilanes**

Alkoxysilanes are the most widely used compounds for stone consolidation due to their transparent nature, low viscosity, low toxicity, hydrophobicity, and the ability to cure at ambient temperatures via the sol-gel reaction.<sup>44</sup> Easily applied by brush, spray or immersion, alkoxysilanes penetrate porous stone materials by capillary force. As the alkoxysilanes interact with trapped water within the stone, the alkoxy groups hydrolyze, forming silanols that further condense to produce a sol-gel network.<sup>45, 46</sup>

Arthur Pillans Laurie published some of the initial patents in alkoxysilane stone consolidants in the early 1920's, where he describes a method for treating stone materials with a solution of silicic ether. Laurie claimed that "hydrated silica is deposited in the pores so as to form a continuous film which binds together the remaining portions of the stone".<sup>47, 48</sup> One of the challenges with early consolidant formulations included the use of silicon tetrachloride, which hydrolyzes to form hydrochloric acid. The formation of acidic byproducts on stone substrates only accelerates degradation, specifically with calcareous stone materials. In the 1930's, ethyl silicate soon become a more widely-used alternative to silicon tetrachloride in both protective stone materials and general paint formulations.<sup>49, 50</sup> Throughout the 1940's and 1950's, research into effective alkoxysilane consolidants for the preservation of stone materials became more abundant,<sup>51-54</sup> and silicon esters were recognized as some of the most successful consolidating materials.<sup>55, 56</sup> Throughout the 1960's and 1970's, exploration of the effect of alkoxysilanes and mineral composition of stone materials indicated that chemical bonds formed between siliceous stones (granite, quartz) and consolidants, however calcareous stone materials exhibited no

chemical bonding with alkoxy silanes.<sup>57-59</sup> As a result, the focus on consolidation of calcareous stone materials has driven stone consolidation research.

Three major alkoxy silane compounds have been utilized in consolidant formulations: tetraethylorthosilicate (TEOS), methyltrimethoxysilane (MTMOS), and methyltriethoxysilane (MTEOS).<sup>44</sup> Tradeoffs between reactivity and volatility must be considered when choosing an alkoxy silane. MTMOS is the most reactive alkoxy silane as well as having the largest vapor pressure at 31 mm Hg. TEOS has the lowest reactivity, with a vapor pressure of 5 mm Hg.<sup>44</sup> Additionally, tradeoffs between steric hindrance and inductive effects also influence alkoxy silane reactivity. Commercial consolidants primarily contain TEOS, as a slower reactivity allows for sufficient saturation within the stone's pores.

Much of the published literature on alkoxy silane formulations incorporate the addition of water for increasing the rate of hydrolysis. As a result, solvent such as methanol or ethanol is commonly added for miscibility between the alkoxy silane and water.<sup>60-64</sup> The incorporation of water and solvent effectively increases the volatile content, requiring more coats of material for sufficient consolidation. One way to reduce the amount of water and solvent is to incorporate a catalyst. Catalysts such as acids, bases and organotin compounds are commonly used in alkoxy silane consolidant formulations for increasing the rate of hydrolysis.<sup>44</sup> Acid-catalyzed hydrolysis proceeds by nucleophilic attack of water on the silicon atom. The resulting silanols are easily protonated, making them more susceptible to nucleophilic attack by the unprotonated silanols. The condensation reaction proceeds, forming oligomeric siloxanes. In the acid-catalyzed system, monomeric silanols are more basic than the oligomeric silanols, making the monomeric compounds preferentially protonated. After all monomeric silanols have all reacted to form oligomers, network formation by oligomeric condensation proceeds. Silanols on the ends

of oligomers are considered to more basic than silanols in the middle of the chain, resulting in the formation of a linear network with fewer branches. For base-catalyzed consolidants, hydrolysis proceeds via nucleophilic attack of the silicon atom by the base, forming the silanols. Condensation then occurs by deprotonation of one of the silanols by the hydroxyl anion, forming water. The silanol anion attacks another silicon atom, forming a siloxane bond. Opposite of the acid catalyst crosslinking, central silanols on oligomeric chains are more prone to reaction due to higher acidity, forming more crosslinked and branched structures. Organotin catalysts, such as dibutyltin dilaurate (DBTDL), are the most commonly used catalysts in commercial alkoxysilane consolidants.<sup>65</sup> In the presence of water, the organotin compound hydrolyzes, forming a hydroxy-tin and organic acid. The hydroxy-tin then condenses with an alkoxysilane, forming a reactive siloxane-tin. Silanols are capable of condensing with the siloxane-tin, kicking off the tin catalyst and forming an Si-O-Si bond. The hydroxy-tin is regenerated and continues catalyzing the condensation reaction. Similar to base catalysts, organotin compounds produce more branched networks.<sup>44</sup>

Although alkoxysilanes have been heavily investigated, demands for improvements in commercial formulations have led to research efforts focused on increasing flexibility, “breathability” and durability.

### **1.3. Lignin**

Petrochemical materials have a well-established market within the area of coatings and polymeric materials, however, demands for reducing oil dependence have led to the investigation into renewable materials.<sup>66</sup> Found in the cell walls of woody plants, lignin is the second most abundant biopolymer after cellulose. However, unlike cellulose, lignin is comprised of an aromatic structure, offering unique properties such as mechanical strength and integrity.<sup>67</sup> The



three structural units that make up lignin are coumaryl alcohol, coniferyl alcohol and sinapyl alcohol, which vary in abundance depending on the environment.<sup>67</sup> As a result, the structural blueprint of lignin is highly variable.

### **1.3.1. Use of lignin in polymeric systems**

As a byproduct of the Kraft Pulp process, lignin is considered a waste stream, sparking recent interests in producing value-added chemicals from lignin. Lignin by itself is highly rigid and brittle, and therefore must be functionalized for any practical end use. Polyurethanes systems utilizing unmodified lignin have been shown to produce rigid sheets and foams.<sup>68, 69</sup> Chemical modifications of lignin have been carried out by nitration,<sup>70</sup> dealkylation,<sup>71</sup> hydroxyalkylation,<sup>72, 73</sup> sulfomethylation<sup>74</sup> and amination.<sup>75</sup> Applications of modified lignin has been explored, primarily in epoxy systems.<sup>76</sup> Given the abundance of phenol and alcohol groups on lignin, epoxidation using epichlorohydrin has been utilized.<sup>77, 78</sup> The persistent challenges of lignin such as brittleness and insolubility must be overcome before any practical applications are developed.<sup>79</sup>

### **1.3.2. Aromatic biomass from lignin**

Depolymerization of lignin results in small molecular-weight aromatic compounds, including p-hydroxybenzaldehyde, vanillin, syringic aldehyde, p-hydroxybenzoic acid, vanillic acid, syringic acid, 5-formyl vanillic acid, 5-carboxyvanillin and acetovanillone (Figure 1.2).<sup>80</sup> Vanillin is one of the most abundant by-products from oxidative depolymerization of lignin, with yields ranging from 6-12% in softwoods.<sup>81, 82</sup> While 85% of vanillin is synthetically produced from guaiacol, 15% of the global production comes from lignin-derived vanillin, being the only commercialized lignin-derived monomer.<sup>83</sup> The multi-functional aspect of vanillin indicates the

potential be used as a crosslinker within thermoset coating systems via step-growth polymerization, however little work has been done in this area.

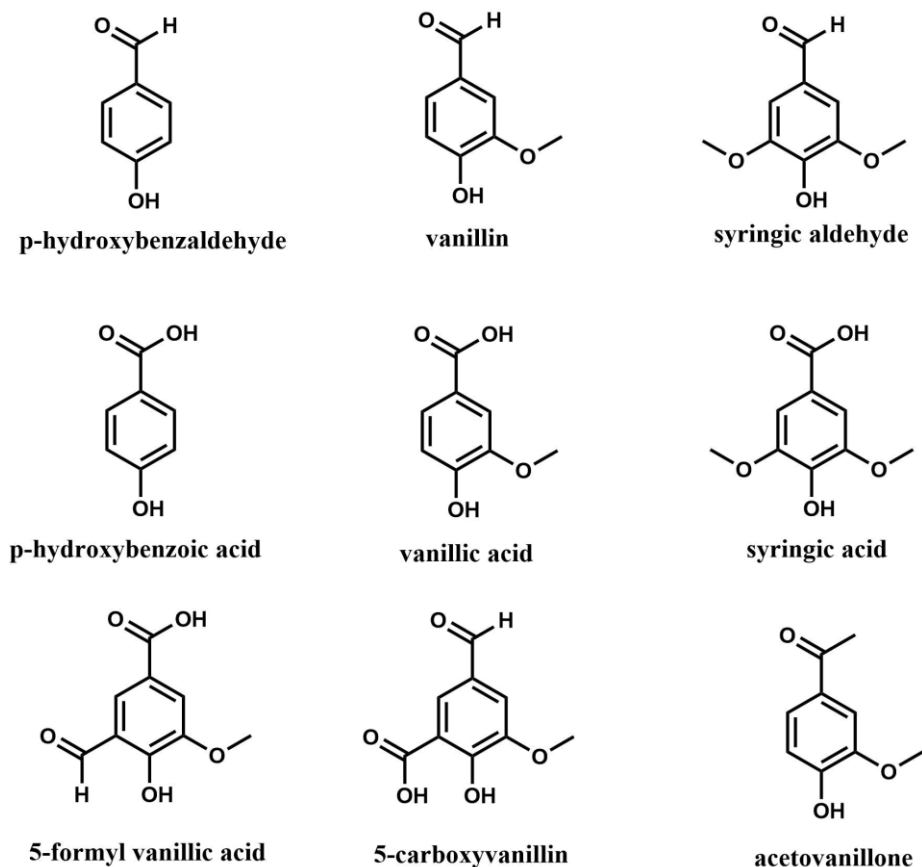


**Figure 1.2. Lignin depolymerization products**

Biobased epoxy monomers and thermosets utilizing vanillin have been extensively investigated by Caillol et al., and will be thoroughly detailed in Chapter 4. Polyurethane elastomers based on vanillin were developed by Kim et al. via the synthesis of divanillin-ethanol amine conjugates.<sup>84</sup> The developed divanillin monomers were used as chain extenders for the replacement of 1,4-butanediol, resulting in increased strain and modulus without compromising thermal properties. Fache et al. synthesized a platform of functionalized vanillin monomers for epoxies, polyhydroxyurethanes, polycarbonates, polyesters, polyacrylates, polyimides,

polyureas, and polyamides by incorporating functional groups of epoxy, cyclic carbonates, alcohols, amines, and carboxylic acids.<sup>85</sup> The majority of thermoset development from these functionalized monomers have focused primarily on biobased epoxies,<sup>86-91</sup> however, the platform of functionalized vanillin monomers opens the door to novel biobased thermoset systems.

#### **1.4. Conclusions**

Incorporating green chemistry principles into scientific endeavors is essential for creating a sustainable future. Within the field of stone consolidants, room for sustainable development includes the elimination of solvents without compromising consolidant performance. Additionally, lignin-derived vanillin offers potential as a biobased crosslinker in protective coating systems due to the unique aldehyde and phenol functionality.

#### **1.5. References**

1. National Environmental Policy Act of 1969. **1969**; Vol. Sec. 2 [42 U.S. Code § 4321].
2. Anastas, P. T.; Warner, J. C., *Green chemistry: theory and practice*. Oxford University Press: **2000**.
3. Cartwright, T.; Belmin, V., *Illustrated Glossary on Stone Deterioration Patterns*. Paris, **2008**.
4. Doehne, E.; Price, C. A., *Stone Conservation: An Overview of Current Research*. Getty Conservation Institute: Los Angeles, **2010**.
5. Herrera, L. K.; Videla, H. A., The importance of atmospheric effects on biodeterioration of cultural heritage constructional materials. *International Biodeterioration & Biodegradation* **2004**, 54 (2), 125-134.
6. Charola, A. E., Chem I supplement: Acid rain effects on stone monuments. *Journal of Chemical Education* **1987**, 64 (5), 436-437.

7. Charola, A. E.; Ware, R., Acid deposition and the deterioration of stone: a brief review of a broad topic. *Geological Society, London, Special Publications* **2002**, 205 (1), 393.
8. Zanardini, E.; Abbruscato, P.; Ghedini, N.; Realini, M.; Sorlini, C., Influence of atmospheric pollutants on the biodeterioration of stone. *Int. Biodeterior. Biodegrad.* **2000**, 45 (1-2), 35-42.
9. Ishizaki, T., Deterioration of porous materials of cultural properties. *Netsu Bussei* **2008**, 22 (2), 125-129.
10. Rodriguez-Navarro, C.; Linares-Fernandez, L.; Doehne, E.; Sebastian, E., Effects of ferrocyanide ions on NaCl crystallization in porous stone. *J. Cryst. Growth* **2002**, 243 (3-4), 503-516.
11. Matovic, V.; Eric, S.; Sreckovic-Batocanin, D.; Colomban, P.; Kremenovic, A., The influence of building materials on salt formation in rural environments. *Environ. Earth Sci.* **2014**, 72 (6), 1939-1951.
12. Gibson, L. T.; Cooksey, B. G.; Littlejohn, D.; Tennent, N. H., Investigation of the composition of a unique efflorescence on calcareous museum artifacts. *Anal. Chim. Acta* **1997**, 337 (3), 253-264.
13. Heiner, S., Salt efflorescence as indicator for sources of damaging salts on historic buildings and monuments: a statistical approach. *Environmental earth sciences.* **2018**, 77 (16), 1.
14. Scheerer, S.; Ortega-Morales, O.; Gaylarde, C., Microbial deterioration of stone monuments-an update overview. *Adv. Appl. Microbiol.* **2009**, 66, 97-139.
15. Sierra-Fernandez, A.; Gomez-Villalba, L. S.; Fort, R.; Rabanal, M. E.; De, I. R.-G. S. C.; Gomez-Cornelio, S.; Quintana, P., Synthesis, Photocatalytic, and Antifungal

- Properties of MgO, ZnO and Zn/Mg Oxide Nanoparticles for the Protection of Calcareous Stone Heritage. *ACS Appl Mater Interfaces* **2017**, 9 (29), 24873-24886.
16. Li, Q.; Zhang, B.; Yang, X.; Ge, Q., Deterioration-Associated Microbiome of Stone Monuments: Structure, Variation, and Assembly. *Appl Environ Microbiol* **2018**, 84 (7).
  17. Warscheid, T.; Braams, J., Biodeterioration of stone: a review. *International Biodeterioration & Biodegradation* **2000**, 46 (4), 343-368.
  18. Cappitelli, F.; Zanardini, E.; Sorlini, C., The biodeterioration of synthetic resins used in conservation. *Macromol. Biosci.* **2004**, 4 (4), 399-406.
  19. Gadd, G. M., Geomicrobiology of the built environment. *Nature Microbiology* **2017**, 2, 16275.
  20. Saiz-Jimenez, C., Biodeterioration of Stone in Historic Buildings and Monuments. **1994**, pp 587-604.
  21. Ashurst, J.; Dimes, F. G., *Conservation of Building and Decorative Stone*. Butterworth-Heinemann: London and Boston, **1998**; Vol. 2.
  22. Hansen, E.; Doehne, E.; Fidler, J.; Larson, J.; Martin, B.; Matteini, M.; Rodriguez-Navarro, C.; Pardo, E. S.; Price, C.; de Tagle, A.; Teutonico, J. M.; Weiss, N., A review of selected inorganic consolidants and protective treatments for porous calcareous materials. *Rev. Conserv.* **2003**, 4, 13-25.
  23. Price, C.; Ross, K.; White, G. A further appraisal of the "lime technique" for limestone consolidation, using a radioactive tracer. *Studies in Conservation* [Online], **1988**, p. 178-86.
  24. Rodriguez-Navarro, C.; Suzuki, A.; Ruiz-Agudo, E., Alcohol Dispersions of Calcium Hydroxide Nanoparticles for Stone Conservation. *Langmuir* **2013**, 29 (36), 11457-11470.

25. Daehne, A.; Herm, C., Calcium hydroxide nanosols for the consolidation of porous building materials - results from EU-STONECORE. *Heritage Sci.* **2013**, *1*, 11/1-11/9, 9 pp.
26. Drdacky, M.; Slizkova, Z.; Ziegenbalg, G., A nano approach to consolidation of degraded historic lime mortars. *J. Nano Res.* **2009**, *8*, 13-22.
27. Ziegenbalg, G.; Bruemmer, K.; Pianski, J., Nano-lime - a new material for the consolidation and conservation of historic mortars. *RILEM Proc.* **2010**, *PRO 78* (2nd Conference on Historic Mortars and RILEM TC 203-RHM Final Workshop, **2010**, 1301-1309.
28. D'Armada, P.; Hirst, E., Nano-Lime for Consolidation of Plaster and Stone. *Journal of Architectural Conservation* **2012**, *18* (1), 63-80.
29. Vojtechovsky, J., Surface consolidation of wall paintings using lime nano-suspensions. *Acta Polytech.* **2017**, *57* (2), 139-148.
30. Cather, S.; Courtauld Institute of, A.; Getty Conservation, I. In *The conservation of wall paintings : proceedings of a symposium organized by the Courtauld Institute of Art and the Getty Conservation Institute, London, July 13-16, 1987*, [Marina del Rey, CA], **1991**; Getty Conservation Institute: [Marina del Rey, CA].
31. Schnabel, L., Evaluation of the barium hydroxide-urea consolidation method. In *7th International Congress, Deterioration and Conservation of Stone*, Lisbon, **1992**; pp 1063-1072.
32. Lewin, S. Z.; Baer, N. S., Rationale of the barium hydroxide-urea treatment of decayed stone. *Studies in Conservation* **1974**, *19* (1), 24-35.

33. Selwitz, C. M. C., The Use of Epoxy Resins for Stone Consolidation. *MRS Proceedings* **1990**, 185, 181.
34. Selwitz, C., The Use of Epoxy Resins for the Stabilization of Deteriorated Masonry. *APT Bulletin* **1995**, 26 (4), 27-34.
35. Cavalletti, R., *A new type of epoxy resin for the structural consolidation of badly decayed stones*. Presses polytechniques romandes: Lausanne, **1985**; p 769.
36. Ginell, W. S.; Coffman, R., Epoxy Resin-Consolidated Stone: Appearance Change on Aging. *Studies in Conservation* **1998**, 43 (4), 242-248.
37. Muhcu, D.; Terzi, E.; Kartal, S. N.; Yoshimura, T., Biological performance, water absorption, and swelling of wood treated with nano-particles combined with the application of Paraloid B72. *J. For. Res. (Harbin, China)* **2017**, 28 (2), 381-394.
38. Crisci, G. M.; La Russa, M. F.; Malagodi, M.; Ruffolo, S. A., Consolidating properties of Regalrez 1126 and Paraloid B72 applied to wood. *Journal of Cultural Heritage* **2010**, 11 (3), 304-308.
39. Svadlena, J.; Stoulil, J., Evaluation of protective properties of acrylate varnishes used for conservation of historical metal artefacts. *Koroze a Ochrana Materiálu* **2017**, 61 (1), 25-31.
40. Tan, T., Multi-Scale Adhesion and Fracture: From Eco-friendly Structures to Biomedical Devices. Soboyejo, W., Ed. ProQuest Dissertations Publishing: **2011**.
41. Zhou, Y.; Zhang, B.-j., Technological conditions for consolidation and protection of fragile silk fabrics relics with acrylic resin Paraloid B72 and evaluation of consolidation effect. *Canye Kexue* **2012**, 38 (5), 879-884.

42. Wheeler, G. S.; Shearer, G. L.; Fleming, S.; Kelts, L. W.; Vega, A.; Koestler, R. J., Toward a better understanding of B72 acrylic resin/methyltrimethoxysilane stone consolidants. *Mater. Res. Soc. Symp. Proc.* **1991**, *185* (Mater. Issues Art Archaeol. 2), 209-26.
43. Melo, M. J.; Bracci, S.; Camaiti, M.; Chiantore, O.; Piacenti, F., Photodegradation of acrylic resins used in the conservation of stone. *Polym. Degrad. Stab.* **1999**, *66* (1), 23-30.
44. Wheeler, G., *Alkoxysilanes and the Consolidation of Stone*. Getty Publications: Los Angeles, **2005**.
45. Wright, J. D.; Sommerdijk, N. A. J. M., *Sol-Gel Materials: Chemistry and Applications*. Gordon and Breach Science Publishers: Amsterdam, **2001**.
46. Brinker, C. J.; Scherer, G. W., CHAPTER 3 - Hydrolysis and Condensation II: Silicates. In *Sol-Gel Science*, Academic Press: San Diego, **1990**; pp 96-233.
47. Laurie, A. P. Improvements relating to the preservation of stone. **1923**.
48. Laurie, A. P. Preservation of stone. **1925**.
49. George, K.; Threlfall, R. Material for forming coatings, for use as impregnating agents or for like purposes. **1928**.
50. Vaughn, T. H. Hydrolysis of the organic esters of inorganic acids. **1936**.
51. Emblem, H. G.; Sos, F. L., Organosilicon compounds. *Chem. Ind. (London, U. K.)* **1946**, 450-2.
52. Emblem, H. G., Silicon ester paints. *Paint Manuf.* **1946**, *16*, 291-2.
53. Cogan, H.; Setterstrom, C., Ethyl Silicates. *Industrial & Engineering Chemistry* **1947**, *39* (11), 1364-1368.



54. Cogan, H. D.; Setterstrom, C. A., Properties of ethyl silicate. *Chem. Eng. News* **1946**, *24*, 2499-2501.
55. Plenderleith, H. J., *The Conservation of antiquities and works of art : treatment, repair, and restoration / by H. J. Plenderleith*. Oxford University Press: London, **1956**.
56. Shore, B. C. G., *Stones of Britain*. Leonard Hill Books: London, **1957**.
57. Snethlage, R.; Klemm, D. D. Scanning electron microscopic investigation on impregnated sandstones *Deterioration and Protection of Stone Monuments* [Online], **1978**.
58. Goins, E. S. Alkoxysilane stone consolidants: the effect of stone substrate on the polymerization process. University College London, University of London, **1995**.
59. Kumar, R., Fourier transform infrared spectroscopic study of silane/stone interface. *Materials Issues in Art and Archeology* **1995**.
60. Xu, F.; Li, D.; Zhang, H.; Peng, W., TEOS/HDTMS inorganic-organic hybrid compound used for stone protection. *J. Sol-Gel Sci. Technol.* **2012**, *61* (2), 429-435.
61. Li, D.; Xu, F.; Shao, L.; Wang, M., Effect of the addition of 3-glycidoxypropyltrimethoxysilane to tetraethoxyorthosilicate-based stone protective coating using n-octylamine as a catalyst. *Bull. Mater. Sci.* **2015**, *38* (1), 49-55.
62. Mosquera, M. J.; de los Santos, D. M.; Rivas, T., Surfactant-Synthesized Ormosils with Application to Stone Restoration. *Langmuir* **2010**, *26* (9), 6737-6745.
63. Mosquera, M. J.; de Santos, D. M.; Montes, A.; Valdez-Castro, L., New Nanomaterials for Consolidating Stone. *Langmuir* **2008**, *24* (6), 2772-2778.

64. Sena da Fonseca, B.; Picarra, S.; Ferreira Pinto, A. P.; Ferreira, M. J.; Montemor, M. F., TEOS-based consolidants for carbonate stones: the role of N1-(3-trimethoxysilylpropyl)diethylenetriamine. *New J. Chem.* **2017**, *41* (6), 2458-2467.
65. Méndez-Vivar, J., *The interaction of dibutyltin dilaureate with tetraethyl orthosilicate in sol-gel systems.* **2006**; p 159-166.
66. Roddy, D., *Biomass in a petrochemical world.* **2013**; p 20120038.
67. Chung, H.; Washburn, N. R., Chemistry of lignin-based materials. *Green Mater.* **2013**, *1* (3), 137-160.
68. Xu, C.; Ferdosian, F., Lignin-Based Polyurethane (PU) Resins and Foams. **2017**; pp 133-156.
69. Gadhawe, R. V.; Mahanwar, P. A.; Gadekar, P. T., Lignin-polyurethane based biodegradable foam. *Open J. Polym. Chem.* **2018**, *8* (1), 1-10.
70. Zhang, L.; Huang, J., Effects of nitrolignin on mechanical properties of polyurethane–nitrolignin films. *Journal of Applied Polymer Science* **2001**, *80* (8), 1213-1219.
71. Liu, Y.; Li, K., Preparation and Characterization of Demethylated Lignin-Polyethylenimine Adhesives. *The Journal of Adhesion* **2006**, *82* (6), 593-605.
72. Gonçalves, A. R.; Benar, P., Hydroxymethylation and oxidation of Organosolv lignins and utilization of the products. *Bioresource Technology* **2001**, *79* (2), 103-111.
73. Hu, L.; Pan, H.; Zhou, Y.; Zhang, M., *Methods to improve lignin's reactivity as a phenol substitute and as replacement for other phenolic compounds: A brief review.* **2011**.
74. Laurichesse, S.; Avérous, L., Chemical modification of lignins: Towards biobased polymers. *Progress in Polymer Science* **2014**, *39* (7), 1266-1290.

75. Yue, X.; Chen, F.; Zhou, X., *Improved interfacial bonding of PVC/wood-flour composites by lignin amine modification*. **2011**.
76. Calvo-Flores, F. G.; Dobado, J. A., Lignin as Renewable Raw Material. *ChemSusChem* **2010**, *3*, 1227-1235.
77. Effendi, A.; Gerhauser, H.; Bridgwater, A. V., Production of renewable phenolic resins by thermochemical conversion of biomass: a review. *Renewable and sustainable energy reviews* **2008**, *12* (8), 2092-2116.
78. Ferdosian, F.; Yuan, Z.; Anderson, M.; Xu, C., Synthesis of lignin-based epoxy resins: optimization of reaction parameters using response surface methodology. *RSC Advances* **2014**, *4* (60), 31745-31753.
79. Fu, M.; Chen, F.; Cen, L.; Zhou, Y., Research progress in modification of lignin and its application in plastics. *Zhongguo Suliao* **2012**, *26* (11), 14-21.
80. Sun, Z.; Fridrich, B.; de Santi, A.; Elangovan, S.; Barta, K., Bright Side of Lignin Depolymerization: Toward New Platform Chemicals. *Chemical Reviews* **2018**, *118* (2), 614-678.
81. Fache, M.; Boutevin, B.; Caillol, S., Vanillin Production from Lignin and Its Use as a Renewable Chemical. *ACS Sustainable Chem. Eng.* **2016**, *4* (1), 35-46.
82. Araújo, J. D. P.; Grande, C. A.; Rodrigues, A. E., Vanillin production from lignin oxidation in a batch reactor. *Chemical Engineering Research and Design* **2010**, *88* (8), 1024-1032.
83. Borregaard The Home of Sustainable Vanillin. <https://www.vanillin.com/>.
84. Gang, H.; Lee, D.; Choi, K.-Y.; Kim, H.-N.; Ryu, H.; Lee, D.-S.; Kim, B.-G., Development of High Performance Polyurethane Elastomers Using Vanillin-Based Green

- Polyol Chain Extender Originating from Lignocellulosic Biomass. *ACS Sustainable Chem. Eng.* **2017**, *5* (6), 4582-4588.
85. Fache, M.; Darroman, E.; Besse, V.; Auvergne, R.; Caillol, S.; Boutevin, B., Vanillin, a promising biobased building-block for monomer synthesis. *Green Chemistry* **2014**, *16* (4), 1987-1998.
  86. Caillol, S. In *New platform of lignin based building blocks for polymers*, American Chemical Society: **2016**; pp GC+E-193.
  87. Fache, M.; Monteremal, C.; Boutevin, B.; Caillol, S., Amine hardeners and epoxy cross-linker from aromatic renewable resources. *Eur. Polym. J.* **2015**, *73*, 344-362.
  88. Fache, M.; Viola, A.; Auvergne, R.; Boutevin, B.; Caillol, S., Biobased epoxy thermosets from vanillin-derived oligomers. *Eur. Polym. J.* **2015**, *68*, 526-535.
  89. Fache, M.; Auvergne, R.; Boutevin, B.; Caillol, S., New vanillin-derived diepoxy monomers for the synthesis of biobased thermosets. *Eur. Polym. J.* **2015**, *67*, 527-538.
  90. Fache, M.; Boutevin, B.; Caillol, S., Vanillin, a key-intermediate of biobased polymers. *Eur. Polym. J.* **2015**, *68*, 488-502.
  91. Fache, M.; Boutevin, B.; Caillol, S., Epoxy thermosets from model mixtures of the lignin-to-vanillin process. *Green Chem.* **2016**, *18* (3), 712-725.

## CHAPTER 2. FORMATION AND HYDROLYTIC STABILITY OF THE SILANOL-ISOCYANATE REACTION

### 2.1. Introduction

Block copolymers of materials with dissimilar surface energies result in amphiphilic systems commonly containing hydrophobic and hydrophilic components. Low surface energy blocks consist of materials such as polysiloxanes and fluoropolymers, whereas higher surface energy components contain hydrophilic polymers such as polyethylene glycol (PEG).

Amphiphilic block copolymers have shown great success within the biomedical field for applications such as drug delivery, forming micellar structures capable of delivering hydrophobic drugs.<sup>3</sup> Within the field of marine coatings, amphiphilic siloxane-polyurethanes have shown promising potential for effectively preventing barnacles and other organisms from permanently attaching to the surface of ship hulls.<sup>4,5</sup> The siloxane self-stratifies to the surface, creating a low surface energy for the organisms to adhere to. Typical siloxane segments such as polydimethylsiloxane (PDMS) are incorporated into the polyurethane via carbinol-terminated chain ends that react with isocyanates to produce a polyurethane coating, however, recent literature has incorporated silanol-terminated PDMS in producing siloxane-polyurethane pre-polymers.<sup>6-13</sup> While certain literature may suggest the formation of a silyl carbamate linkage, very little information on the feasibility of the silanol-isocyanate reaction has been published since the early 1960's. Andrianov et al. was first to acknowledge the reaction between a silanol and an isocyanate, stating that "the resulting compounds are readily hydrolysed by water and decomposed by alcohols".<sup>14-16</sup> They suggested that a silyl carbamate linkage will react with water to form an intermediate carbamic acid, which readily decomposes into amine and carbon dioxide. Andrianov further proved that carbinol-terminated polydimethylsiloxane formed stable

urethane bonds in the presence of isocyanates, stating that “rupture does not occur at either the siloxane or the silicon-carbon bonds”.<sup>16</sup> Mironov et al. validated Andrianov’s findings by stating “all o-silylurethanes are readily hydrolyzed in air, with the exception of PhNHCO<sub>2</sub> which is surprisingly stable in air”.<sup>17</sup>

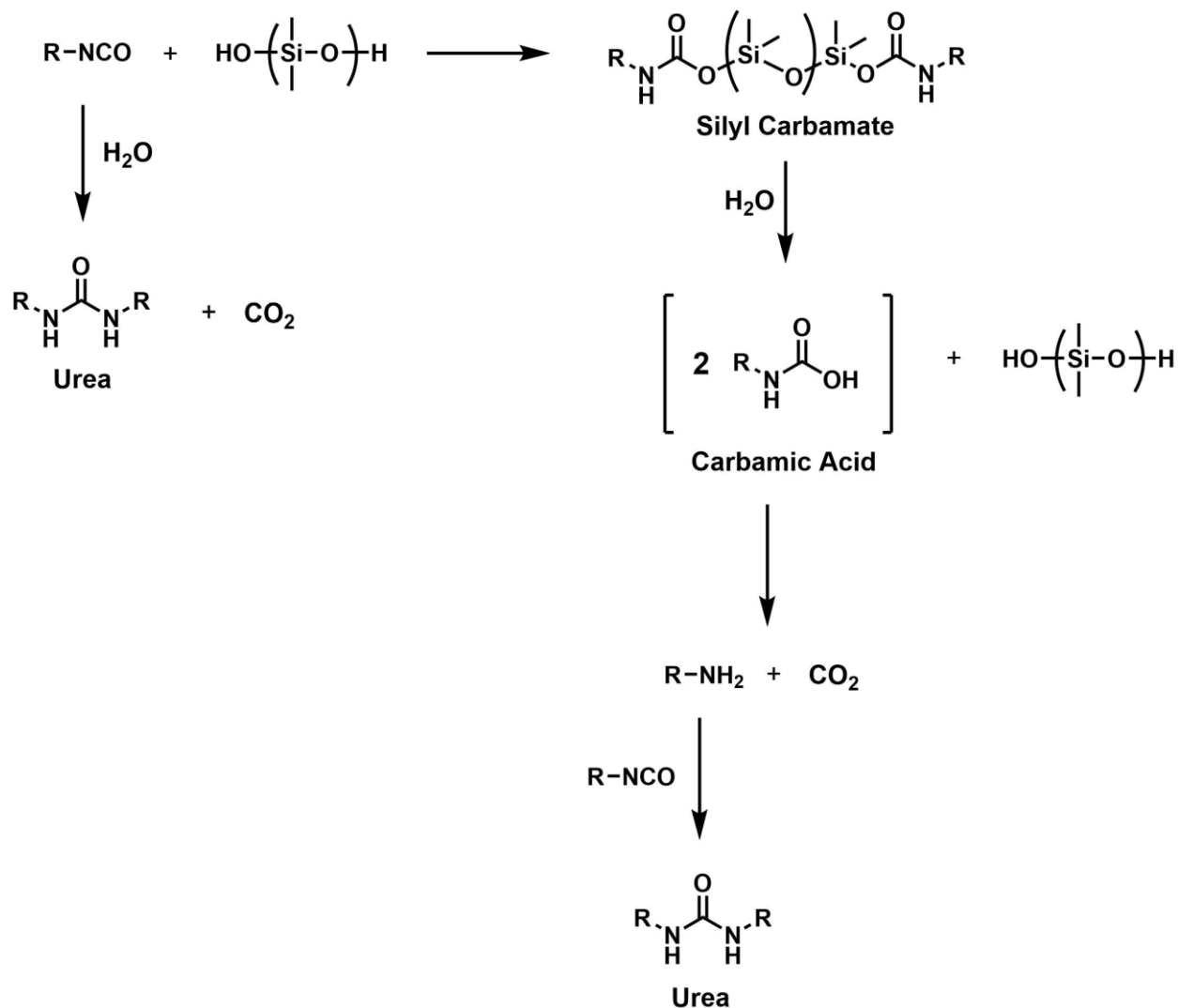
Up until the last decade, almost all published literature on siloxane-polyurethane systems as they relate to fouling-release marine coatings have utilized carbinol-terminated polydimethylsiloxane. Recent publications, however, express ambiguity of the end chain functionality of polydimethylsiloxane by using terminology such as “hydroxy-terminated PDMS” to describe silanol-terminated PDMS, a term that was traditionally used in reference to carbinol-terminated PDMS. Rath et al. created an isocyanate-capped prepolymer by reacting hydroxy-terminated PDMS (silanol end chain) with toluene diisocyanate and characterized simply by Fourier Transform Infrared spectroscopy (FTIR), confirming the appearance of a carbonyl peak at 1715 cm<sup>-1</sup>.<sup>11</sup> Su et al. developed waterborne polyurethaneureas using  $\alpha,\omega$ -dihydroxypropyl[(3,3,3-trifluoropropyl)methylsiloxane] (PTFPMS, a silanol-terminated PDMS derivative) and isophoronediiisocyanate (IPDI) as the prepolymer which was further incorporated into a waterborne polyurethane-urea, however no characterization was reported of the prepolymer.<sup>12</sup> Rahman et al. developed waterborne polyurethane adhesives starting with hydroxy-terminated PDMS (silanol chain ends), poly(tetramethyleneadipate glycol) (PTAd), and 4,4'-dicyclohexylmethane diisocyanate (H<sub>12</sub>MDI), claiming that “the use of PDMS with benefits in boosting water resistivity might be useful”.<sup>9</sup> FTIR spectra of the prepolymers show a decreasing carbonyl peak that appears to shift to lower wavenumbers as the PDMS content increases. Rahman additionally published on a waterborne polysiloxane-urethane-urea (WBPSUU) for marine coatings which also utilized the silanol-isocyanate reaction.<sup>10</sup> Both

silanol-terminated PDMS and poly(tetramethyleneoxide glycol) (PTMG) in various ratios were reacted with H<sub>12</sub>MDI in the prepolymer process. The prepolymer was then neutralized and dispersed in water, forming a WBPSUU. The formulation with 100% PDMS was noted to be “fully brittle at dried condition and, therefore, was not considered for characterization”.<sup>10</sup> FTIR characterization of the WBPSUU prepolymers was not shown for each individual formulation, however it was stated that carbonyl peaks ranged between 1600 – 1760 cm<sup>-1</sup>. Additionally, molecular weight data suggested that prepolymers with increasing PDMS exhibited decreasing molecular weights.

Choi et al. synthesized a polyurethane-urea bandage material from hydroxy-terminated PDMS (silanol chain ends), polyethylene glycol (PEG), and H<sub>12</sub>MDI, with no characterization of the silyl carbamate prepolymer.<sup>6</sup> Hwang et al. incorporated hydroxy-terminated (silanol chain ends) into a UV-curable polycarbonate-based polyurethane methacrylate dispersions by reacting with isophorone diisocyanate (IPDI), forming a silyl carbamate linkage.<sup>7</sup> It was claimed that the reaction was monitored simply by observing the disappearance of isocyanate peaks using FTIR, however no FTIR spectra were published and therefore a determination of the presence of carbonyl peaks may not be made. Pandey et al. also reacted silanol-terminated PDMS with IPDI in the prepolymer step of forming highly branched siloxane-urethane networks.<sup>8</sup> While no FTIR spectra were published, it was reported that urethane peaks appeared at 1710 cm<sup>-1</sup> and no hydroxyl groups were present. Size exclusion chromatography of the branched polymers indicated a “definitive presence of low molecular weight fractions might contribute to the broadening of the traces in the higher retention time region”, which may correlate with hydrolysis products if the silyl-carbamate linkage is unstable.

Silanols are well known to be more acidic than their corresponding carbinols with  $pK_a$  values ranging from 5-14.<sup>18-21</sup> For example, the  $pK_a$  of trimethyl silanol is 11, whereas tert-butyl alcohol has a  $pK_a$  of 19. While the hydrolytic stability of silyl carbamates has not been investigated, carboxylic acids in reaction with isocyanates may be comparable based on low acidity. Dieckmann et al. described the reaction of carboxylic acids and isocyanates, resulting in a carbamic-carboxylic anhydride.<sup>22</sup> However, this reaction product was determined to be unstable, decomposing into either an amide and  $CO_2$  or urea and acid anhydride.<sup>23-25</sup> While carboxylic acids and isocyanates produce unstable carbamic-carboxylic anhydride compounds, little is known about the silanol-isocyanate reaction. Given the possible instability of the silyl-carbamate linkage, it is important to investigate this reaction fully prior to publishing literature utilizing this chemistry. As Andrianov suggested, the possibility of a silanol reacting with an isocyanate is plausible, however the stability of the silyl-carbamate may readily hydrolyze into a carbamic acid intermediate which may further decompose into amine and carbon dioxide (Scheme 2.1).<sup>16</sup> If the silanol-isocyanate reaction occurs relatively quickly, the hydrolysis and decomposition amine product may react with excess isocyanate to form urea, a competing reaction to the silyl-carbamate formation. Isocyanates are also capable of reacting with water, in which the resulting products are ureas. Therefore, it is important to know the exact route in which ureas are formed to determine whether the silyl carbamate linkage does indeed form.

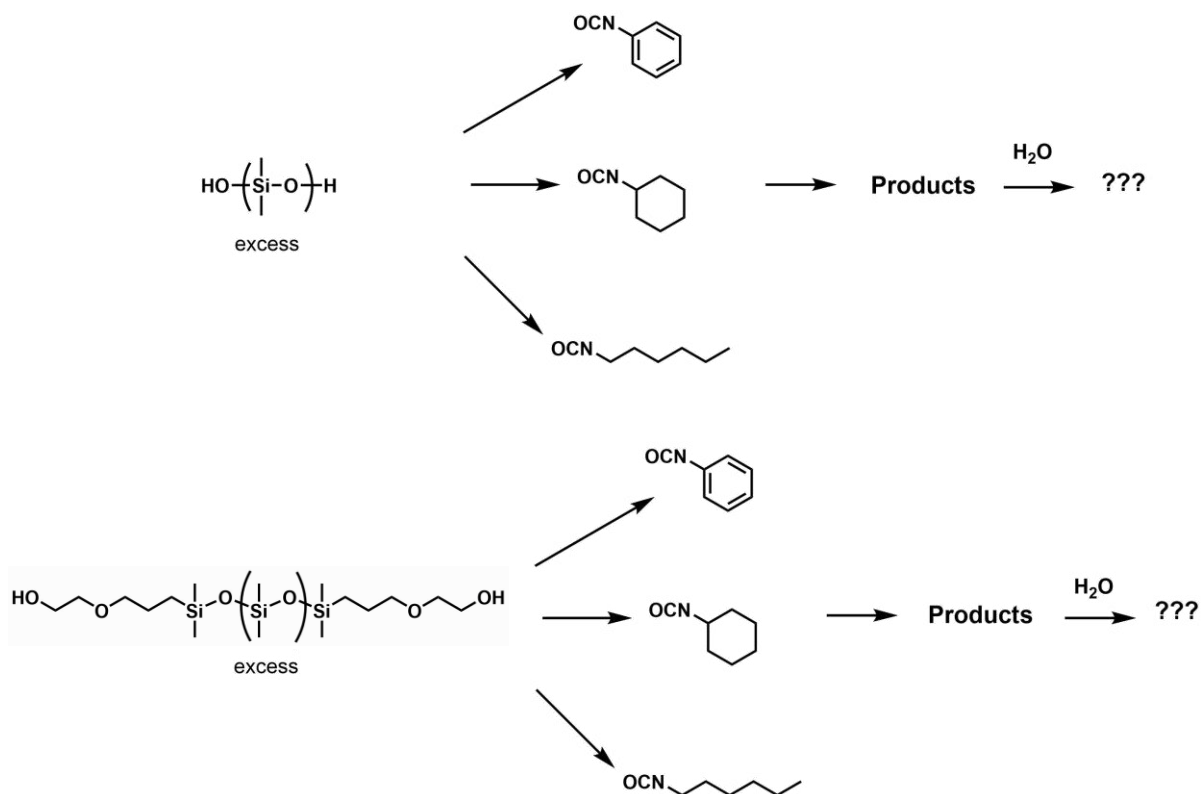




### Scheme 2.1. Silanol-isocyanate reaction mechanism

This study investigates the formation and hydrolytic stability of silyl-carbamates to understand the nature of silyl urethanes in fouling-release polyurethanes. Silanol-terminated PDMS was reacted with monoisocyanates and analyzed using FTIR and NMR (Scheme 2.2). Comparisons were made between traditional urethanes by reacting carbinol-terminated PDMS with the same monoisocyanates. Additionally, computational analysis was run to understand the feasibility and stability of the silanol-isocyanate reaction by understanding the bond stability of the silicon-oxygen bond of the silyl carbamates for each monoisocyanate with silanol. Carbinol-

monoisocyanate reaction products with carbamates were also computationally analyzed and compared to the silyl carbamates.



**Scheme 2.2. Experimental approach for investigation of the silanol-isocyanate study**

## 2.2. Experimental

### 2.2.1. Raw materials

Silanol-terminated polydimethylsiloxane ( $M_n \sim 550$ ), phenyl isocyanate, cyclohexyl isocyanate, hexyl isocyanate, toluene, dibutyltin dilaurate (DBTDL), chloroform-d and dimethyl sulfoxide-d6 were purchased from Sigma Aldrich. Mono-isocyanates were stored at  $1.6^\circ\text{C}$ . Toluene was dried using  $4\text{\AA}$  molecular sieves. Carbinol-terminated polydimethylsiloxane (DMS-C16) was purchased from Gelest. All reagents were used as received with the exception of dried toluene.

### **2.2.2. Synthesis of silyl-carbamate linkages**

Attempts at synthesizing silyl-carbamates were performed by first adding silanol-terminated PDMS into a 20 mL vial followed by adding isocyanate at a 1.2:1 equivalent ratio of silanol to NCO. This ensures that all isocyanate will ideally react leaving a small excess of PDMS. The reaction was carried out at room temperature under nitrogen with 0.05% DBTDL. No solvent was necessary. Reaction completion took between 3-6 hours and was monitored by the disappearance of isocyanate groups at  $\sim 2200\text{-}2300\text{ cm}^{-1}$  using FTIR. The final product appeared as a white solid with a small amount of oil, which was washed using dried toluene and filtered using a vacuum. The filtered product and the toluene filtrate were dried in an oven at  $80^{\circ}\text{C}$  for 30 minutes. The monoisocyanates were also reacted with carbinol-PDMS using the previously mentioned method for comparison. Additionally, each isocyanate was reacted with excess water for 24 hours at room temperature and dried in the oven at  $80^{\circ}\text{C}$  for 3 hours to form the corresponding ureas. The ureas were compared to the products from the silanol-isocyanate reactions.

### **2.2.3. Characterization of silyl-carbamate linkages**

Reaction products from the silanol-isocyanate synthesis were analyzed by Fourier transform infrared spectroscopy (FTIR) using a Thermo Scientific Nicolet 8700 spectrometer. The white solid product was run by making a pellet with potassium bromide (KBr), whereas the oily toluene filtrate was spread across a KBr disc. Additionally, nuclear magnetic resonance spectroscopy (NMR) using a Jeol 400 MHz spectrometer was performed on each product after washed with toluene, the toluene filtrate, and the ureas formed from isocyanates and water. Products were solubilized in either chloroform-d or dimethyl sulfoxide-d<sub>6</sub>. Proton NMR ( $^1\text{H}$

NMR) and carbon NMR ( $^{13}\text{C}$  NMR) were both run for each sample. Integration using Mestrelab Mnova was utilized to quantify the products and byproducts.

#### 2.2.4. Computational calculations on silyl-carbamate linkage<sup>1</sup>

Computational analysis was performed on silanol-monoisocyanate and carbinol-monoisocyanate products to compare the stability of the silyl carbamate linkage. To calculate the bond stability for the products, a computational quantum chemical approach was applied. For this, a density function theory (DFT) method implemented in Gaussian 16 software was used to calculate the Wiberg Bond Index, natural charges on atoms, and dipole/debye value for each carbamate product. Within a DFT method a B3LYP functional together with 6-31g(d) basis set were used for bond stability calculations. Computationally Assisted Science and Technology (CCAST) services were utilized to carry out the computational calculations. Comparisons between the silanol-NCO and carbinol-NCO products were made.

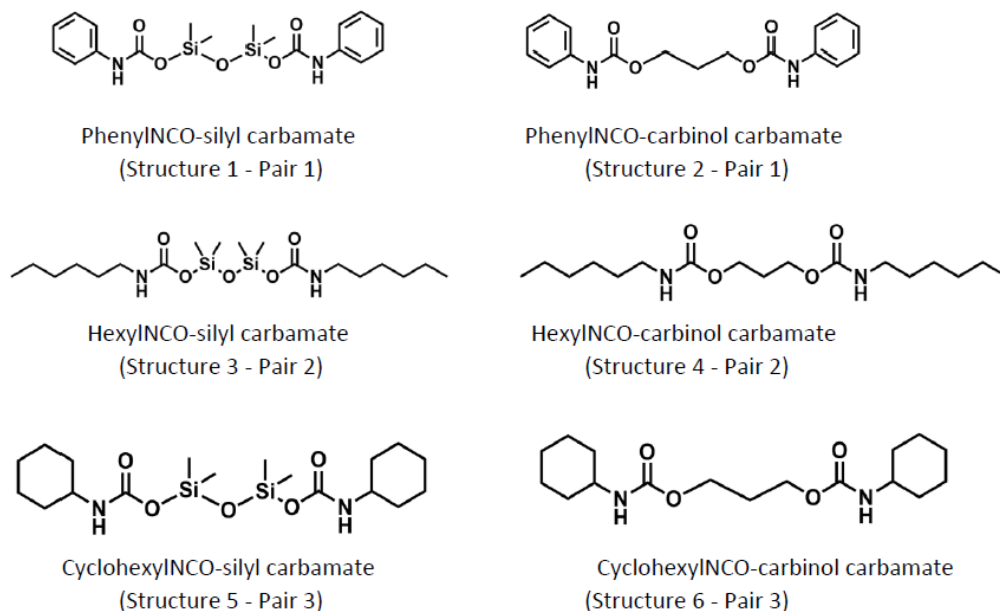


**Figure 2.1. Product structures for bond stability calculations**

<sup>1</sup> This work was done in collaboration with Alireza Rahimi

Six product structures were used as inputs for bond stability calculations (Figure 2.1). Each product represents a phenyl, cyclohexyl and hexyl isocyanate with either silanol (structures 1,3,5) or carbinol (structures 2,4,6). For simplicity in the calculations, only the carbamate linkage was studied, and therefore the silanol-PDMS was minimized to two repeat units.

## 2.3. Results and discussion

### 2.3.1. Silanol-isocyanate synthesis

All silanol-isocyanate products appeared as a homogenous oily white solid, whereas the carbinol-isocyanate products showed phase separation of a white solid on the bottom with a transparent oil on top (Figure 2.2). The transparent oil was characterized using NMR and FTIR and was found to be unreacted PDMS due to formulating with excess carbinol-terminated PDMS.



**Figure 2.2. Carbinol-isocyanate (left) and silanol-isocyanate (right) product appearance**

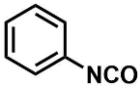
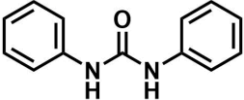
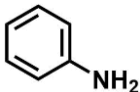
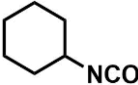
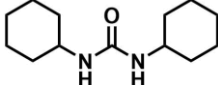
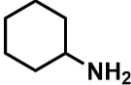
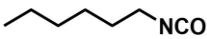
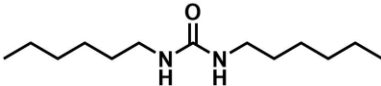
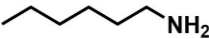
After washing all the products with dried toluene and filtering the oil from the solid, excess unreacted PDMS was consistently found to be the only compound in the toluene filtrate. As a result, any unreacted isocyanate, carbamate, urea or amine remained in the white solid

portion and was considered the “product”, whereas the toluene filtrate was confirmed to be PDMS only and excluded from further characterization.

### 2.3.2. Characterization of silyl-carbamate formation

The reaction products and byproducts from the silanol-isocyanate reaction were characterized by NMR and FTIR. Initial formulations with an excess of isocyanate resulted in a lack of product solubility in NMR solvents such as chloroform-d, dimethyl sulfoxide-d<sub>6</sub>, and methanol-d<sub>4</sub>. As a result, re-formulating with an excess of silanol helped overcome many of the previous solubility issues in order to proceed with product characterization. NMR was used to characterize and quantify the presence of silyl carbamate, urea, and/or amine, whereas FTIR was primarily utilized in observing the presence and location of the carbonyl peaks. The potential observable byproducts from the silanol reaction with phenyl, cyclohexyl and hexyl isocyanates (amines and ureas) are shown in Table 2.1.

**Table 2.1. Potential reaction by-products for each isocyanate reaction**

	Isocyanate	Urea	Amine
Phenyl NCO			
Cyclohexyl NCO			
Hexyl NCO			

Urea by-products were most easily identified through comparison of the FTIR and NMR peaks of the ureas formed from NCO-water products. Amines, however, were more difficult in

their identification using FTIR, and therefore NMR was relied upon for determining the presence of aniline, cyclohexyl amine and hexyl amine.

### 2.3.2.1. Fourier transform infrared spectroscopy

Reaction products from the silanol-terminated PDMS was compared to the carbinol-terminated PDMS in addition to the urea product formed from isocyanate and water. The carbonyl peaks of the silyl carbamate are expected to appear around  $\sim 1700 - 1730 \text{ cm}^{-1}$  whereas urea carbonyl peaks appear between  $\sim 1600 - 1700 \text{ cm}^{-1}$ . Figures 2.3-2.5 show the FTIR spectra for each set of isocyanate products (silanol, carbinol, and urea).

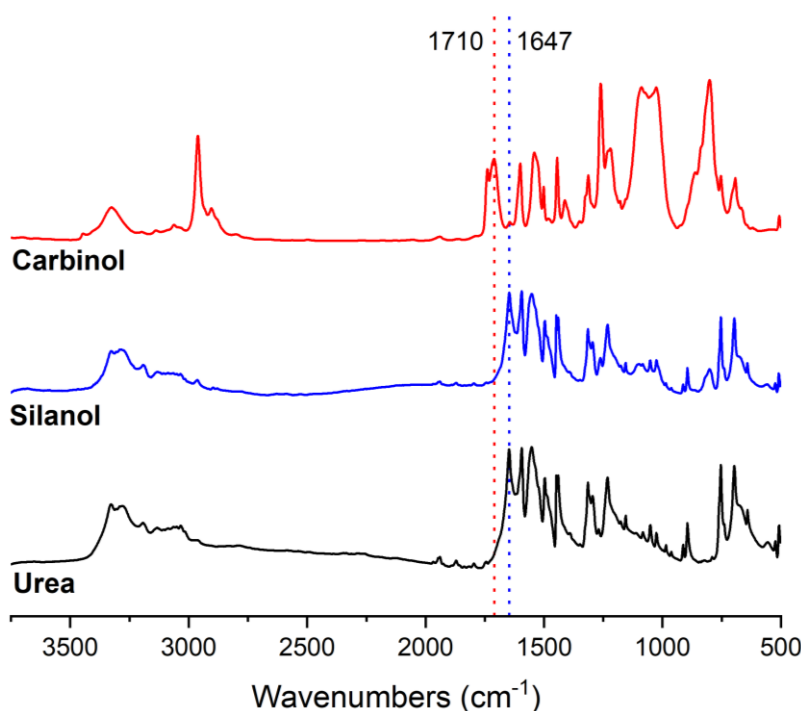


**Figure 2.3. Phenyl isocyanate and carbinol, silanol and urea comparison**

For the carbinol-terminated PDMS and phenyl isocyanate reaction product, a distinct carbonyl peak shows at  $1710 \text{ cm}^{-1}$ , indicating the carbonyl of the carbamate. The siloxane bonds (Si-O-Si) between  $1000-1100 \text{ cm}^{-1}$  show the presence of PDMS. As previously mentioned, unreacted PDMS was removed from the product with toluene, and therefore the presence of

PDMS in addition to the distinct carbonyl from the carbamate signify the carbinol-terminated PDMS has successfully reacted with phenyl isocyanate to form a urethane linkage. Comparing the silanol and urea, little visual difference between peak location and intensity is observed. The carbonyl peak at  $1647\text{ cm}^{-1}$  for both the urea and the silanol product correlates to the carbonyl of diphenyl urea. The silanol product does not contain any carbonyl peaks associated with a silyl carbamate. Additionally, siloxane bonds are not present in the washed silanol product, resulting in no reacted PDMS. From the FTIR of phenyl isocyanate and silanol, it has been concluded that silyl carbamate is not present, rather urea is the prominent observable product. While amines may also be present within the product, distinction of the amine peaks in FTIR proved difficult, and therefore NMR was more useful in identifying amines.

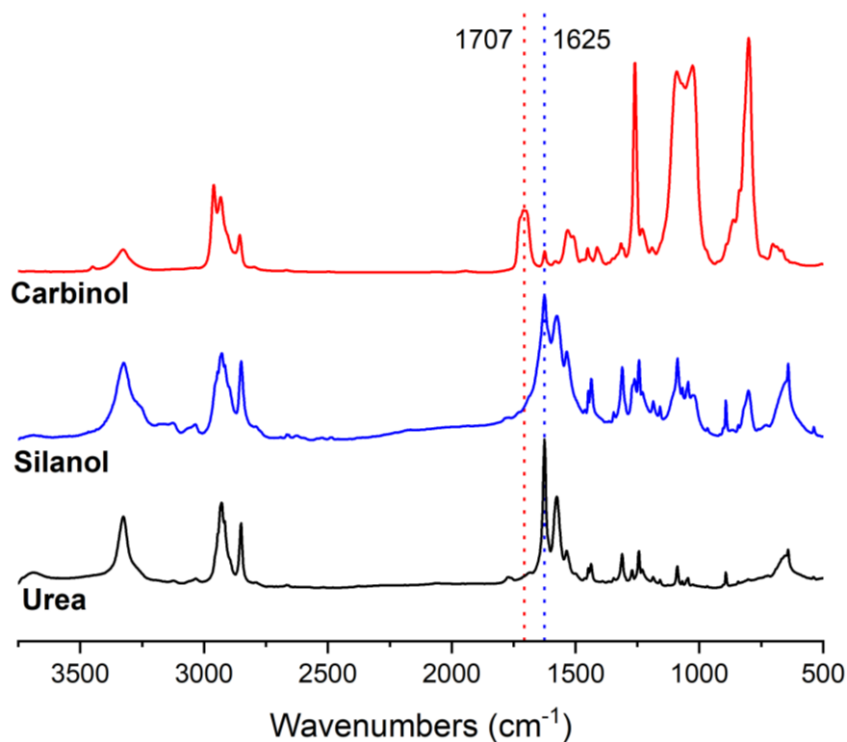


**Figure 2.4. FTIR for cyclohexyl isocyanate and carbinol, silanol and urea comparison**



Cyclohexyl isocyanate products with carbinol and silanol are compared to the urea in Figure 2.4. The carbinol product shows a distinct carbonyl peak at  $1707\text{ cm}^{-1}$  representing the carbamate. The siloxane peaks at  $1000\text{-}1100\text{ cm}^{-1}$  are also present after washing the product with toluene, indicating that PDMS has reacted with cyclohexyl isocyanate to form the urethane linkage. The FTIR spectra of the silanol product shows comparable peaks to the urea product spectra. The carbonyl peak for dicyclohexyl urea is shown at  $1625\text{ cm}^{-1}$  for both silanol and urea product. No silyl carbamate is observed in the silanol product.

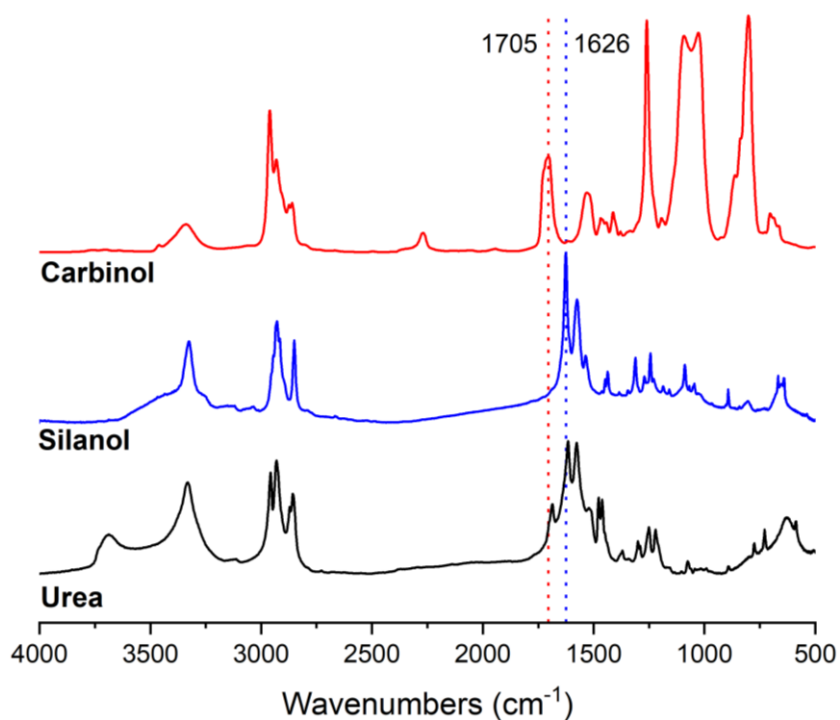


**Figure 2.5. Hexyl isocyanate and carbinol, silanol and urea comparison**

For hexyl isocyanate and carbinol (Figure 2.5), a carbonyl peak at  $1705\text{ cm}^{-1}$  and the presence of siloxanes from  $1000\text{-}1100\text{ cm}^{-1}$  indicates the formation of the carbamate. The silanol and urea product are both similar in the strong urea presence from the carbonyl at  $1626\text{ cm}^{-1}$ . The urea product shows a broad peak around  $3700\text{ cm}^{-1}$  and a small side peak around  $1700\text{ cm}^{-1}$  which indicates the presence of water. The silanol product contains no silyl carbamate as the

carbonyl peak within the 1700's  $\text{cm}^{-1}$  is absent. Any PDMS within the product was washed into the toluene filtrate, indicating no covalent bonds between the PDMS and the isocyanate.

Similar behavior was observed for each monoisocyanate and the silanol/carbinol products. For each isocyanate-carbinol product, a distinct carbonyl peak (1705 – 1710  $\text{cm}^{-1}$ ) indicates the presence of the carbamate linkage. Additionally, the siloxane bonds (Si-O-Si) between 1000-1100  $\text{cm}^{-1}$  indicate the presence of covalently-bonded PDMS. All mono-isocyanates reacted with carbinol-terminated PDMS therefore show the formation of the urethane linkage without the presence of urea, indicating a hydrolytically stable carbamate. For each of the isocyanate-silanol products, carbonyl peaks appear between 1612-1647  $\text{cm}^{-1}$ . The lower shift in wavenumbers is indicative of urea carbonyl peaks rather than silyl-carbamate peaks. No urethane linkage is observed in any of the silanol products. Additionally, after washing the product with toluene to remove unreacted PDMS, each of the silanol products appear identical to the urea spectra, indicating a high presence of urea within the product. This indicates that the silyl-carbamate linkage either did not form or was hydrolytically unstable.

#### **2.3.2.2. Nuclear Magnetic Resonance Spectroscopy**

Proton and carbon NMR were individually analyzed for each product to identify the major components and compared against urea. Figures 2.6-2.8 shows the  $^1\text{H}$  and  $^{13}\text{C}$  NMR spectra for phenyl, cyclohexyl and hexyl isocyanate with silanol and carbinol. The identified product structures are shown on each spectrum, with red indicating amine, blue indicating urea and green indicating carbamate.

The presence of amine indicates that silyl carbamate has indeed formed, however the resulting linkage has been hydrolyzed and decomposed into the corresponding amine and silanol. However, presence of urea gives little indication as to the pathway of formation, which may

occur by two separate routes. The first route includes the reaction of the isocyanate and water, whereas the second route includes the reaction of the hydrolyzed amine by-product of the silyl-carbamate linkage with unreacted isocyanate. The distinction between these two pathways is challenging, and therefore no definitive conclusion on the formation of urea can be made. In the case of the second route, the reaction between the isocyanate and silanol in addition to the rate of hydrolysis and decomposition must proceed relatively quickly for the amine by-product to react with unreacted isocyanate.

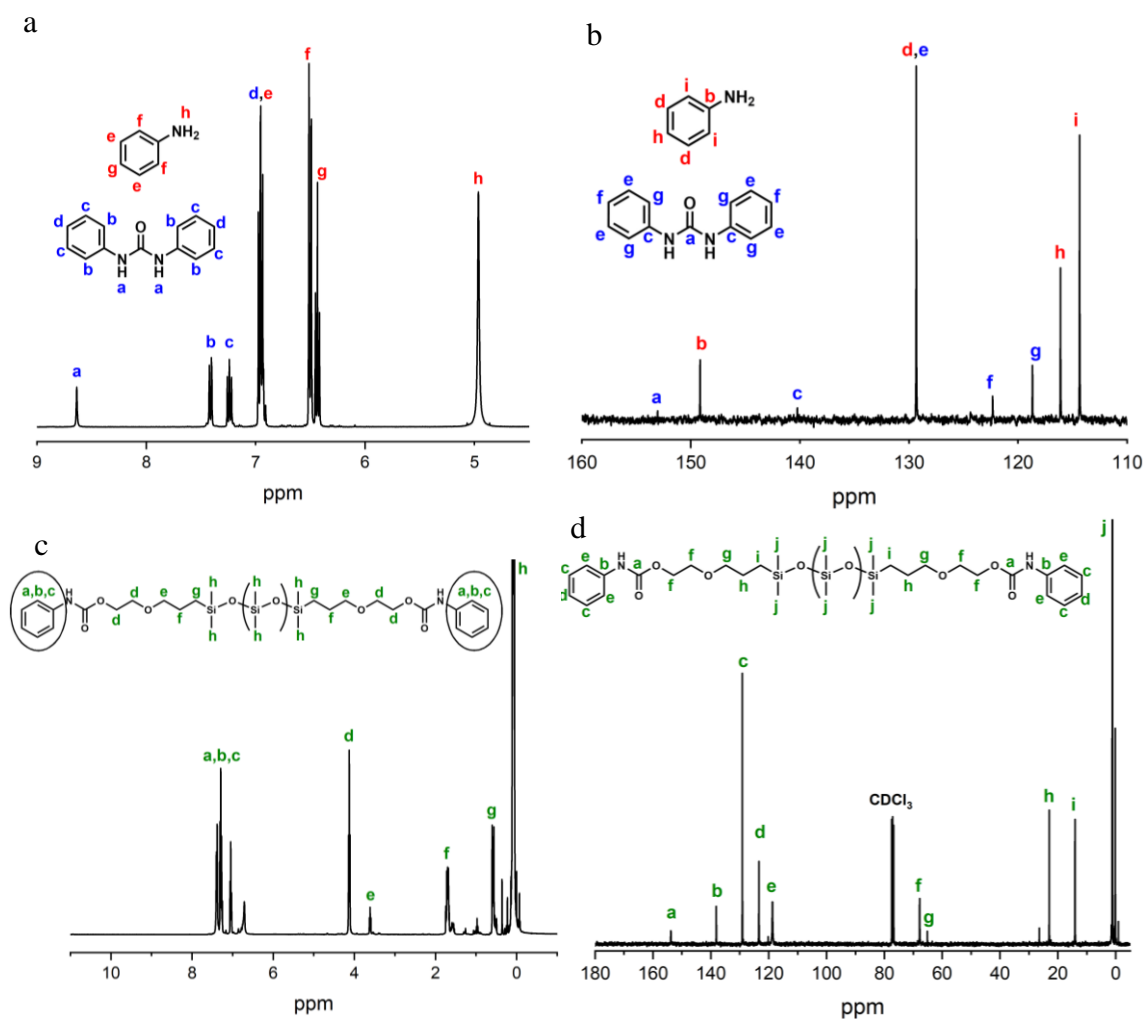


**Figure 2.6. PhenylNCO and a.) silanol  $^1\text{H}$  NMR b.) silanol  $^{13}\text{C}$  NMR c.) carbinoles  $^1\text{H}$  NMR d.) carbinoles  $^{13}\text{C}$  NMR**

From the  $^1\text{H}$  NMR of phenyl isocyanate and silanol (Figure 2.6a), peaks b and f+g were integrated and compared to determine the ratio of amine to urea. It was found that the silanol product consisted of 90% amine and 10% urea. The strong amine presence suggests that the silyl carbamate linkage is formed, however the product is hydrolytically unstable. The carbinol product formed hydrolytically stable carbamates with no presence of amine or urea.

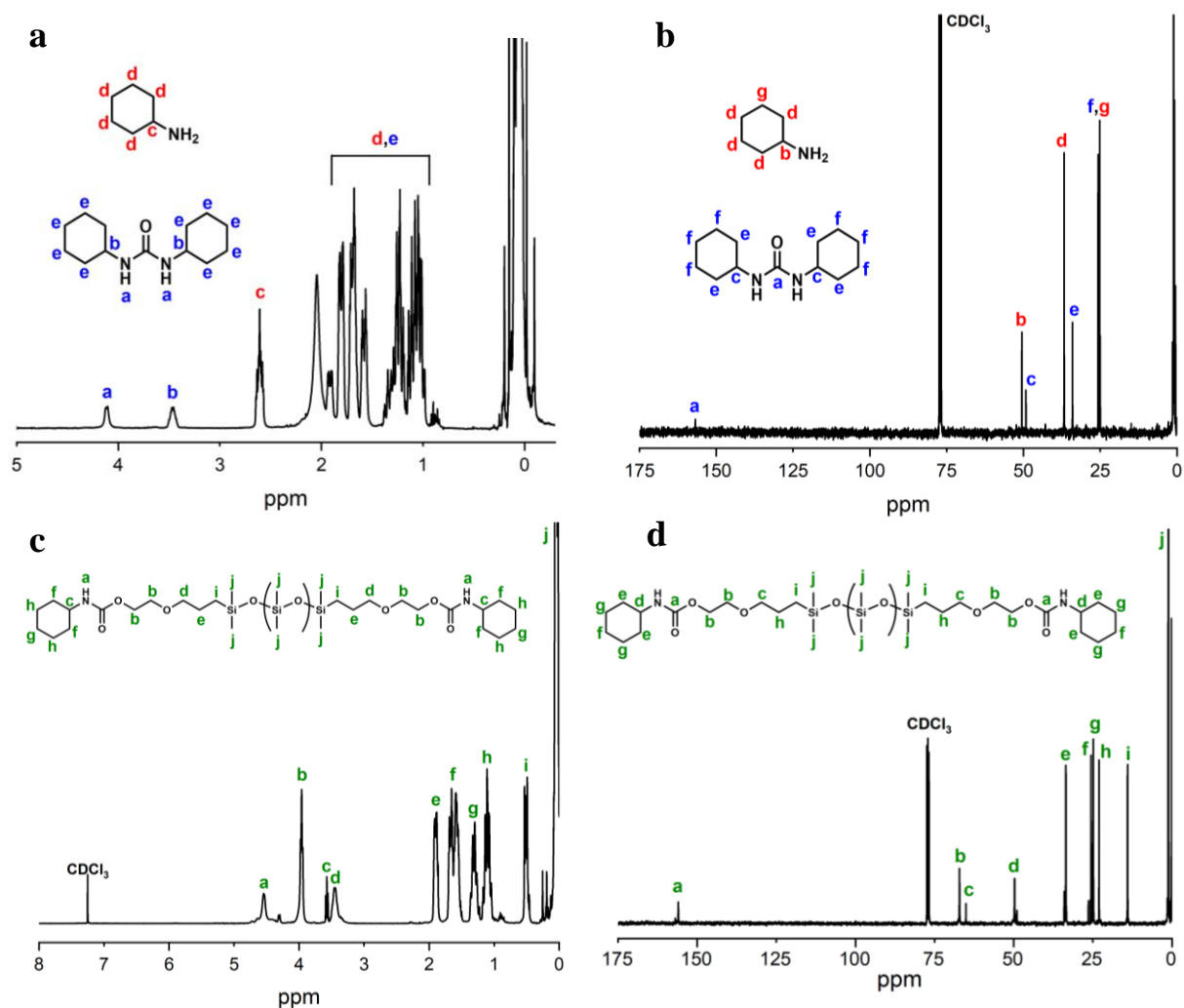


**Figure 2.7. CyclohexylNCO and a.) silanol  $^1\text{H}$  NMR b.) silanol  $^{13}\text{C}$  NMR c.) carbinol  $^1\text{H}$  NMR d.) carbinol  $^{13}\text{C}$  NMR**

Similar to the phenyl isocyanate and silanol reaction, no silyl carbamate linkages were present in the cyclohexyl isocyanate-silanol reaction products. Amine and urea were confirmed in the silanol reaction and integrated using peaks b and c (Figure 2.7a). The product consisted of 88% amine and 12% urea. The cyclohexyl isocyanate and carbinol reaction yielded 100% carbamate with no presence of amine or urea.

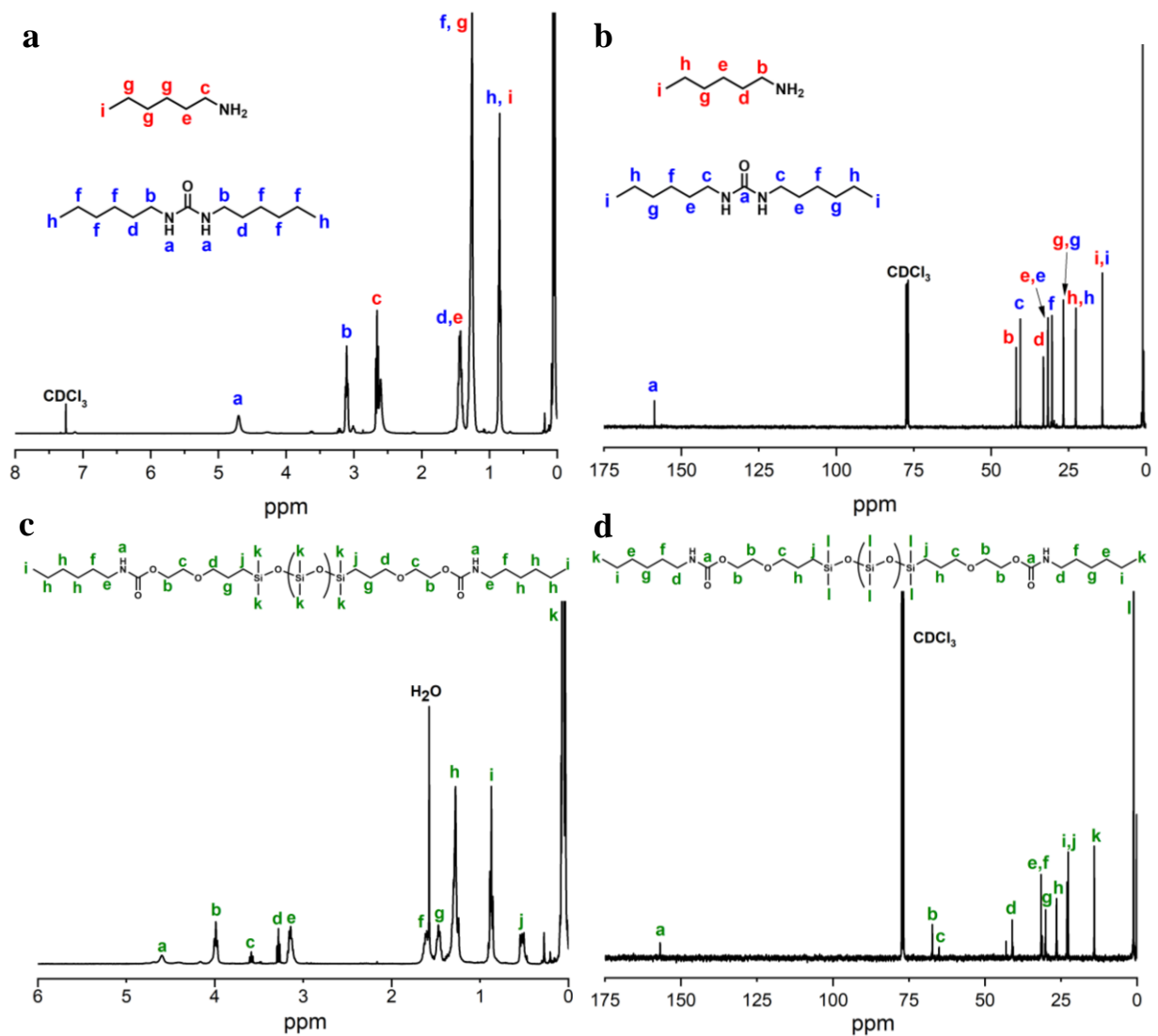


**Figure 2.8. HexylNCO and a.) silanol  $^1\text{H}$  NMR b.) silanol  $^{13}\text{C}$  NMR c.) carbinol  $^1\text{H}$  NMR d.) carbinol  $^{13}\text{C}$  NMR**

The hexyl isocyanate and silanol reaction yielded amine and urea only, indicating the hydrolytic instability of the silyl carbamate linkage. Integration of peaks b and c (Figure 2.8a) resulted in 85% amine and 15% urea. The carbinol product contained the carbamate without the presence of amine or urea, indicating a stable urethane linkage under atmospheric conditions.

A summary of the products for each reaction is shown in Table 2.2. None of the silanol reactions produced stable silyl-carbamates, however the high presence of amine (85-90%) indicates the reaction of silanol and isocyanate proceeds. The silyl-carbamates are easily hydrolyzed and decomposed under atmospheric conditions. These results are in agreement with the observed functionality within FTIR.

**Table 2.2. Results of reaction products from isocyanate-PDMS**

<b>NCO</b>	<b>PDMS</b>	<b>Carbamate %</b>	<b>Amine %</b>	<b>Urea %</b>
Phenyl	Si-OH	0	90	10
Cyclohexyl	Si-OH	0	88	12
Hexyl	Si-OH	0	85	15
Phenyl	C-OH	100	0	0
Cyclohexyl	C-OH	100	0	0
Hexyl	C-OH	100	0	0

Phenyl isocyanate and silanol showed the highest percent of amine formation at 90%, followed by cyclohexyl isocyanate at 88% and then hexyl isocyanate at 85%. Correlating to reactivity, aromatic isocyanates are the most reactive, whereas aliphatic isocyanates are the least reactive.<sup>26</sup> Evidence of this trend is seen in the amine content. As phenyl isocyanate has the highest reactivity, more amine is observed as the silyl-carbamate linkage rapidly forms and hydrolyzes. However, too fast of a reaction leads to the potential of the amine by-product reacting with excess isocyanate, resulting in higher urea content. As the amine reactivity slows, it

is possible that isocyanate is more likely to react with atmospheric moisture, producing higher amounts of urea within the system. While the route of urea formation has not been determined, it is suggested that the lower reactivity of cyclohexyl and hexyl isocyanate allows for isocyanate to react with water, and therefore the urea content is observed to increase with a decreasing amine reactivity.

### 2.3.3. Computational calculation correlations

Wiberg Bond Index values, natural charges on atoms, and dipole moment were all calculated for each silanol and carbinol product to compare the carbamate stability. Table 2.3 shows the Wiberg Bond Index values for the silicon-oxygen or silicon-carbon bond and the nitrogen-carbon bond to understand the bond strength.

**Table 2.3. Wiberg Bond Index values**

Structure #	NCO	PDMS	Si-O	C-O	N-C
1	Phenyl	Si-OH	0.4926	-	1.1219
2	Phenyl	C-OH	-	0.7991	1.1048
3	Hexyl	Si-OH	0.4867	-	1.1422
4	Hexyl	C-OH	-	0.8089	1.1584
5	Cyclohexyl	Si-OH	0.4995	-	1.1684
6	Cyclohexyl	C-OH	-	0.8167	1.1530

The Wiberg Bond Index (WBI) is comparable to bond order from valence bond theory, signifying the number of chemical bonds between atoms. Higher bond orders are commonly correlated with stronger bonds.<sup>27</sup> All silanol products show WBI values of the silicon-oxygen bond around 0.49, whereas all carbinol products have values for the carbon-oxygen bond near 0.80. The smaller WBI for Si-O indicates a weaker bond compared to the O-C bond on the

carbinol product. As a result, the WBI values suggest the silyl carbamate to be less stable than alkyl carbamate. From the nitrogen-carbon bond, higher WBI values between 1.10 – 1.17 indicate relatively stable bonds. If hydrolysis were to occur at any point in the carbamate linkage, the silicon-oxygen bond would be most susceptible to cleavage based on the lower WBI.

**Table 2.4. Natural charges on carbamate atoms and absolute charge difference of Si-O and C-O bonds in carbamate linkage**

Structure	NCO	PDMS	Si	C	O	Si - O	C - O
1	Phenyl	Si-OH	2.2199	-	-0.8937	3.1136	-
2	Phenyl	C-OH	-	-0.11075	-0.58369	-	0.4729
3	Hexyl	Si-OH	2.2245	-	-0.8981	3.1226	-
4	Hexyl	C-OH	-	-0.11137	-0.57823	-	0.4669
5	Cyclohexyl	Si-OH	2.2214	-	-0.8985	3.1199	-
6	Cyclohexyl	C-OH	-	-0.11517	-0.58895	-	0.4738

Natural charges on the silicon/carbon and oxygen of the Si-O or C-O bonds within the carbamate linkage were determined (Table 2.4). The absolute difference in charges is shown in the last two columns (|Si - O| and |C - O|). From the silanol products, a large natural charge on the silicon atom creates a significantly large charge differential (~3.12) between the silicon-oxygen bond. The carbon charge in a traditional carbamate shows a low partial negative charge, resulting in an absolute charge differential of ~0.47 between the carbon-oxygen bond. The large charge differential between the silicon-oxygen bond lowers the overall bond stability, making it more susceptible to nucleophilic attack or hydrolysis. The low charge differential of the carbon-oxygen bond in the carbinol products indicates a more stable link. The results of the natural



atomic charge demonstrate the hydrolytic instability within the silyl carbamate, indicating the potential for cleavage at the silicon-oxygen bond. The carbon-oxygen bond on a traditional carbamate linkage, however, remains stable.

**Table 2.5. Dipole values of carbamate structures**

Structure #	NCO	PDMS	Dipole ( $1 \times 10^{-18}$ statC*cm)
1	Phenyl	Si-OH	3.79
2	Phenyl	C-OH	1.42
3	Hexyl	Si-OH	4.87
4	Hexyl	C-OH	3.42
5	Cyclohexyl	Si-OH	4.34
6	Cyclohexyl	C-OH	0.67

Molecular dipole moments shown in Table 2.5 indicate that the silanol products are generally more polar than the carbinol products. Higher dipole moments of structures 1, 3 and 5 leads to potentially unstable silyl carbamates as certain atoms become susceptible to nucleophilic/electrophilic attacks. Structure #4, consisting of hexyl isocyanate and carbinol, also results in a relatively high dipole moment. One possible explanation is the lack of resonance available on hexyl isocyanate, resulting in larger localized dipole moments that contribute to a large molecular dipole. The other carbinol products, structures 2 and 6, have lower dipole moments of 1.42 and 0.67 respectively. It is suggested that the carbamates formed from isocyanates and carbinols are therefore more stable than silyl carbamates.

Silanols are well known to be inherently more acidic than their corresponding carbinols, with aryl silanols more acidic than alkyl silanols.<sup>18-21</sup> As a result, silanols are capable of

hydrogen bonding with each other in addition to other molecules, with more electronegative substituents increasing the acidity of the silanol.<sup>21</sup> In the case of silyl carbamates, the electronegative urethane group increases the acidity of the oxygen directly attached to the silanol, increasing the potential for hydrogen bonding when in contact with water. Less acidic carbinol carbamates, however, remain stable when in contact water. From the computational calculations of silanol and carbinol products, silyl carbamates are unstable due to the low WBI value, large natural charge on the silicon atom, and the high dipole moment associated with the molecular carbamate. These computational findings agree with the experimental spectroscopic data. It is therefore determined that while silanols do react with isocyanates, they are highly unstable and readily hydrolyze and decompose into their corresponding amines and silanols. It is recommended that silanols should not be used as the polyol component for forming polyurethane materials, especially in the case of waterborne polyurethanes.

#### **2.4. Conclusions**

PDMS silanols and carbinols were reacted with monoisocyanates to understand and compare the formation and stability of silyl carbamates relative to traditional carbamates. Spectroscopic data shows that silanols do react with isocyanates, however they are readily hydrolyzed under atmospheric conditions into amines and silanols. Depending on amine reactivity, excess isocyanates can react with the amine byproducts to form urea. The carbinol-isocyanate products were found to form stable carbamate linkages that do not readily hydrolyze.

Computational calculations of the Wiberg Index Value, natural charges on atoms and molecular dipole moment agree with the experimental data, suggesting that silyl carbamates are unstable at the silicon-oxygen bond. It is suspected that hydrolysis occurs at this site based on the large molecular dipole moment, low bond order, and large charge differential on the silicon-

oxygen bond. It is therefore suggested that silanols are not used as the polyol components in polyurethane materials as a result of their instability.

## 2.5. References

1. Alexandridis, P., Amphiphilic copolymers and their applications. *Curr. Opin. Colloid Interface Sci.* **1996**, *1* (4), 490-501.
2. Sommer, S.; Ekin, A.; Webster, D. C.; Stafslie, S. J.; Daniels, J.; Vander Wal, L. J.; Thompson, S. E. M.; Callow, M. E.; Callow, J. A., A preliminary study on the properties and fouling-release performance of siloxane-polyurethane coatings prepared from poly(dimethylsiloxane) (PDMS) macromers. *Biofouling* **2010**, *26* (8), 961-972.
3. Bodkhe, R. B.; Stafslie, S. J.; Cilz, N.; Daniels, J.; Thompson, S. E. M.; Callow, M. E.; Callow, J. A.; Webster, D. C., Polyurethanes with amphiphilic surfaces made using telechelic functional PDMS having orthogonal acid functional groups. *Prog. Org. Coat.* **2012**, *75* (1-2), 38-48.
4. Choi, S.-J.; Lee, J.-H.; Lee, Y.-H.; Hwang, D.-Y.; Kim, H.-D., Synthesis and properties of polyurethane-urea-based liquid bandage materials. *J. Appl. Polym. Sci.* **2011**, *121* (6), 3516-3524.
5. Hwang, H.-D.; Kim, H.-J., Enhanced thermal and surface properties of waterborne UV-curable polycarbonate-based polyurethane (meth)acrylate dispersion by incorporation of polydimethylsiloxane. *React. Funct. Polym.* **2011**, *71* (6), 655-665.
6. Pandey, S.; Rath, S. K.; Samui, A. B., Structure-Thermomechanical Property Correlations of Highly Branched Siloxane-Urethane Networks. *Ind. Eng. Chem. Res.* **2012**, *51* (9), 3531-3540.

7. Rahman, M. M.; Hasneen, A.; Kim, H.-D.; Lee, W. K., Preparation and properties of polydimethylsiloxane (PDMS)/polytetramethylene adipate glycol (PTAd)-based waterborne polyurethane adhesives: Effect of PDMS molecular weight and content. *J. Appl. Polym. Sci.* **2012**, *125* (1), 88-96.
8. Rahman, M. M.; Chun, H.-H.; Park, H., Waterborne polysiloxane-urethane-urea for potential marine coatings. *J. Coat. Technol. Res.* **2011**, *8* (3), 389-399.
9. Rath, S. K.; Chavan, J. G.; Sasane, S.; Srivastava, A.; Patri, M.; Samui, A. B.; Chakraborty, B. C.; Sawant, S. N., Coatings of PDMS-modified epoxy via urethane linkage: Segmental correlation length, phase morphology, thermomechanical and surface behavior. *Prog. Org. Coat.* **2009**, *65* (3), 366-374.
10. Su, T.; Wang, G. Y.; Wang, S. L.; Hu, C. P., Fluorinated siloxane-containing waterborne polyurethane ureas with excellent hemocompatibility, waterproof and mechanical properties. *Eur. Polym. J.* **2010**, *46* (3), 472-483.
11. Yang, H.; Wang, X.; Yu, B.; Yuan, H.; Song, L.; Hu, Y.; Yuen, R. K. K.; Yeoh, G. H., A novel polyurethane prepolymer as toughening agent: Preparation, characterization, and its influence on mechanical and flame retardant properties of phenolic foam. *J. Appl. Polym. Sci.* **2013**, *128* (5), 2720-2728.
12. Astakhin, V. V.; Losev, I. P.; Andrianov, K. A., Reaction of organohydroxysilanes with isocyanates. Synthesis of organosilicon urethans. *Dokl. Akad. Nauk SSSR* **1957**, *113*, 581-4.
13. Andrianov, K. A.; Astakhin, V. V., Reaction of organosilicon urethans and organomonohydroxysilanes with alcohols. *Zh. Obshch. Khim.* **1959**, *29*, 2698-701.

14. Andrianov, K. A.; Makarova, L. I., The reaction of diatomic organosilicon alcohols with diisocyanates. *Vysokomol. Soedin.* **1961**, *3*, 966-70.
15. Sheludyakov, V. D.; Kirilin, A. D.; Mironov, V. F. Silyl carbamates. SU540869A1, **1976**.
16. Lickiss, P. D., The synthesis and structure of organosilanols. *Adv. Inorg. Chem.* **1995**, *42*, 147-262.
17. Badger, R. M.; Bauer, S. H., Spectroscopic Studies of the Hydrogen Bond. II. The Shift of the O–H Vibrational Frequency in the Formation of the Hydrogen Bond. *The Journal of Chemical Physics* **1937**, *5* (11), 839-851.
18. Sommer, L. H.; Pietrusza, E. W.; Whitmore, F. C., Properties of the Silicon—Hydroxyl Bond in Trialkylsilanols<sup>1</sup>. *Journal of the American Chemical Society* **1946**, *68* (11), 2282-2284.
19. Chandrasekhar, V.; Boomishankar, R.; Nagendran, S., Recent developments in the synthesis and structure of organosilanols. *Chemical reviews* **2004**, *104* (12), 5847-5910.
20. Dieckmann, W.; Breest, F., Notiz über das Verhalten von Carbonsäuren gegen Phenylisocyanat. *Berichte der deutschen chemischen Gesellschaft* **1906**, *39* (3), 3052-3055.
21. Blagbrough, I. S.; Mackenzie, N. E.; Ortiz, C.; Scott, A. I., The condensation reaction between isocyanates and carboxylic acids. A practical synthesis of substituted amides and anilides. *Tetrahedron Letters* **1986**, *27* (11), 1251-1254.
22. Naegeli, C.; Tyabji, A., Ein modifizierter Curtius'scher Abbau VII. Der Abbau der aromatischen Säuren. *Helvetica Chimica Acta* **1933**, *16* (1), 349-366.

23. Sorenson, W. R., Reaction of an Isocyanate and a Carboxylic Acid in Dimethyl Sulfoxide. *The Journal of Organic Chemistry* **1959**, 24 (7), 978-980.
24. Sonnenschein, M. F., *Polyurethanes: Science, Technology, Markets and Trends*. Wiley: Hoboken, NJ, **2015**.
25. Harper, L. K.; Shoaf, A. L.; Bayse, C. A., Predicting Trigger Bonds in Explosive Materials through Wiberg Bond Index Analysis. *ChemPhysChem* **2015**, 16 (18), 3886-3892.

## CHAPTER 3. ALKOXYSILANE SOL-GEL CONSOLIDANTS FOR CALCAREOUS STONE MATERIALS

### 3.1. Introduction

Stone consolidants are an integral solution for the preservation of historic stone structures and artifacts from natural degradation processes such as air pollution, efflorescence, and biodeterioration. The essential function of a stone consolidant is to bind any loose granular particles within the stones internal structure, filling in the pores at the surface to prevent further material degradation. In the cases of severe degradation, some level of structural integrity may potentially be restored with the use of consolidating materials. Fundamental stone consolidant properties require a low viscosity to penetrate the stones pores, hydrophobicity to repel water from entering the stone, transparency to prevent alterations in stone appearance, and the ability to cure at ambient temperatures. As consolidants are traditionally brush or spray applied, it is also essential they are non-toxic to those who apply the materials.

Deficiencies in commercially available stone consolidants arise in limited flexibility, breathability and long-term durability and weatherability. Current commercial stone consolidants such as Silres BS OH 100 (Wacker) and Conservare OH100 (Prosoco) consist mainly of monomeric and oligomeric tetraethylorthosilicate (TEOS). TEOS is a tetra functional alkoxy silane, producing a dense gel network that forms a highly brittle consolidant. Once inside the pores of a stone substrate, the curing of TEOS generates significant shrinkage stresses, resulting in cracks, in which the material becomes ineffective at consolidating the granular particles within the stone and preventing the uptake of water. Flexibility within the sol-gel network can be achieved by incorporating less functional alkoxy silanes in addition to unreactive alkyl chains that provide hydrophobicity (Figure 3.1).

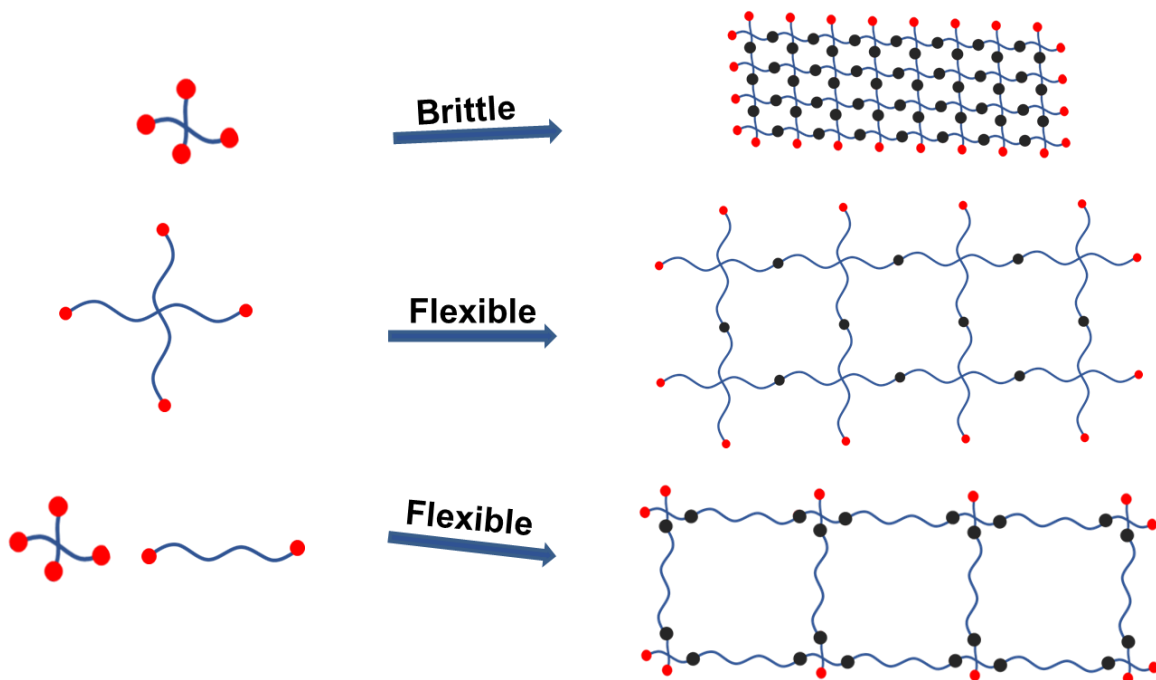


**Figure 3.1. Structure-property relationship of alkoxy silane**

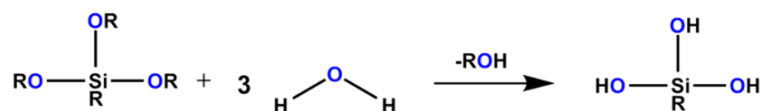
Alkoxy silanes are proven to be effective materials for the consolidation of stone substrates. Other materials such as epoxies,<sup>28-32</sup> acrylics,<sup>33-36</sup> and epoxy/acrylic hybrids<sup>37, 38</sup> have been explored, however there are practical challenges to overcome before considering these reactive systems over alkoxy silanes. Epoxy consolidants are limited in their high viscosity, consequentially leading to difficulty in penetrating the stones porous structure. While the use of a vacuum can overcome this challenge,<sup>39</sup> the impractical nature of reduced-pressure applications creates significant challenges for conservators in the field. Additionally, epoxies are commonly known to exhibit brittleness and yellowing over time. Acrylic consolidants consist mostly of Paraloid B72, an ethyl-methacrylate resin used in combination with alkoxy silanes. Widely used in the field of conservation, B72 is primarily effective as an adhesive for ceramic and glass materials.<sup>40</sup> Despite the claims of B72 imparting beneficial adhesion properties, achieving deep



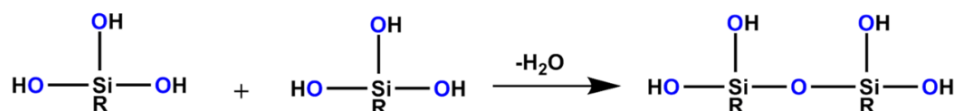
impregnation of acrylic consolidants into porous stone structures remains a challenge due to high viscosity.<sup>34</sup>

Due to their transparent nature, low viscosity, and ambient curing conditions, alkoxysilanes are the primary materials utilized in stone consolidant formulations.<sup>41-43</sup> Once alkoxysilanes are applied to stone materials, the sol-gel reaction proceeds via a two-step reaction (Scheme 3.1). First, alkoxysilanes are hydrolyzed by either atmospheric moisture or the addition of water into the formulation. The resulting silanols condense to form a siloxane network, releasing water which may further catalyze the hydrolysis reaction.<sup>44</sup> The thermal and UV stability of siloxanes make them favorable for outdoor consolidants.<sup>45</sup> Solvents such as ethanol and methanol have been traditionally used in consolidant formulations as alkoxysilanes and water are not miscible. However, as hydrolysis proceeds, alcohols such as ethanol and methanol are produced, resulting in a self-generated solvent supply. Catalysts are commonly used to accelerate the hydrolysis step. While acids and bases have been used, commercial consolidants use organotin catalysts such as dibutyltin dilaurate (DBTDL).

Hydrolysis



Condensation



**Scheme 3.1. Sol-gel reaction: hydrolysis and condensation**

Attempts at improving the commercial alkoxysilane consolidants have been under investigation by changing the alkoxysilane structure, catalyst, solvent, and/or additive components to the formulation. For improvements in flexibility, the incorporation of polydimethylsiloxane (PDMS)<sup>46-57</sup>, colloidal silica (SiO<sub>2</sub>)<sup>48, 49, 53, 56-62</sup> (3-glycidyloxypropyl)trimethoxy silane (GPTMS)<sup>52, 62-64</sup>, polyhedral oligomeric silsesquioxane (POSS)<sup>64</sup> have been investigated.

PDMS has been well-studied in consolidant formulations, acting as an elastic chain extender for improving flexibility. Given the limited functionality, PDMS lowers the crosslink density of TEOS by adding space to the network. In addition to flexibility, Illescas et al. found PDMS to “improve robustness, hydrophobicity, water repellency, and stain resistance when applied to carbonate stones”.<sup>46</sup>

Colloidal silica has been utilized in stone consolidant formulations for enhanced flexibility as well as increasing hydrophobicity for water repellency applications.<sup>48, 49, 53, 56, 57, 59-61, 65</sup> The addition of colloidal silica has been notable in minimizing crack formation during the drying process by acting as a particle spacer within the sol-gel matrix, however, undesirable increases in viscosity requires more solvent within the formulation.<sup>61</sup> Mosquera et al. observed a noticeable increase in viscosity upon the addition of colloidal silica to a simple TEOS-based consolidant, requiring additional ethanol to maintain a low-viscosity solution.<sup>61</sup> However, it was concluded that the addition of colloidal silica changed the network structure from a dense and microporous material to a mesoporous material with a higher pore volume, contributing to reduced cracking of the consolidant during the drying phase. Additionally, Mosquera et al. studied the hydrophobic properties through the incorporation of colloidal silica, in which static contact angle measurements with SiO<sub>2</sub> measured around 149°.<sup>57</sup>

GPTMS is an alkoxy silane with an epoxy functional moiety that has been utilized in hybrid epoxy consolidant formulations by crosslinking with (3-aminopropyl)triethoxysilane.<sup>52, 63</sup> GPTMS has been found to increase flexibility in addition to lowering water absorption of consolidated stone.<sup>62</sup> Epoxies are generally known for their high viscosity and yellowing upon ageing, making them unsuitable for consolidant applications. Additionally, shrinkage stresses upon epoxy curing within a siloxane network leads to brittle gels. Investigation into utilizing GPTMS as an alkoxy silane without crosslinking the epoxy moiety has been investigated.<sup>62, 64</sup> Kim et al. discovered that GPTMS increases flexibility while also decreasing the water absorption within the stone, making it a useful alkoxy silane component for reducing brittleness and hydrophobicity.

POSS has a rigid cage-like structure (Figure 3.2), acting as a particle spacer that allows for the movement of water vapor. Given the nanometer-sized cage-like structure of POSS, trapped water vapor within the stone's internal porous structure is theoretically capable of exiting through the nanometer-sized pores within the POSS cage,<sup>64</sup> however, POSS may additionally create pores within the consolidant that allow for the diffusion of water. This "breathability" aspect decreases the amount of internal erosion within the stone caused by trapped water. Son et al. incorporated polyhedral oligomeric silsesquioxane (POSS) into a consolidant formulation, showing a reduction in water absorptivity of the consolidated stone.<sup>64</sup>

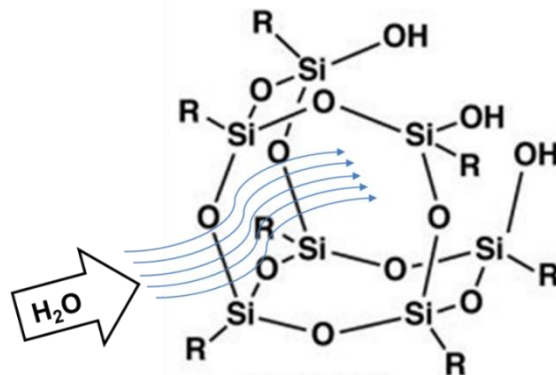


**Figure 3.2. Breathability of stone consolidants via POSS**

Ocyltriethoxy silane (OTES) is commonly used in water repellent formulations for concrete substrates, however few applications have been identified in stone consolidation.<sup>66</sup> The alkyl octyl chain has been notable for enhanced hydrophobicity, and therefore further investigation into the potential use of OTES in alkoxy silane stone consolidants is necessary.<sup>67</sup>

While many variations of these components have been studied in isolation, no optimized formulation incorporating all components through a statistical design approach has been developed. The goal of this study was to improve and optimize alkoxy silane stone consolidants with an emphasis on improving flexibility, breathability, and durability. Structure-property relationships were studied with various alkoxy silane monomers using Design Expert for statistical analysis. Design A investigated three common alkoxy silanes and the effect each one has on gelation and cure rate. Design B incorporates GPTMS, SiO<sub>2</sub> and POSS for increasing flexibility and breathability into the system. Design C incorporates PDMS into the system as a flexible chain extender in addition to studying the effects ethanol has on consolidant properties. Design D, the largest design, incorporates GPTMS, PDMS, POSS and OTES as a final optimization of flexible components within the consolidant formulations. Once the formulation components were determined, optimization was performed to select ideal ratios of monomers to

achieve the desired properties such as contact angle, % solids, hardness, and/or cure rate. Optimized formulations were applied to limestone and marble and exposed to accelerated weathering. Water absorption and color change was monitored throughout weathering to understand consolidant durability. Water vapor permeability was performed to determine the breathability of the optimized consolidant.

## **3.2. Experimental**

### **3.2.1. Raw materials**

Alkoxysilanes were purchased through Sigma Aldrich and include tetraethylorthosilicate (TEOS), methyltrimethoxysilane (MTMOS), methyltriethoxysilane (MTEOS), octyltriethoxysilane (OTES), and 3-glycidyloxypropyl trimethoxy silane (GPTMS). Colloidal silica (Ludox-TM-40), dibutyltin dilaurate (DBTDL), and ethanol were also purchased through Sigma Aldrich. Silanol-terminated polydimethylsiloxane (16-32 cSt) was purchased through Gelest. Trisilanolisooctyl polyhedral oligomeric silsesquioxane (IO-POSS) and trisilanolphenyl polyhedral oligomeric silsesquioxane (P-POSS) were purchased from Hybrid Plastics.

### **3.2.2. Methods**

#### **3.2.2.1. Xerogel/film property methods**

Xerogels were formed by pouring consolidants into small aluminum pans (28mm diameter) and cured for 14 days at ambient conditions. Films were made by spraying consolidant onto substrate using a G22 dual-action gravity feed airbrush (0.3 mm needle). Consolidants were applied in 3 repeated “cycles”, each cycle consisting of three successive applications every 10 minutes with a wait period of 20 minutes in between cycles, for a total of 9 passes over each substrate. Substrates included phosphorylated steel panels (Bondrite), Leneta 2A opacity charts,

and/or Whatman circular filter papers (42.5 mm). Consolidated substrates were cured for 14 days at ambient conditions prior to testing.

The overall appearance of the xerogel or film was analyzed through observation of transparency, film uniformity, and the presence of any defects or cracks. Comparisons were made to commercial consolidants Conservare OH100 and Silres BS OH 100.

Weight loss measurements were taken on the consolidants poured into aluminum pans every hour for 6 hours, followed by measurements every 24 hours, up to 400 hours. Weight loss % over time was charted to understand the cure properties of the consolidants in comparison to commercial consolidants.

Static contact angle measurements using FTÅ 125 Contact Angle/Surface Tension Analyzer were performed on the consolidated Leneta 2A opacity charts. Measurements were taken 1 minute after the droplet had set on the surface. An average of 10 contact angle measurements were taken per sample on a single opacity chart.

Opacity measurements were performed on the Leneta 2A opacity charts using an X-Rite SP64 portable spectrophotometer. A total of 3 readings for the CIE Y value were taken, the first over the black portion of the 2A opacity chart, then over the white portion of the 2A chart, and finally a measurement of the unconsolidated white chart. The X-Rite spectrophotometer automatically calculated % opacity by dividing the reflectance over the black portion by the reflectance over the white portion.

Non-volatile content of consolidant formulations was determined according to ASTM D5095. Briefly, ~ 3 grams of 0.5% pTSA in ethanol was poured into a pre-weighed aluminum pan (58mm diameter) and the weight was recorded. 1 gram of consolidant was added and the solution, weighed, and thoroughly mixed with catalyst solution. Materials in Al pan were left to

stand at room temperature for 60 minutes. The consolidant and catalyst solution were then heated in a forced-draft oven for 60 min at 110°C. The dish was left to cool at room temperature in a desiccator and the weight was recorded. Nonvolatile content was calculated according to equations from ASTM D5095.

Hardness values were measured by pencil hardness method (ASTM D3363) and/or König pendulum hardness (ASTM D4366). Briefly, pencil hardness was carried out by using pencils of various hardness levels to determine the hardest pencil that does not gouge or scratch the surface of the coating. For König pendulum hardness, damping time was measured by an oscillating pendulum on the surface of the coating.

Water vapor permeability was conducted according to ASTM E96/E96M-16. Consolidated Whatman circular filter papers (42.5 mm) were used (Figure 3.3a), as 1.7” diameter xerogels were too brittle to clamp between permeability cups. Filter papers were then clamped into BYK Permeability Cup S (Figure 3.3b) with a 10 cm<sup>2</sup> exposure area. Triplicates were performed for each sample. Briefly, perm cups were filled half way with water and the filter paper was placed over top and clamped into place. Initial weight measurements were recorded. Perm cups were placed into a controlled temperature and humidity chamber (Espec Platinous) at 73.4°F and 50% humidity and weight measurements were taken every 2 hours for 24-48 hours. Weight measurements were plotted against time in minutes and the water vapor transmission rate was calculated from the slope of each line. Water vapor transmission rate was reported in g/m<sup>2</sup> per 24 hours.

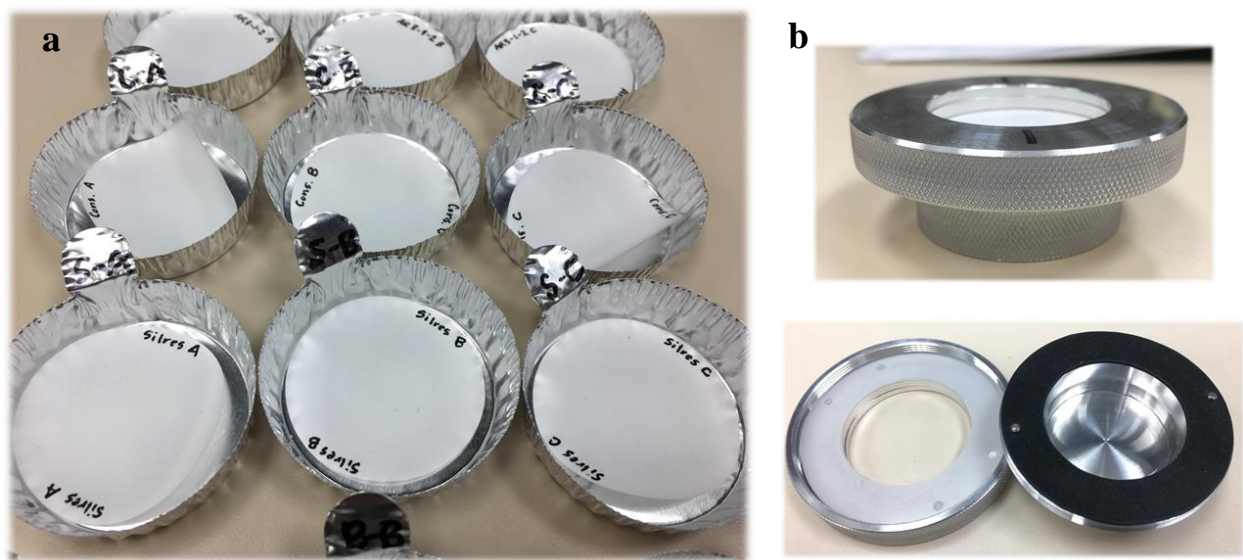


**Figure 3.3. a.) Consolidated filter paper samples and b.) BYK permeability cup S**

Coated and uncoated filter papers were attached to cylindrical aluminum mounts with 3M XYZ-Axis Electrical Conductive tape (Ted Pella, Redding, California, USA), and then sputter coated (Cressington 108auto, Ted Pella, Redding, California USA) with a conductive layer of gold. Images were obtained with a JEOL JSM-6490LV scanning electron microscope (JEOL USA, Inc., Peabody, Massachusetts USA) at an accelerating voltage of 15 kV.

### **3.2.2.2. Stone property methods**

Experimental and commercial consolidants were spray applied onto all faces of circular Royal Danby marble samples (diameter of 2", width of 0.5") and square Indiana limestone samples (2" x 2" x 0.5") using a G22 dual-action gravity feed airbrush (0.3 mm needle). Consolidants were applied in 3 repeated "cycles", each cycle consisting of three successive applications every 10 minutes with a wait period of 20 minutes in between cycles, for a total of 9 passes over each substrate. Replicates were made for each formulation on each substrate, for a total of 10 limestone samples and 10 marble samples. Consolidants were cured at ambient conditions for 14 days prior to analysis.



Consolidated and unconsolidated stones were attached to cylindrical aluminum mounts with 3M XYZ-Axis Electrical Conductive tape (Ted Pella, Redding, California, USA), and then sputter coated (Cressington 108auto, Ted Pella, Redding, California USA) with a conductive layer of gold. Images were obtained with a JEOL JSM-6490LV scanning electron microscope (JEOL USA, Inc., Peabody, Massachusetts USA) at an accelerating voltage of 15 kV.

Consolidant penetration depth into the stone substrate was initially attempted using Thermo Scientific K-Alpha X-ray Photoelectron Spectrometer system. Cross-sectional samples of consolidated and unconsolidated stones were cut using an IsoMet 4000 linear precision saw and dried in the oven at 40°C for 2 hours. XPS measurements were limited to 1 mm from the edge of the cross-section sample. Each measurement included 50 scans with a focus on the binding energy of Si2p. Three XPS measurements were taken across the sample (Figure 3.4).

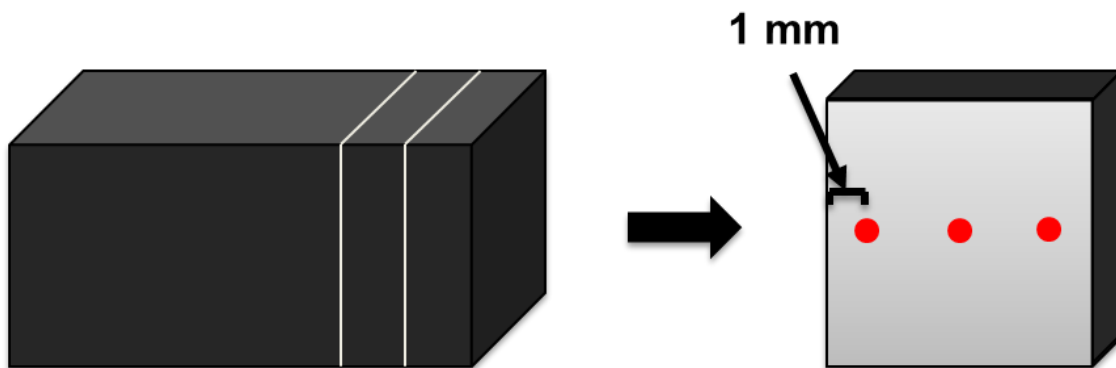


**Figure 3.4. XPS of cross-section of consolidated stone**

Penetration depth of experimental consolidants was also measured using fluorescence microscopy. Lectin was added as a fluorescing agent into both experimental and Conservare consolidant formulations. Indiana limestone samples were consolidated with the lectin-containing consolidant formulations following the previously detailed spray application method. Additionally, a set of limestone samples were consolidated by immersing the stone in a jar of

consolidant for 1 minute, taking out the stone, and exposing to ambient atmospheric conditions for 5 minutes. This process was repeated 2 more times, correlating to 1 cycle. A total of 3 cycles of immersion were performed. After 14 days, cross-sectional samples were cut using the IsoMet 4000 linear precision saw and dried in the oven at 40°C for 2 hours. Samples were analyzed using a Zeiss Axio Observer Z1 LSM 700 and the depth of consolidation was calculated using Imaris 3D/4D Real-Time Interactive Data Visualization and Management Software by Bitplane.

Consolidated and unconsolidated marble and limestone samples were placed in QUV chambers with UVA radiation (340 nm) according to ASTM D6695-16 cycle 1; 8 hours of UV at 60°C followed by 4 hours condensation at 50°C. Samples were checked at 100, 200, 300, 400, 500, 750 and 1000 hours. Weathering checks were performed when the program was at least 5 hours into the UV cycle to ensure the stones were fully dried.

Water absorption was measured after each weathering check on the consolidated and unconsolidated marble and limestone using the Rilem tube method<sup>68</sup>. Briefly, a graduated horizontal Rilem tube from 0 – 5 mL is secured to the surface of the stone using putty. The Rilem tube is filled with deionized water up until the 0 mL marker. Water absorption into the stone was measured after 60 minutes.

Color change was monitored after each weathering check on the consolidated and unconsolidated limestone and marble. Using an X-Rite SP64 portable spectrophotometer, L\*a\*b\* values were recorded. ΔE values were calculated using Equation 3.1.

$$\Delta E = \sqrt{(L_2 - L_1)^2 + (a_2 - a_1)^2 + (b_2 - b_1)^2} \quad (\text{Equation 3.1})$$

### 3.2.3. Mixture designs

The initial selection of alkoxy silane components was determined using a series of mixture and response surface methodology designs (Design A – D) developed using Stat-Ease Design

Expert software. Input variables included the specific alkoxy silanes, a minimum and maximum amount for each component, and the number of formulations and replicates necessary to conduct the mixture design. The response variables commonly included consolidant properties such as gelation within the vial prior to application, cure time, weight loss, opacity, water contact angle, pencil hardness, König pendulum hardness, and/or general appearance. Target metrics for each property are shown in Table 3.1. Through analysis of the response variables, optimization of the formulation was performed, either through elimination of specific alkoxy silane components or determination of the ideal amount of an alkoxy silane to obtain a desired property.

**Table 3.1. Stone consolidant property targets**

<b>Property</b>	<b>Target</b>
Gelation	0 (no gel)
Cure time	< 14 days
Weight Loss	> 50%
Opacity	< 2
Contact Angle	> 80
Pencil Hardness	3B – 3H
Appearance	Smooth, no cracks

**3.2.3.1. Design A: TEOS – MTEOS – MTMOS**

In this mixture design, tetraethoxysilane (TEOS), methyltriethoxysilane (MTEOS), and methyltrimethoxysilane (MTMOS) were formulated using a simplex centroid design model with a total of 14 runs (Figure 3.5). Each black dot represents one formulation, totaling 10 formulations with 4 replicate runs to provide a check for the model.

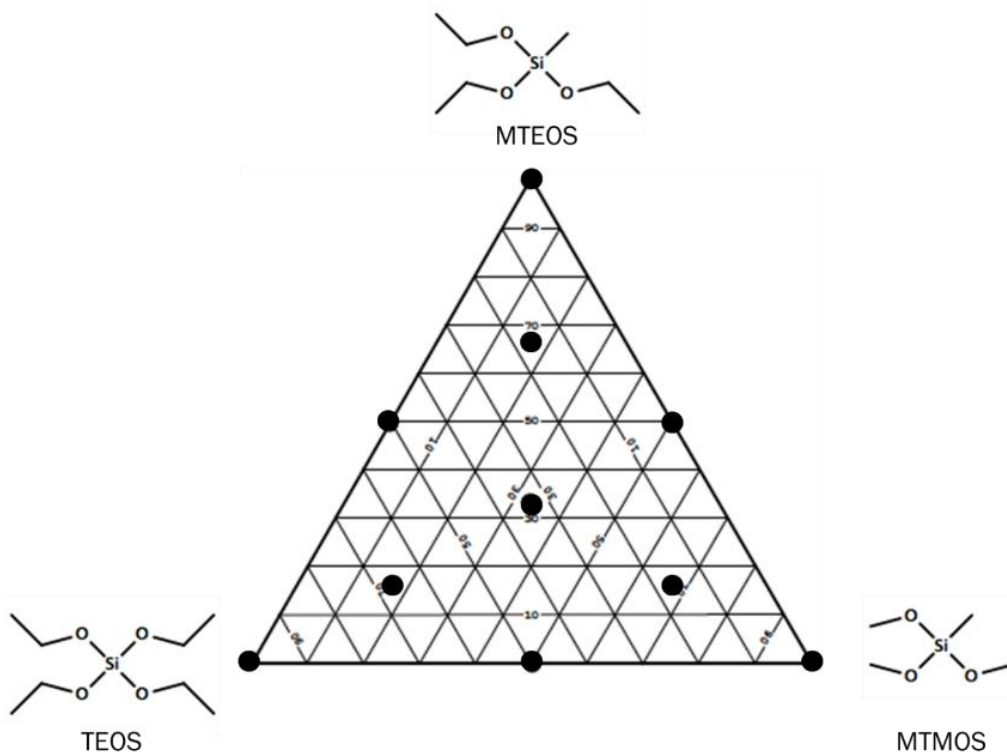


**Figure 3.5. Mixture Design A: TEOS-MTEOS-MTMOS**

Formulations were based off traditional consolidant formulations that incorporate water as an accelerator for hydrolysis and solvent (ethanol or methanol) to solubilize both alkoxy silane and water. Alkoxy silane content totaled 49% of the overall formulation. Each individual alkoxy silane component ranged from 0-100% of the total alkoxy silane content. Water was stoichiometrically added to hydrolyze the alkoxy silanes (~15% by weight) followed by 35% ethanol. DBTDL was added as a catalyst at 0.5%. Table 3.2 shows the general formulation for the TEOS-MTEOS-MTMOS consolidants. Each component was added to a 20mL vial and vortexed for ~1 minute before adding the next component. The order of addition was as follows: TEOS/MTEOS/MTMOS, ethanol, water, and DBTDL. The formulations were left to mix

overnight at room temperature. Gelation, weight loss, and overall appearance were analyzed as input variables to determine the optimal alkoxy silane for future consolidant formulations.

**Table 3.2. Design A general formulation for TEOS-MTEOS-MTMOS in weight %**

Component	%
Alkoxysilanes	49
Ethanol	35
Water	15
DBTDL	1

**3.2.3.2. Design B: GPTMS – POSS – SiO<sub>2</sub>**

A mixture design consisting of 10 formulations and 4 replicates (ideal for estimating pure error) was developed utilizing GPTMS, SiO<sub>2</sub> and IO-POSS to understand the effects of each component in conjunction with TEOS (Figure 3.6).

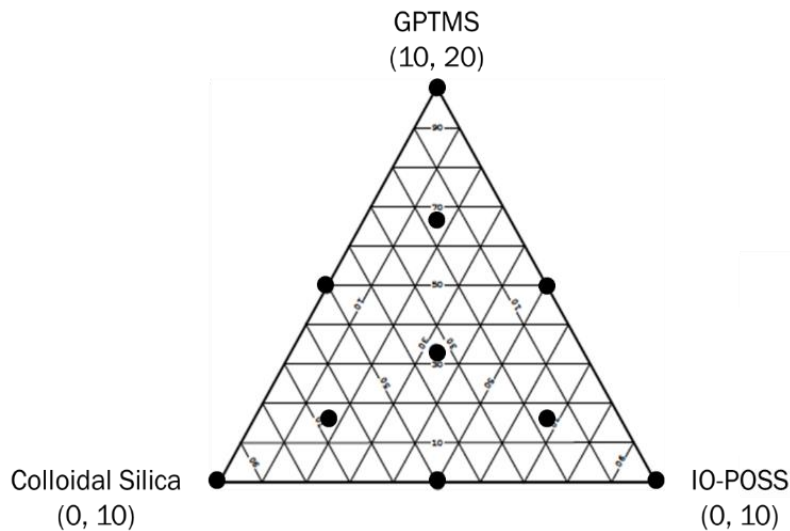


**Figure 3.6. Mixture Design B: GPTMS-POSS-SiO<sub>2</sub>**

Ludox HS-40 is a 40% weight solution of SiO<sub>2</sub> suspension in water with particles sizes of ~12 nanometers. GPTMS was formulated between 10-20% while SiO<sub>2</sub> and IO-POSS content ranged from 0-10%. The remaining 80% of the formulation consisted of 29% TEOS, 35% ethanol, 15% water (including the water in Ludox HS-40) and 1% DBTDL. Each component was added to a 20mL vial and vortexed for ~1 minute before adding the next component. The order of addition was as follows: IO-POSS, TEOS, GPTMS, SiO<sub>2</sub>, ethanol, water, and DBTDL. The formulations were left to mix overnight at room temperature. Table 3.3 shows the mixture design space and the corresponding formulations.

**Table 3.3. Design B formulations for GPTMS-POSS-SiO<sub>2</sub> in weight %**

<b>Component</b>	<b>%</b>
GPTMS	10-20
POSS	0-10
SiO <sub>2</sub>	0-10
TEOS	29
Ethanol	35
Water	15
DBTDL	1

Xerogels of the consolidants were made in aluminum pans. Additionally, films were sprayed on phosphorylated steel panels (Bondrite) and Leneta 2A opacity charts. Static contact angle and opacity values were measured on Leneta paper. Weight loss was measured over time from the consolidants in the Al pans. Consolidant performance was measured against Conservare OH 100 and Silres BS OH 100.

### 3.2.3.3. Design C: GPTMS – PDMS – ethanol

The response surface methodology design of GPTM – PDMS – ethanol was carried out using Design Expert. GPTMS and PDMS were formulated between 5-10%, while ethanol ranged from 10-20%. A total of 15 formulations were developed with no replicates. P-POSS was added at 3%, catalyst at 1% (DBTDL), and TEOS ranged from 50-70% (Table 3.4). Formulations were made using 20 mL vials, adding all components in the following order: P-POSS, TEOS, GPTMS, PDMS, ethanol, and DBTDL. Formulations were mixed at room temperature for 24 hours. Xerogels of the consolidants were made in aluminum pans. Additionally, films were sprayed on phosphorylated steel panels (Bondrite) and Leneta 2A opacity charts.

**Table 3.4. Design C formulations for GPTMS-PDMS-ethanol in weight %**

<b>Component</b>	<b>%</b>
GPTMS	5-10
PDMS	5-10
Ethanol	10-20
TEOS	64-74
P-POSS	3
DBTDL	1

Static contact angle and opacity values were measured on Leneta paper. Weight loss was measured over time from the consolidants in the Al pans. Coated steel panels were analyzed using pencil hardness (ASTM D3363) and König pendulum hardness (ASTM D4366). Consolidant performance was compared against Conservare OH 100 and Silres BS OH 100.

### 3.2.3.4. Design D: GPTMS – PDMS – OTES – TEOS

The 4-component mixture design of GPTM – PDMS – OTES – TEOS was developed, analyzed and optimized using Design Expert. Regression analysis was utilized as a way of

determining the relationship between each component and the response variables. GPTMS, PDMS, and OTES were formulated between 5-15%, while TEOS ranged from 51-81%. All four alkoxysilane components totaled 96% by weight of the formulation, in addition to 3% P-POSS and 1% DBTDL. A total of 24 formulations were made, including 5 replicates and 5 lack-of-fit points. All components were added to 20 mL vials and mixed overnight at room temperature. Components were added in the following order: P-POSS, TEOS, GPTMS, OTES, PDMS, and DBTDL. Formulations were mixed at room temperature for 24 hours. Xerogels of the consolidants were made in aluminum pans. Additionally, films were sprayed on phosphorylated steel panels (Bondrite) and Leneta 2A opacity charts. Table 3.5 shows the corresponding formulations for Design D.

**Table 3.5. Design D formulations for GPTMS-PDSM-OTES-TEOS in weight %**

<b>Component</b>	<b>%</b>
GPTMS	5-15
PDMS	5-15
OTES	5-15
TEOS	51-81
P-POSS	3
DBTDL	1

Certain formulations were observed to gel within the vial after 30 days. As a result, gelation was included as a response variable for the mixture design as a measure of formulation stability. Static contact angle and opacity values were measured on Leneta paper. Weight loss was measured over time from the consolidants in the Al pans. Coated steel panels were analyzed



using pencil hardness and König pendulum hardness. Consolidant performance was compared against Conservare OH 100 and Silres BS OH 100.

### 3.2.4. Optimized formulations

#### 3.2.4.1. Optimization using Design Expert

Using Design Expert’s numerical optimization capabilities, the most important response factors were weighted and ranked based on desired properties. Table 3.6 indicates the target values for gelation, % solids, and opacity.

**Table 3.6. Optimization: Target properties and importance**

<b>Property</b>	<b>Target</b>	<b>Weight</b>
Gelation	0	+++++
% Solids	Maximize	+++
Opacity	Minimize	+++

Four optimal formulations consisting of TEOS, GPTMS, PDMS, OTES, P-POSS and DBTDL were produced. The four experimental consolidants were formulated by adding all components to 20 mL vials and mixed overnight at room temperature. Components were added in the following order: P-POSS, TEOS, GPTMS, OTES, PDMS, and DBTDL. Xerogels were made by pouring consolidants into Al pans. Leneta and filter paper were coated by previously described methods. Indiana limestone and Royal Danby marble stones were consolidated by spray application as previously described. All consolidated substrates cured for 14 days prior to testing.

#### **3.2.4.2. Optimized consolidant characterization and performance**

Weight loss, % solids, opacity, static contact angle and general appearance were all measured on the optimized experimental consolidants in the form of xerogels or coated Leneta paper. Comparisons were made against commercial consolidants Conservare and/or Silres. Penetration depth of consolidants on Indiana limestone was measured using XPS and fluorescence microscopy. Water vapor permeability of only the top 2 experimental consolidants was performed on filter paper and measured against commercial consolidants. Consolidated filter papers were qualitatively analyzed by SEM prior to water vapor permeability tests. Cured consolidants on limestone and marble were exposed to QUV weathering and measured for color change ( $\Delta E$ ) and water absorption. SEM images were qualitatively analyzed of unconsolidated and consolidated limestone and marble prior to weathering.

#### **3.2.5. POSS study**

Previous studies utilized either P-POSS or IO-POSS, however there is no indication as to how these materials vary in terms of consolidant performance. P-POSS is a solid white powder, whereas IO-POSS is a high viscosity, transparent liquid. Figure 3.7 shows the structures of each of these POSS materials. It is suggested that P-POSS may be more susceptible to UV degradation due to the aromatic ring. IO-POSS, however, does not contain any chromophores, and therefore may be less susceptible to color change from weathering. As a result, each compound was investigated in various ratios to understand the difference in performance and weatherability applied to stone consolidants.

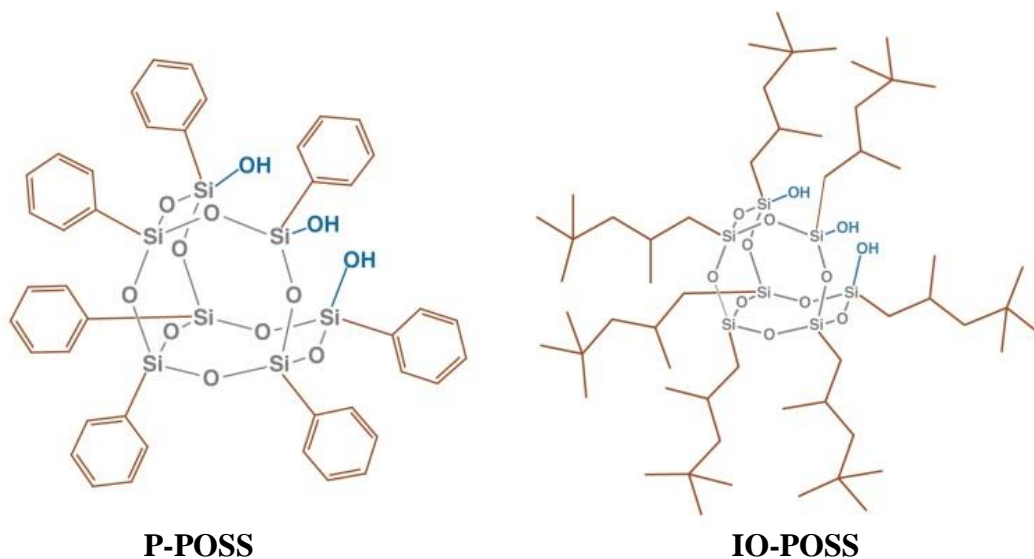


**Figure 3.7. a.) Phenyl-POSS and b.) Isooctyl-POSS**

P-POSS and IO-POSS were formulated at 1%, 3% and 5% loading (Table 3.7). All materials were added to 20 mL vials in the following order: 1. POSS, 2. GPTMS, 3. PDMS, 4. TEOS, and 5. DBTDL. A stir bar was added to the vial and the formulations were mixed overnight at room temperature. After 24 hours of mixing, consolidants were poured into Al pans and weight loss measurements were taken over time. Additionally, the experimental formulations were sprayed onto all sides of square Indiana limestone samples (2" x 2" x 0.5") and circular Royal Danby Marble stones (diameter of 2", 0.5" width) in addition to Leneta paper for contact angle measurements. Replicates were made for each formulation on each stone type, with a total of 24 stone samples. Stone samples were cured for 14 days at room temperature prior to testing. Consolidated stone samples were exposed to 1000 hours of QUV accelerated weathering. Color changes and water absorptivity were recorded every 100 hours of weathering up to 500 hours, followed by 250-hour incremental checks from 500-1000 hours. Performance of the experimental POSS consolidants were compared to Conservare OH 100.

**Table 3.7. POSS consolidant formulations in weight %**

	P- 1	P- 3	P- 5	IO- 1	IO- 3	IO- 5
TEOS	75	73	71	75	73	71
GPTMS	15	15	15	15	15	15
PDMS	8	8	8	8	8	8
DBTDL	1	1	1	1	1	1
P-POSS	1	3	5	-	-	-
IO- POSS	-	-	-	1	3	5

### 3.3. Results and discussion

Due to the complex and multivariate nature of the consolidant compositions, a statistical experimental design approach allows for efficient exploration of the variable space, understanding structure-property relationships, and expedited development of an optimized consolidant formulation. A series of mixture designs (A-D) were carried out to study the effect of each alkoxy silane/inorganic component on the properties of the xerogel, thin film and consolidated stone materials. The primary alkoxy silane was chosen based on the results of Design A, whereas Designs B and C narrowed the selection to alkoxy silane additives while eliminating colloidal silica and solvent. Finally, Design D resulted in four optimized formulations using multiple alkoxy silane additives at varying concentrations to maximize consolidant performance. The four optimized formulations were compared against commercial consolidants and found to exhibit superior consolidating properties.

### 3.3.1. Mixture designs

#### 3.3.1.1. Design A: TEOS – MTEOS – MTMOS

In Design A, the primary alkoxysilane for the consolidant formulation was determined from three possible materials: methyltriethoxysilane, methyltrimethoxysilane, and tetraethylorthosilicate. A mixture design of MTEOS, MTMOS and TEOS was developed and formulations were analyzed based on their gelation time and cure rate (weight loss over time) to identify the optimal primary alkoxysilane.

After mixing each formulation overnight at room temperature, 6/10 formulations had prematurely gelled in the vial prior to consolidant application (Figure 3.8). The remaining 4 formulations are labeled A-D. The formulations high in MTEOS and MTMOS indicated a higher rate of hydrolysis and condensation as compared to TEOS, resulting in a faster gel time inside the vial. MTMOS and MTEOS have larger vapor pressures than TEOS, leading to high volatility of the monomer before hydrolysis and condensation occurs.

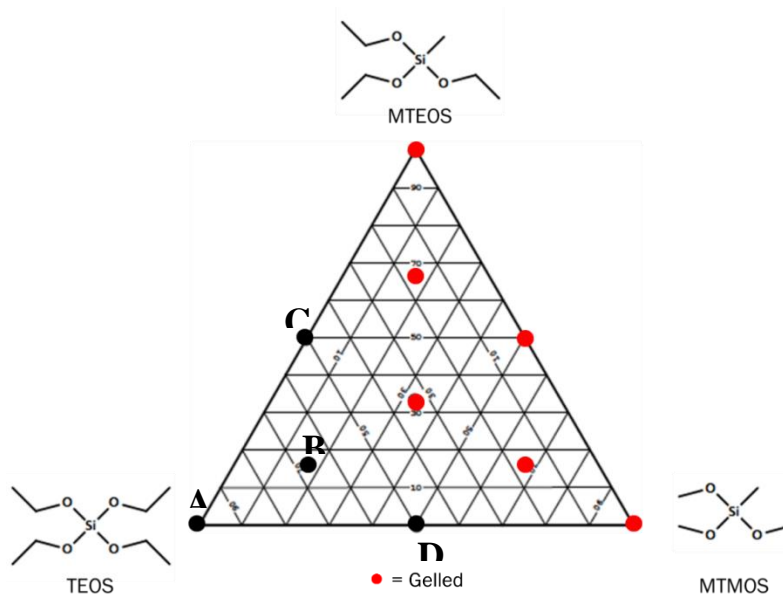
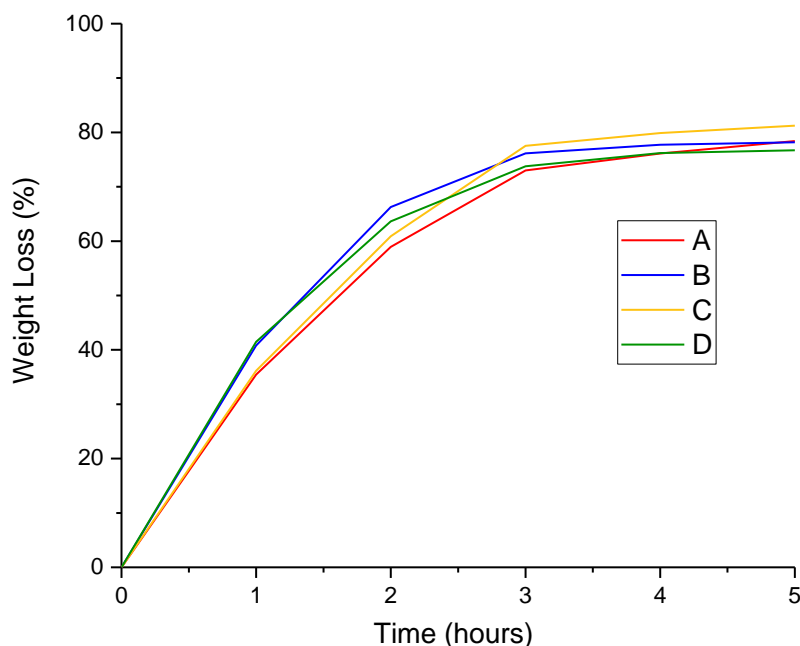


Figure 3.8. Gelation of TEOS-MTEOS-MTMOS formulations

Weight loss measurements of the remaining 4 formulations indicated no significant differentiation between the alkoxy silane monomer and cure rate (Figure 3.9). TEOS does appear to have a slower rate of cure. The rate of hydrolysis for each monomer is dependent on a variety of factors including catalyst type and amount, solvent, water to alkoxide ratio, etc. Bulkier alkyl chains add steric hindrance during the hydrolysis step, generally increasing the rate of gel formation. As a result, TEOS is expected to have the slowest cure rate relative to MTEOS and MTMOS.



**Figure 3.9. Weight loss of Design A TEOS-MTEOS-MTMOS formulations**

As the primary alkoxy silane in commercial consolidants, TEOS offers a slower rate of hydrolysis and condensation with lower volatility of monomer, allowing sufficient working time and shelf life. Based on the rapid gelation, MTEOS and MTMOS were eliminated and TEOS was chosen as the primary alkoxy silane for future consolidant formulations.

### 3.3.1.2. Design B: GPTMS – POSS – SiO<sub>2</sub>

After TEOS was chosen as the primary alkoxy silane, additional components were explored to enhance flexibility of the consolidant. GPTMS, POSS and colloidal silica have previously been found to enhance flexibility within TEOS-based consolidant formulations,<sup>48, 64</sup> however no comprehensive mixture design containing each of these components has been done. In this design, GPTMS, POSS and SiO<sub>2</sub> formulations were examined as xerogels and thin films for understanding the effect each component has on gelation, opacity, weight loss and contact angle.

The formulations are labeled A-I in the GPTMS – POSS – SiO<sub>2</sub> mixture design (Figure 3.10a). Only one formulation gelled prior to application, which was excluded from further characterization. This formulation had the highest percentage of colloidal silica at 10%. Initial appearance of the consolidant films in Al pans indicate that SiO<sub>2</sub> contributes to a more brittle and opaque appearance, both undesirable properties for a stone consolidant. One important factor in conservation of materials is to minimize the change of appearance due to consolidants. As a result, development of a transparent system is crucial. Opacity measurements were performed to understand the appearance of the consolidant (Figure 3.10 b).

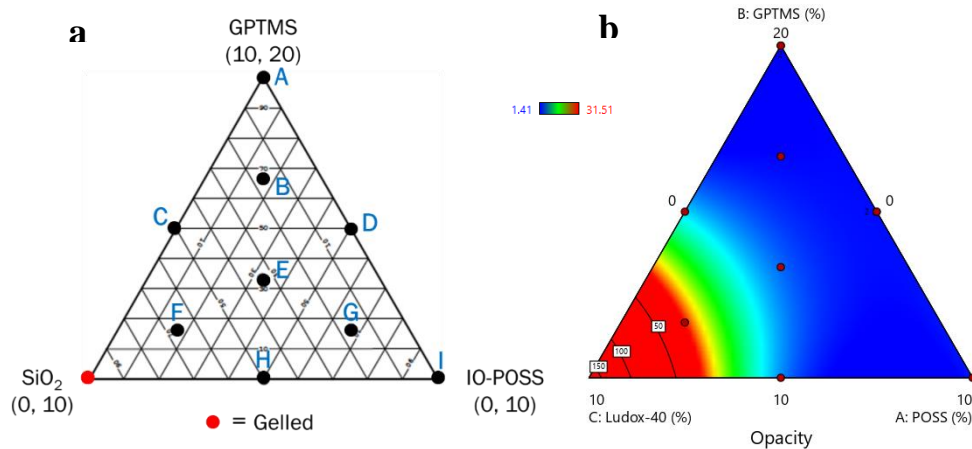


**Figure 3.10. a.) Gelation and b.) opacity of GPTMS-POSS-SiO<sub>2</sub> formulations**

Silicon dioxide directly correlates with a sharp increase in opacity values as shown in Figure 3.10 b, whereas GPTMS and POSS maintain transparency throughout the consolidant. As a result, SiO<sub>2</sub> is undesirable as an additive for stone consolidants simply based on the opaque and brittle appearance.

The weight loss profiles of samples A-I were monitored, specifically within the first 5 hours of cure. Figure 3.11 shows the weight loss profile over time in addition to the contour plot of the final weight loss value after 30 days. The experimental consolidants show a rapid increase in weight loss within the first 1-3 hours, reaching a plateau around 60-70% weight loss after 4-5 hours. In comparison, the commercial consolidants (Silres and Conservare) show a steady cure rate, only reaching 10% after the first 5 hours. The contour plot of the final weight loss for each formulation in the mixture design indicates a lower weight loss value with increasing GPTMS and colloidal silica.

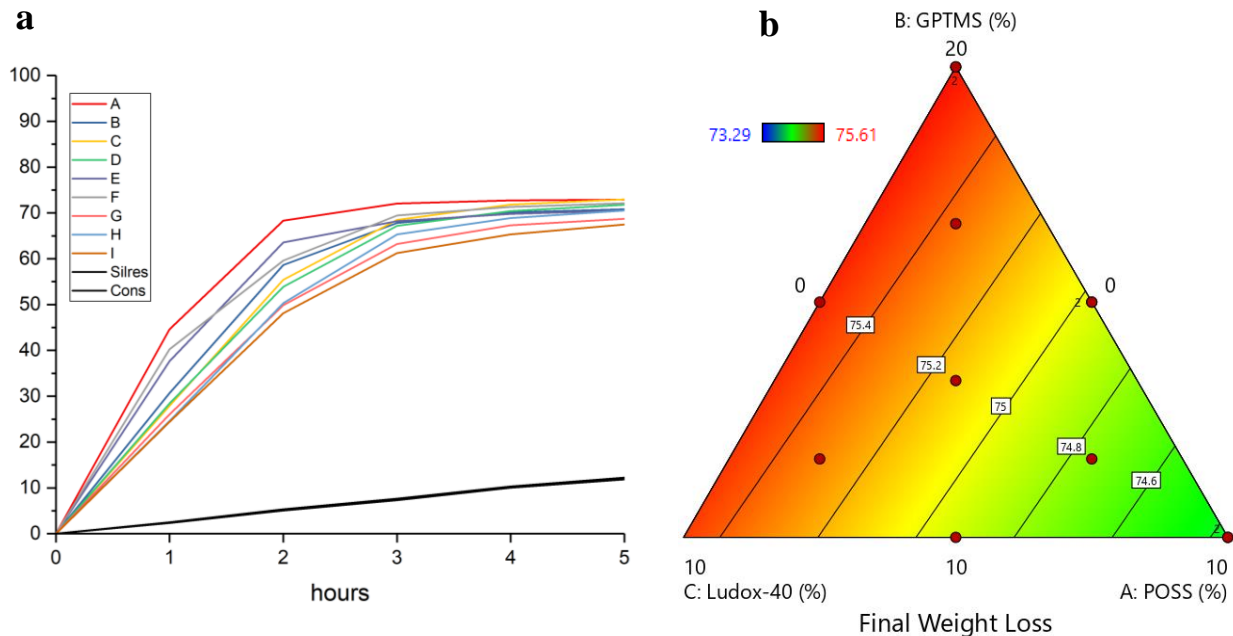


**Figure 3.11. % Weight loss profile of GPTMS-POSS-SiO<sub>2</sub> formulations a.) within first 5 hours and b.) contour plot of final weight loss values after 30 days**



Contact angle measurements were performed on all experimental formulations except for C, F and H. These 3 formulations contained the highest amount of SiO<sub>2</sub>, and appeared flaky and opaque on the Leneta paper, making contact angle measurements difficult to obtain. The contact angle measurements on the remaining formulations indicated that experimental consolidants, apart from A, all had higher contact angle values compared to the commercial consolidants (Figure 3.12). Formulation A containing the highest amount of GPTMS (20%) shows more hydrophilic behavior, a direct correlation with the glycidyoxypropyl group. Therefore, additional hydrophobic alkoxy silanes are required in combination with GPTMS to obtain a contact angle greater than 70°. It is evident that SiO<sub>2</sub> contributes greatly to the consolidant hydrophobicity, however the opaque and flaky appearance hinders the usage of SiO<sub>2</sub> as an effective additive for stone consolidants. Additionally, POSS increases the hydrophobic nature of the consolidants, a beneficial contribution of the siloxane-cage structure.

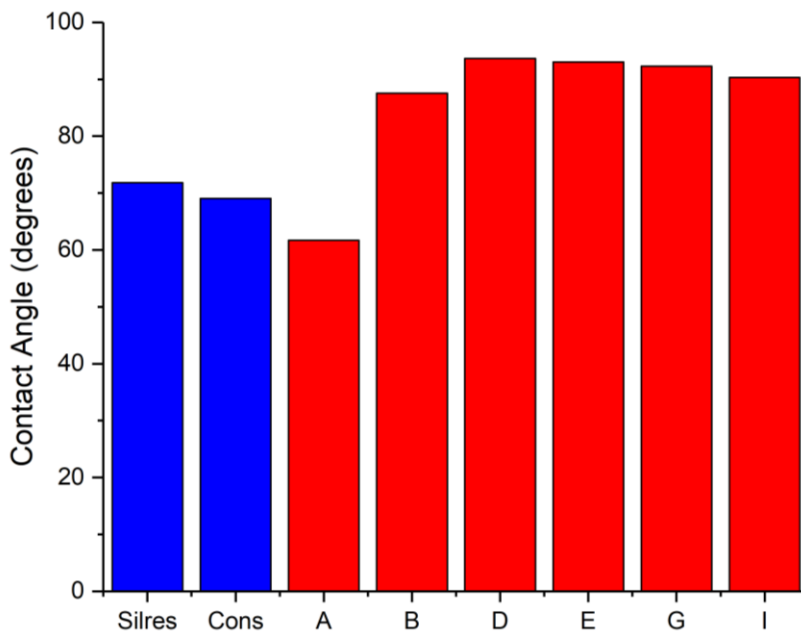


**Figure 3.12. Contact angle of GPTMS-POSS-SiO<sub>2</sub>**

Based on the gelation, opacity and overall appearance, colloidal silica will be removed from all future formulations. GPTMS provides an overall lower weight loss, however, the hydrophilic nature of the glycidyoxypropyl group requires additional hydrophobic alkoxy silanes to repel water from entering the stone. POSS showed beneficial hydrophobic properties in addition to sufficient transparency and overall uniform appearance of the xerogels.

### **3.3.1.3. Design C: GPTMS – PDMS – ethanol**

After the elimination of colloidal silica as a potential particle spacer for stone consolidants, a known flexible component, PDMS, was explored in which direct condensation into the gel network occurs. Additionally, the effect of solvent on consolidant properties was explored, as traditional alkoxy silane consolidants utilize ethanol or methanol to accelerate hydrolysis by solubilizing water and alkoxy silanes. However, as hydrolysis proceeds, ethanol and/or methanol is produced, and it was therefore of interest to investigate the necessity of additional solvent within alkoxy silane consolidant formulations. To minimize the introduction of all new variable, GPTMS remained a component of investigation for Design C. Film and xerogel appearance in addition to weight loss, % solids, contact angle and hardness values were all measured.

Unlike the previous Designs A and B, response surface methodology (RSM) was utilized instead of a mixture design. RSM is useful in understanding the direct relationship between multiple variables (input factors) and optimizing each variable based on the response variables (output factors). In this RSM design, 3-4 consolidant components were formulated and analyzed by consolidant performance tests to understand the relationship between each variable. Optimization using Design Expert allows for determination of the optimal amount of each component to achieve a certain performance property.

All formulations produced smooth transparent films as seen in Figure 3.13. Conservare contained minor defects throughout the film that later cracked and flaked off the panel, proving the brittleness of the commercial consolidants. While some shrinkage was observed on the films cured in aluminum pans, all experimental formulations remained intact while the Conservare films became brittle after 14 days.

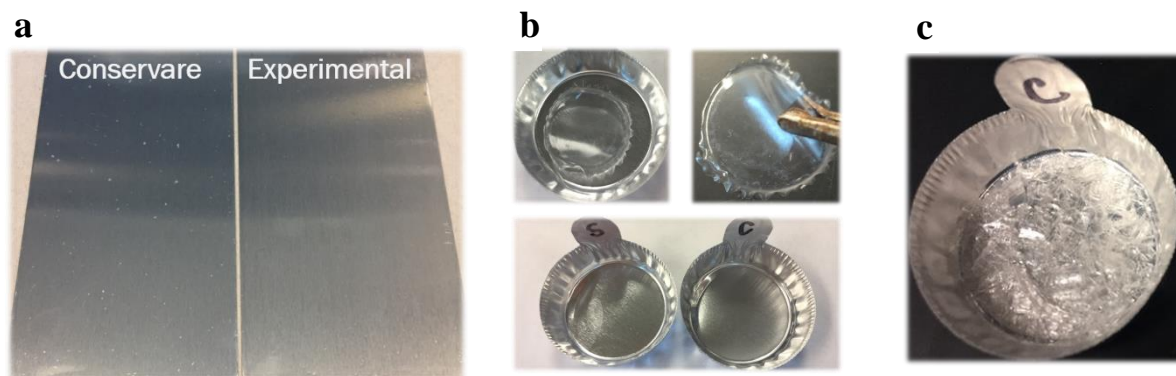


**Figure 3.13. a) Conservare vs Experimental films on steel panels b) transparent films in Al pans after 3 days c) Conservare after 14 days**

Performance properties, or response variables, of the stone consolidants were measured using weight loss, % solids, opacity, contact angle, pencil hardness and König hardness. Each response was analyzed using Design Expert and specific variable was correlated with GPTMS, PDMS, and/or ethanol. Table 3.8 outlines the model significance based on p-values that designate significance ( $p < 0.05$ ) or insignificance ( $P > 0.05$ ) to each model regarding each response variable. The components that contribute to model significance are also identified based on p-values. Contact angle and König hardness were the only response variables that are not dependent on GPTMS, PDMS or ethanol. As a result, no correlation for these properties can be made. However, weight loss, % solids, opacity and pencil hardness were all significant models.

**Table 3.8. Design C GPTMS-PDMS-ethanol model significance and component p-values**

	<b>Model p-values</b>	<b>GPTMS</b>	<b>PDMS</b>	<b>Ethanol</b>
Weight Loss	<b>0.0004</b>	<b>0.0016</b>	<b>0.0004</b>	0.8682
% Solids	<b>&lt;0.0001</b>	<b>0.0003</b>	<b>&lt; 0.0001</b>	0.7796
Opacity	<b>0.0012</b>	0.7723	<b>0.0001</b>	0.3725
Contact Angle	0.1591	0.2212	0.3009	0.3612
Pencil Hardness	<b>0.0036</b>	0.1126	<b>0.0007</b>	0.5552
König Hardness	0.0956	0.1602	0.9002	0.0398

One of the most notable results is the minimal impact that ethanol plays on film formation. Weight loss and % solids are surprisingly independent of ethanol content as observed by a p value greater than 0.05, but rather dependent on the GPTMS and PDMS content. Figure 3.14 shows the contour plots for both weight loss and % solids. As GPTMS and PDMS increase, the weight loss % decreases. Similarly, with % solids, as GPTMS and PDMS increase, the % solids also increase. This indicates that GPTMS and PDMS each formulated between 10-15% offers a competitive advantage by lowering the amount of ethanol hydrolyzing from TEOS.

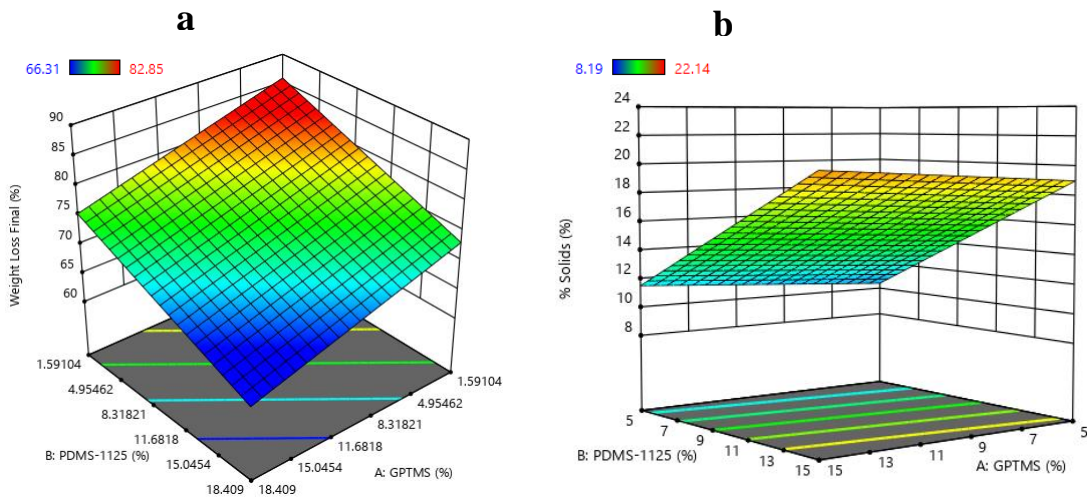


**Figure 3.14. Contour plots of a.) weight loss and b.) % solids for GPTMS-PDMS-ethanol**

Opacity and pencil hardness were both found to be dependent only on PDMS. The contour plot for each of these response variables is shown in Figure 3.15. The alphanumeric pencil hardness scale was converted to a simple numeric scale of 1-19, with 1 equaling 8B and 19 being 9H. Increasing PDMS significantly lowers both opacity and pencil hardness, however all opacity values remained below 2.17, offering sufficient transparency at 5% PDMS.

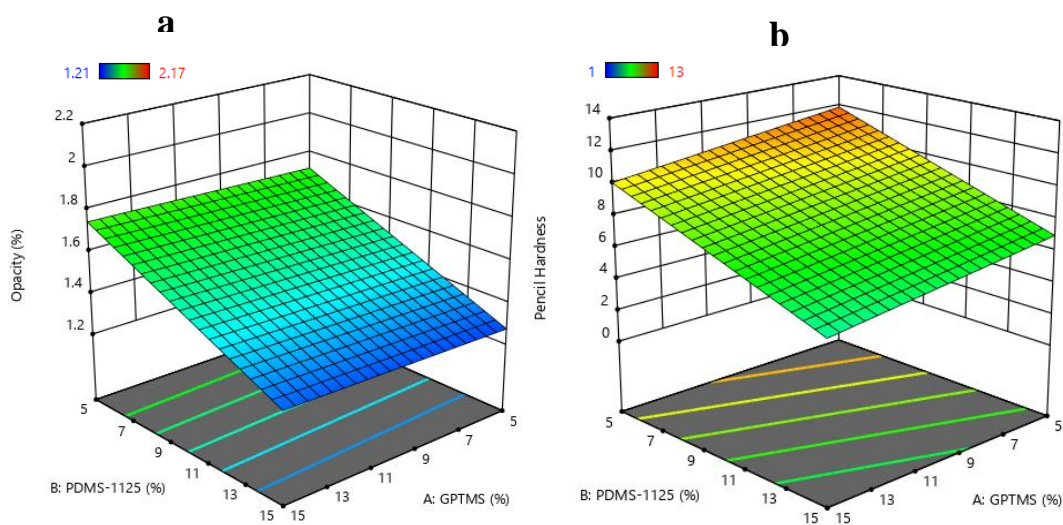


**Figure 3.15. Contour plots a.) opacity and b.) pencil hardness for GPTMS-PDMS-Ethanol**

While traditional alkoxysilane consolidants commonly contain solvent, it was determined from Design C that ethanol provides minimal benefits to alkoxysilane consolidants and may therefore be removed from future formulations. As alkoxysilanes hydrolyze in the presence of atmospheric moisture, ethanol and methanol are released, providing sufficient solvent for miscibility between alkoxysilanes and water produced from the condensation reaction. As the reaction proceeds, more solvent is produced, and therefore no additional solvent or water are necessary for catalyzing the hydrolysis and condensation reactions. Additionally, higher percentages of PDMS and GPTMS aid in minimizing weight loss and increasing % solids.

Increasing PDMS content decreased opacity values, however, all opacity values remained sufficiently transparent for stone consolidation.

#### **3.3.1.4. Design D: GPTMS – PDMS – OTES – TEOS**

Designs A-C focused on exploring potential additives for improving consolidant properties and eliminating unnecessary components from the formulations. From the previous Design C, solvent was eliminated from the formulation as no beneficial properties were imparted to the consolidant from the incorporation of ethanol. However, PDMS and GPTMS were found to be valuable components in increasing flexibility and % solids, and were therefore further explored in Design D. From Design B, xerogels and films containing POSS were not indicative of water vapor permeability, and therefore further investigation of POSS in alkoxy silane consolidants was necessary to understand consolidant performance on stone substrates. Given the low formulating range of POSS (1-5%), 3% POSS was chosen for the optimization Design D, and therefore POSS was eliminated as a mixture design variable within the system. One final alkoxy silane additive of interest, OTES, was explored in combination with GPTMS, PDMS and TEOS to determine the ideal formulation for stone consolidation. Xerogel and film properties were analyzed, and four optimal formulations were chosen for further consolidation testing on limestone and marble substrates.

All 24 formulations were tested for gelation after 30 days, opacity, % solids, pencil hardness, and contact angle. Table 3.9 shows the model significance based on p-values and the gradient values based on coded proportional relationships between each component. The more negative or positive the gradient value, the more that component contributes to a decrease or increase respectively in the response variable. For example, TEOS has a -34.91-gradient value

for % solids while PDMS has a gradient value of 91.31. As the TEOS content in a formulation increases, the % solids decrease, whereas an increase in PDMS content has a larger impact on increasing the % solids than TEOS has on decreasing the % solids.

**Table 3.9. GPTMS-PDMS-OTES-TEOS model significance and component gradient values**

	<b>Model p-values</b>	<b>GPTMS</b>	<b>PDMS</b>	<b>OTES</b>	<b>TEOS</b>
Gelation	< 0.0001	-2.95	10.95	-3.63	-1.90
% Solids	< 0.0001	-2.97	91.31	-7.97	-34.91
Opacity	0.4215	0.3074	-0.6075	0.2681	0.0139
Contact Angle	< 0.0001	-50.42	6.09	-10.72	23.91
Pencil Hardness	0.0142	-4.80	-61.84	10.77	24.27

Due to the complex nature of the 4-component mixture design, comparisons using gradient values are more identifiable than contour plots. Gelation of formulations within the vial after 30 days was directly related to PDMS loading greater than 10%. However, a higher PDMS loading resulted in a desirably higher % solids. Because of these two variables PDMS loading should be considered between 7-9% for future formulations in order to prevent gelation while increasing % solids. All opacity measurements were below 2.20, resulting in all formulation having sufficient transparency. Due to minimal opacity value differentials, no model significance was found. Contact angle was found to significantly decrease with higher levels of GPTMS. Formulation of GPTMS is optimal at the minimal loading of 5% to maximize contact angle values. One of the more unexpected results shows contact angle increasing with TEOS content. Commercial consolidant formulations consisting of monomeric and oligomeric TEOS show relatively low contact angles around 75°, and it would therefore be expected to lower the contact angle of experimental formulations. OTES also shows a minimal impact on lowering contact angle, which

should be considered when optimizing the formulation. Pencil hardness values were mostly dependent on PDMS, which softens the consolidant at higher levels. OTES and TEOS content increases pencil hardness values.

### 3.3.2. Formulation optimization

Using Design Expert’s optimization feature, criteria for each response variable was set based on the GPTMS-PDMS-OTES-TEOS results for gelation, % solids, contact angle and pencil hardness. Response variable criteria was weighted based on importance. The order of importance was weighted as follows: gelation > solids > contact angle > hardness > opacity. Four optimal formulations were produced from Design Expert’s numerical optimization capabilities. Table 3.10 displays the four optimized formulations, labeled 1-4.

**Table 3.10. Optimized formulations 1-4 based on weight %**

	<b>1</b>	<b>2</b>	<b>3</b>	<b>4</b>
GPTMS	15.00	5.00	15.00	15.00
PDMS	8.91	7.54	8.11	7.75
OTES	5.00	13.03	11.68	15.00
TEOS	67.09	70.43	61.21	58.25
P-POSS	3.00	3.00	3.00	3.00
DBTDL	1.00	1.00	1.00	1.00

### 3.3.3. Optimized consolidant characterization and performance

#### 3.3.3.1. Consolidant curing and appearance

All four experimental formulations were transparent with no noticeable defects. Figure 3.16 shows the commercial and experimental consolidant formulations as films on Leneta paper and xerogels in Al pans. Commercial consolidant Conservare and Silres both appeared flaky and



brittle simply due to shrinkage stress upon cure. As a result, it is suspected that commercial consolidants break within the pores of the stone, rendering them ineffective at consolidation. Experimental formulations show promising potential in flexibility due to minimized shrinkage stress, allowing for effective consolidation within the pores of stone materials.

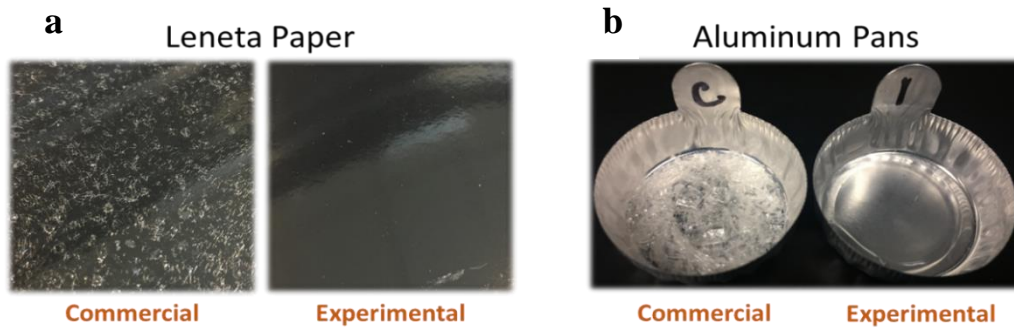


**Figure 3.16. Commercial and experimental consolidants a) film on Leneta paper and b) xerogel in Al pan**

Weight loss over time was measured and compared against Conservare. Figure 3.17 shows the initial 6-hour weight loss behavior in addition to the overall weight loss profile over 400 hours. From Figure 3.17 a, all four experimental consolidants show a fast cure rate than Conservare, however Figure 3.17 b indicates that Conservare has an overall larger weight loss % than the majority of experimental consolidants after plateauing around ~200 hours. This indicates that while experimental consolidants have an initially higher cure rate, the overall weight loss of Conservare is ~3-8% higher than  $\frac{3}{4}$  of the experimental formulations.

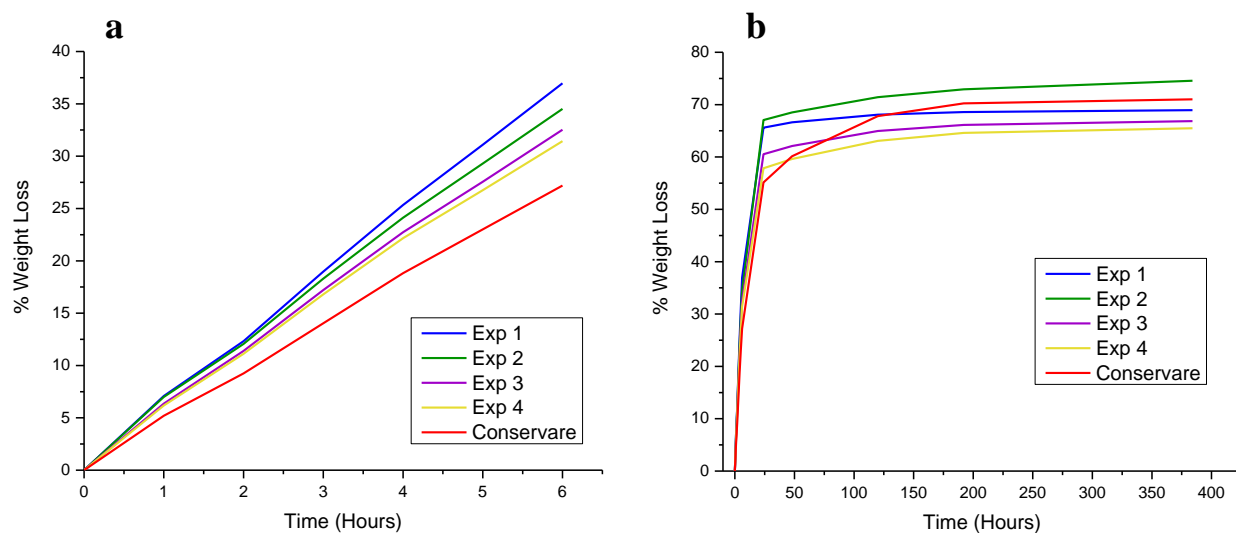


**Figure 3.17. Weight loss of experimental consolidants after a.) 6 hours b.) 400 hours**

Final weight loss values at 400 hours for both experimental and commercial consolidants is reinforced by the overall % solids for each formulation (Figure 3.18). Silres and Conservare both show lower % solid values at 50-52% as compared to the experimental formulations at 52-60%. This improvement in solid content is a direct result of decreasing the functionality within the system by incorporating di and tri-functional alkoxy silanes, lowering the hydrolyzed ethanol and methanol released from the system.

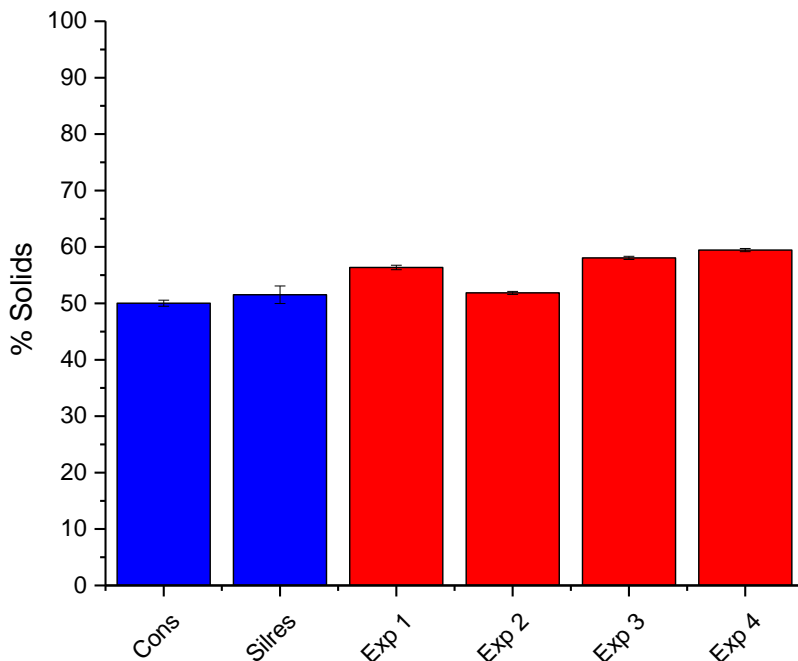


**Figure 3.18. % Solids of experimental and commercial consolidants**

Hydrophobic properties of the experimental consolidants were measured on Leneta paper and compared to commercial consolidants. Figure 3.19 a shows that all four experimental formulations displayed significantly higher contact angles ranging from 89-94°, as compared to Conservare and Silres at 75° and 79° respectively. After 8 months of sitting at ambient conditions, contact angle measurements were re-tested. Conservare and Silres dipped to 69° and 72°, respectively, whereas all experimental formulations slightly increased hydrophobicity by 0.1-2°. Figure 3.19 b shows the contact angle images at 2 weeks and 8 months, indicating a drastic decrease for commercial consolidants.

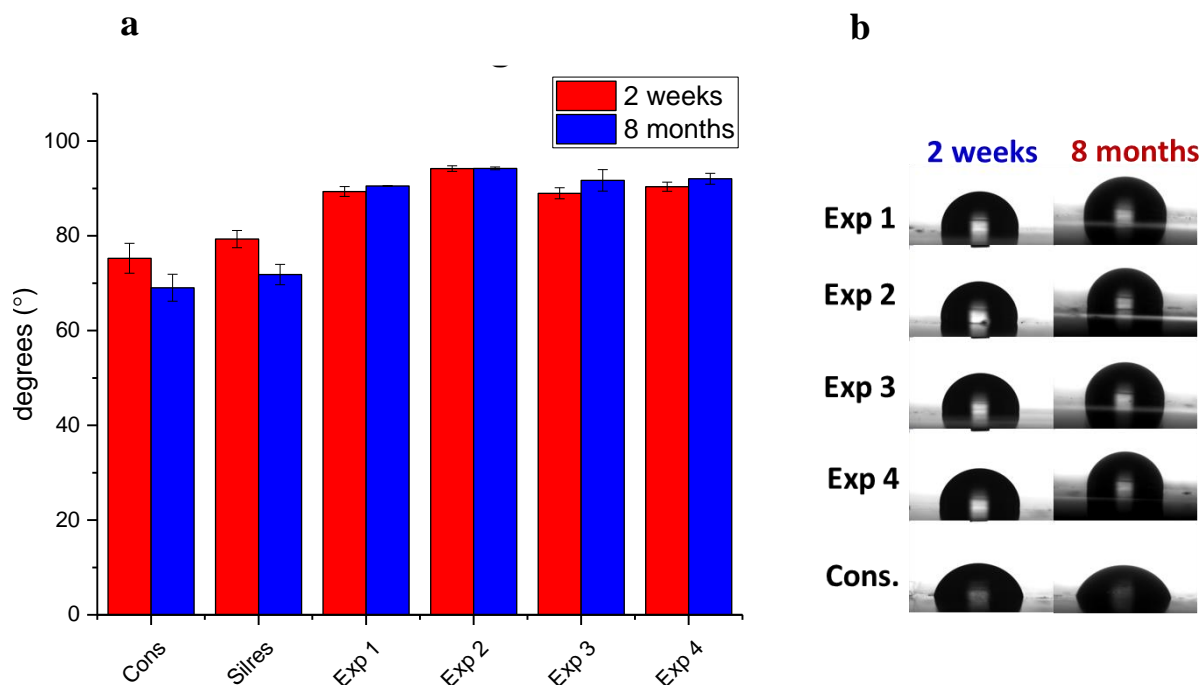


**Figure 3.19. Contact angle measurements a.) chart comparison b.) images**

Initial xerogel and film property tests indicate the potential of the experimental consolidants based on decreased brittleness, increased cure rate with lower final weight loss, increased % solids, and greater hydrophobicity and increased contact angle measurements over time. Future characterization includes performance on stone substrates.

### 3.3.3.2. Consolidant penetration depth

Consolidated limestone and marble substrates were first analyzed by understanding how far the consolidant penetrates the stone's pores. XPS was initially utilized to measure the atomic content, specifically % silicon, at various points on a cross-section of consolidated limestone. One of the major limitations with this method included a minimum edge distance of 1 mm. Unfortunately, no detectable difference in atomic content was observed between the 1 mm edge and the unconsolidated cross-sectional sample, and it was therefore concluded that consolidant depths did not reach 1 mm.

Fluorescence microscopy was employed to quantify the depth of consolidant penetration. Figure 3.20 shows fluorescence imaging of the consolidant on a cross-section of consolidated stone by both spray and immersion application.

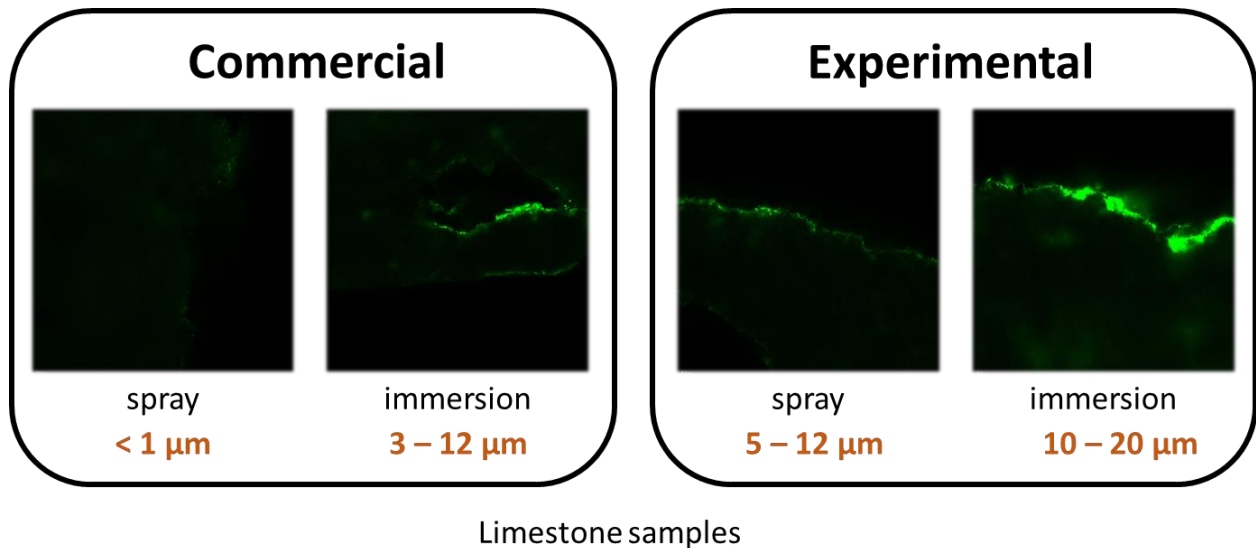


**Figure 3.20. Fluorescence microscopy of consolidation depth for commercial and experimental formulations**

The depth of consolidant penetration for spray application was lower than for immersion application. Spray-applied commercial consolidants showed less than 1 µm depth of consolidation, whereas experimental formulations showed 5-12 µm. For immersion, the commercial consolidants showed 3-12 µm of depth, whereas experimental shows 10-20 µm. The greater depth of consolidation for the experimental formulations indicates a greater chance of more effective stone protection from environmental degradation.

### 3.3.3.3. Consolidant performance on stone

Commercial and experimental consolidants applied to limestone and marble were analyzed by SEM to understand how the consolidant appears on the surface of the stone. Figure 3.21 shows unconsolidated and consolidated limestone and marble samples at 5,000x magnification.

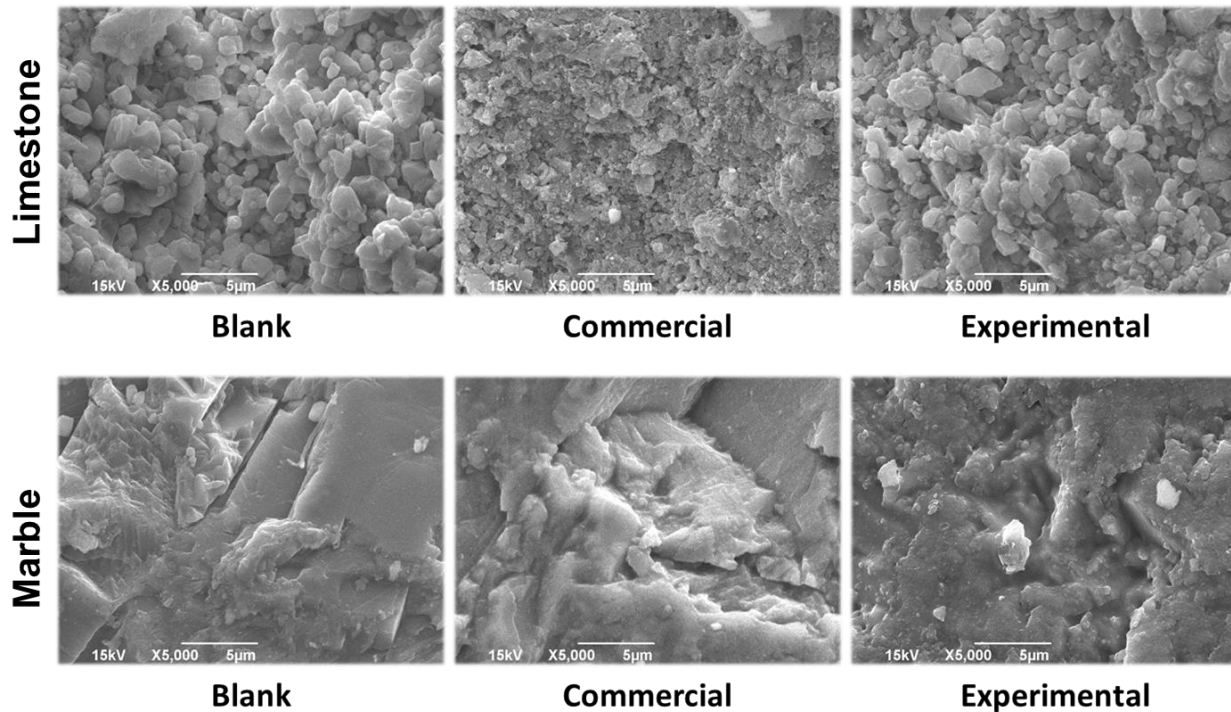


**Figure 3.21. SEM images of consolidated limestone and marble**

For limestone substrates consolidated with the experimental formulations, very little difference in appearance is observed relative to the unconsolidated limestone. For the commercial consolidants however, a web-like blanket of material appears to sit over the granular particles. Given the minimal depth of consolidation for Conservare, it is likely that the consolidant is concentrated at the surface rather than absorbed into the pores. Not only does this effect decrease the consolidant efficiency, it also changes the surface appearance of the stone material, a highly undesirable property in the field of conservation. Because marble is naturally less porous than limestone, the majority of consolidant is concentrated on the surface for both commercial and experimental formulations. As a result, the surface appearance is directly related to the amount of consolidant applied.

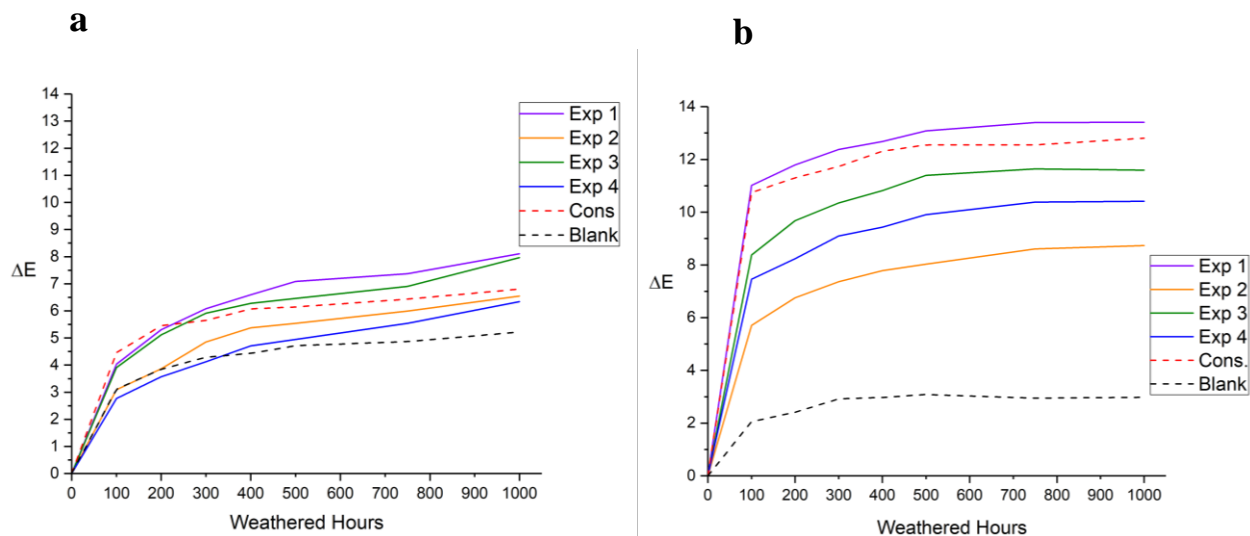


**Figure 3.22. Color change ( $\Delta E$ ) of weathered consolidants on a.) limestone and b.) marble**

Color change values were observed over 1000 hours of accelerated weathering testing. Consolidated limestone samples all showed similar trends in  $\Delta E$  values (Figure 3.22 a), with the largest increase within the first 100 hours of weathering followed by a gradual increase over time. Exp 2 and Exp 4 both show lower  $\Delta E$  values than Conservare. These experimental formulations contain the highest loading of OTES at 13% and 15% respectively. Consolidated marble substrates experienced significantly higher delta E values compared to unconsolidated marble in addition to consolidants on limestone substrates (Figure 3.22 b). This is most likely due to the minimal porosity of marble, as the consolidant sits on the surface of the marble. As a result, accelerated weathering by direct UV exposure is mainly interacting with the concentrated consolidant layer.

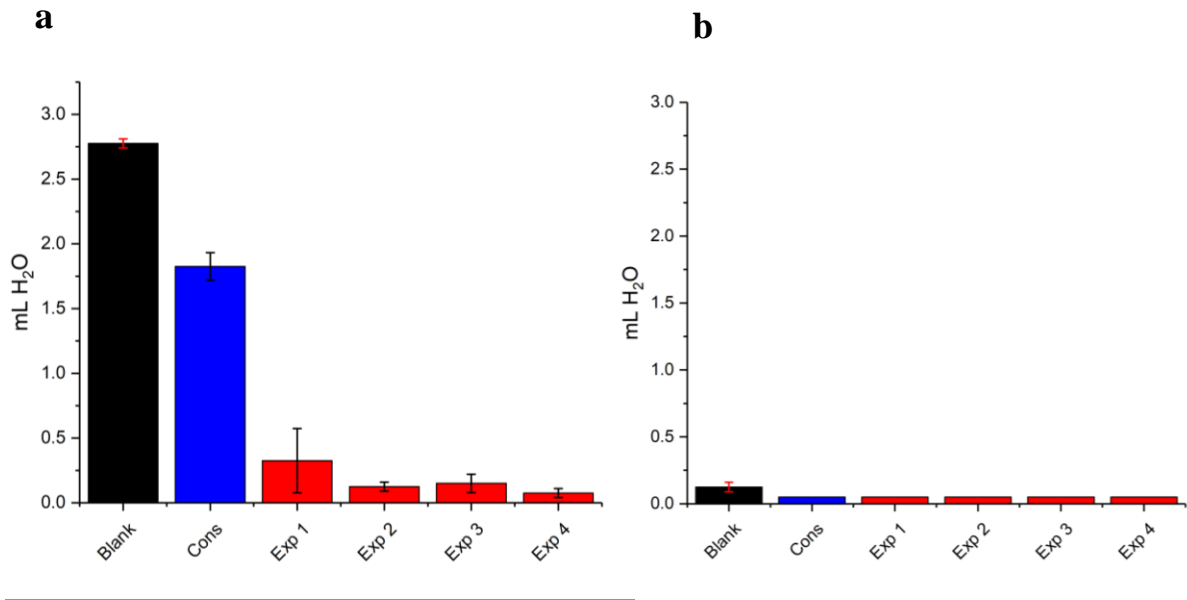


**Figure 3.23. Water absorption of weathered consolidants after 1000 hours on a.) limestone and b.) marble**

The final water absorption measurements on consolidated and unconsolidated stone after 1000 hours of weathering is shown in Figure 3.23. For limestone (Figure 3.23 a), all experimental consolidants show significantly improved water absorption compared to Conservare, only minimizing water absorption by 1.0 mL. Exp 2 and Exp 4 show the lowest water absorption with minimal error between replicates, drastically decreasing water absorption by 2.50 mL. Given the decreased brittleness of the experimental formulations, the consolidation efficacy is drastically improved, whereas the brittle Conservare inside the stone's porous structure allows for water penetration between the cracks of the consolidant caused by shrinkage stress.

Water absorption values on weathered marble (Figure 3.23 b) shows minimal differentiation between unconsolidated and consolidated samples. Based on the non-porous nature of marble, significant consolidation may not be necessary for minimally porous substrates.



#### **3.3.3.4. Water vapor permeability**

Water vapor permeability measurements were performed on consolidated filter papers. SEM images of the filter papers was initially performed to understand the interaction between the consolidant and the fibers. Figure 3.24 a shows the SEM images of consolidated and unconsolidated filter paper. Web-like formations between the paper fibers indicates the presence of the consolidants, however no significant differences appear between the commercial and experimental consolidants. Zoomed in at 5,000x (Figure 3.24 b), however, it becomes evident that both Conservare and Silres show significant cracks in the consolidant between the filter paper fibers, whereas Exp 2 and Exp 4 show no signs of any cracks within the consolidant. This further shows on a microscopic level that the experimental formulations are a substantial improvement from the brittle commercial consolidants.

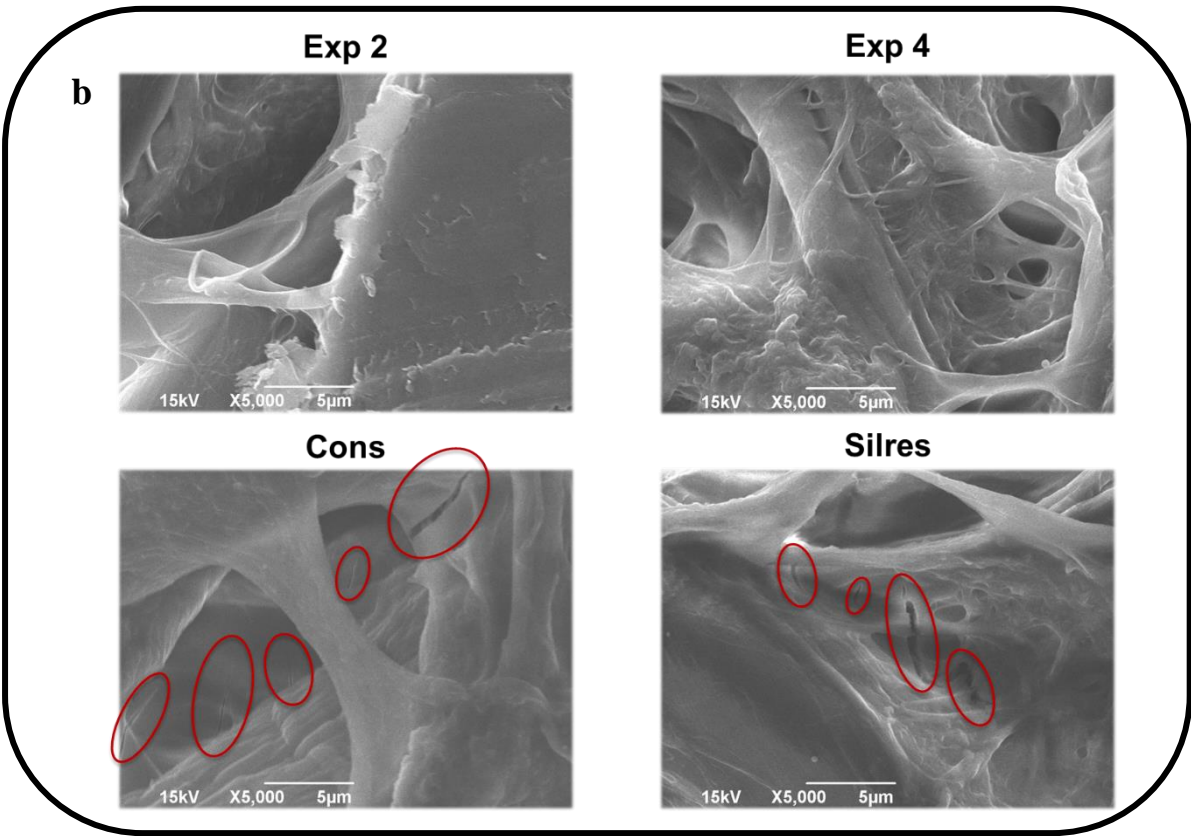
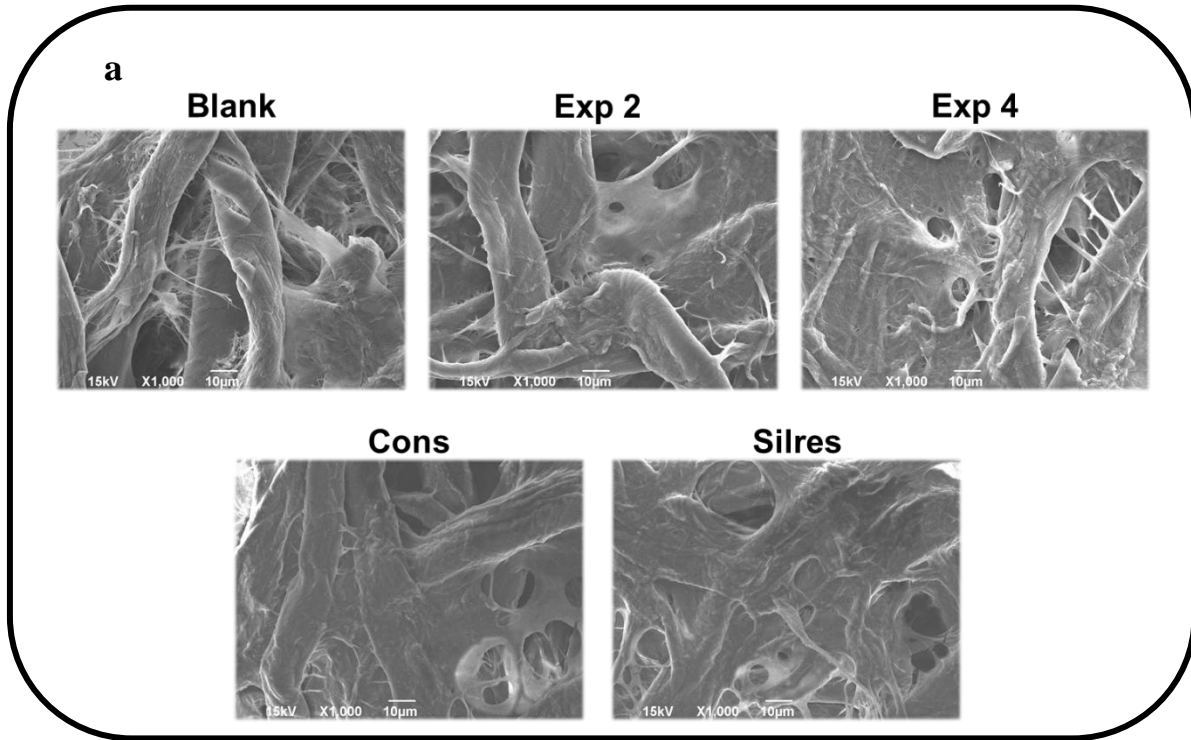


**Figure 3.24. SEM of consolidated filter paper a.) 1000x b.) 5000x**

Water vapor permeability tests were performed on the top two experimental formulations to measure the “breathability” of the experimental consolidants relative to the commercial consolidants. Figure 3.25 shows the water vapor transmission rate in  $\text{g/m}^2$  per 24 hours.

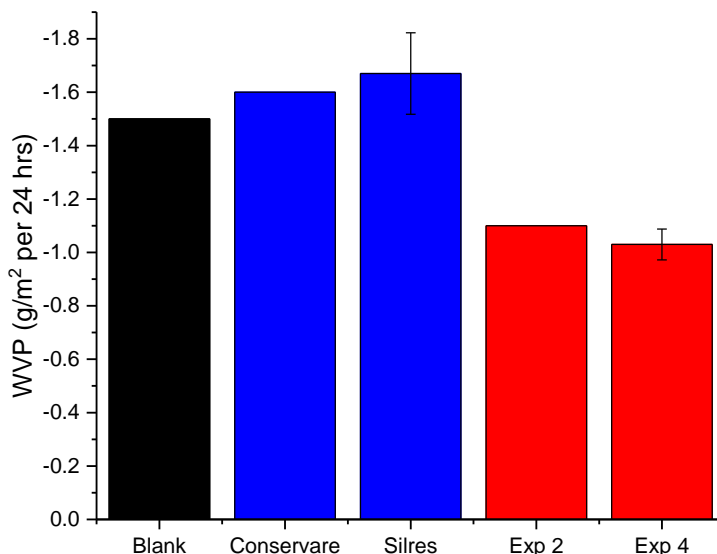


**Figure 3.25. Water vapor transmission rate of experimental and commercial consolidants**

Both Conservare and Silres show higher water vapor transmission rates than an unconsolidated filter paper, indicating a certain level of hydrophilicity that attracts water vapor to flow through the system. Given the relatively low contact angle of the commercial formulations, it is suspected that there is low differentiation between water entering the stone and water vapor exiting out of the stone. Water entering the stone has the ability to cause further degradation inside the pore's, resulting in an ineffective consolidant. Exp 2 and 4 both show lower water vapor transmission rates relative to the unconsolidated filter. While a more hydrophobic system than the commercial consolidants, the experimental formulations still allow for breathability, selectively allowing water vapor to exit the system while limiting the amount of water entering

in. The experimental formulations are therefore excellent candidates for stone consolidants considering the balance of hydrophobicity and breathability.

### **3.3.4. POSS study**

#### **3.3.4.1. Performance properties**

Isooctyl-POSS was initially chosen in Design B based on the hydrophobic alkyl chain ends, however, challenges in workability due to the high viscosity lead to the use of Phenyl-POSS in Designs C and D. From the optimized formulations produced from Design D,  $\Delta E$  values were comparable (if not slightly improved) to commercial consolidants. Isooctyl POSS may be less susceptible to UV degradation due to lack of chromophores available for UV degradation, and therefore a comparison of performance properties of P-POSS vs IO-POSS was explored.

P-POSS and IO-POSS consolidants formulated at 1%, 3% and 5% were cured in Al pans and weight loss was measured over time as shown in Figure 3.26. The 6-hour weight loss profile (Figure 3.26 a) shows Conservare with the slowest cure rate. The POSS consolidants indicate that a higher loading content correlates with a slower cure rate. The overall weight loss profile (Figure 3.26 b) shows a plateau at ~70% weight loss after 24 hours for the experimental consolidants, whereas Conservare does not plateau until ~200 hours. A faster cure rate may be desirable for conservation of outdoor stone materials.

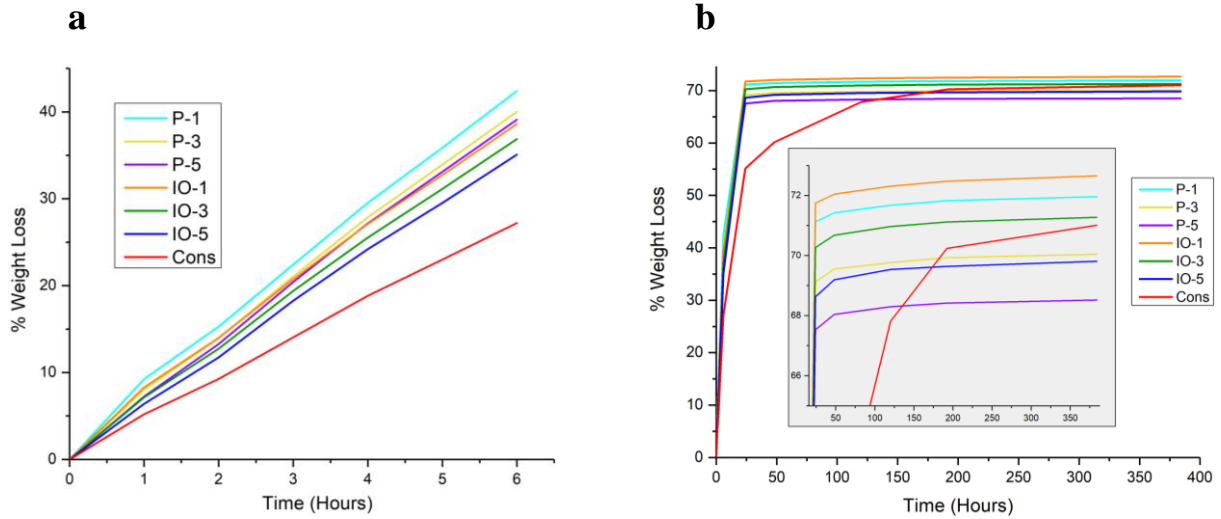


**Figure 3.26. Weight loss of POSS consolidants after a.) 6 hours b.) 400 hours**

Contact angle measurements were performed on consolidated Leneta paper and were compared against Conservare. Figure 3.27 a shows the contact angle images and Figure 3.27 b shows the contact angle values compared to both Silres and Conservare. All experimental formulations are higher compared to Silres and Conservare. P-1 shows the highest contact angle, however each POSS consolidants is comparably within range.

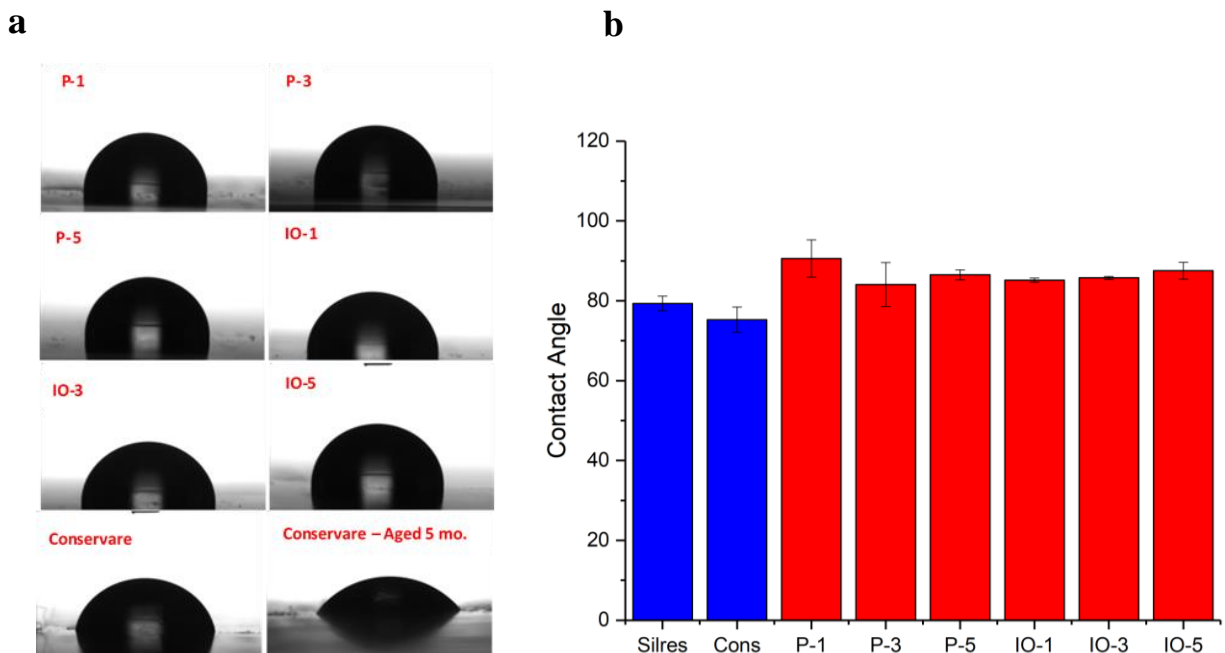


**Figure 3.27. Contact angle of POSS consolidants a.) images b.) values**

Based on the weight loss profiles, the POSS consolidants favor higher loading for a slower cure rate. However, the contact angles indicate no distinct correlation regarding POSS type and loading. As a result, accelerated weathering data will be analyzed to further distinguish the POSS consolidants.

### 3.3.4.2. Accelerated weathering

P-POSS and IO-POSS consolidants were exposed to 1000 hours of accelerated weathering and evaluated by monitoring the color change in addition to water absorption. Figure 3.28 shows the  $\Delta E$  values of each formulation over 1000 hours of weathering on Indiana limestone and Royal Danby marble.

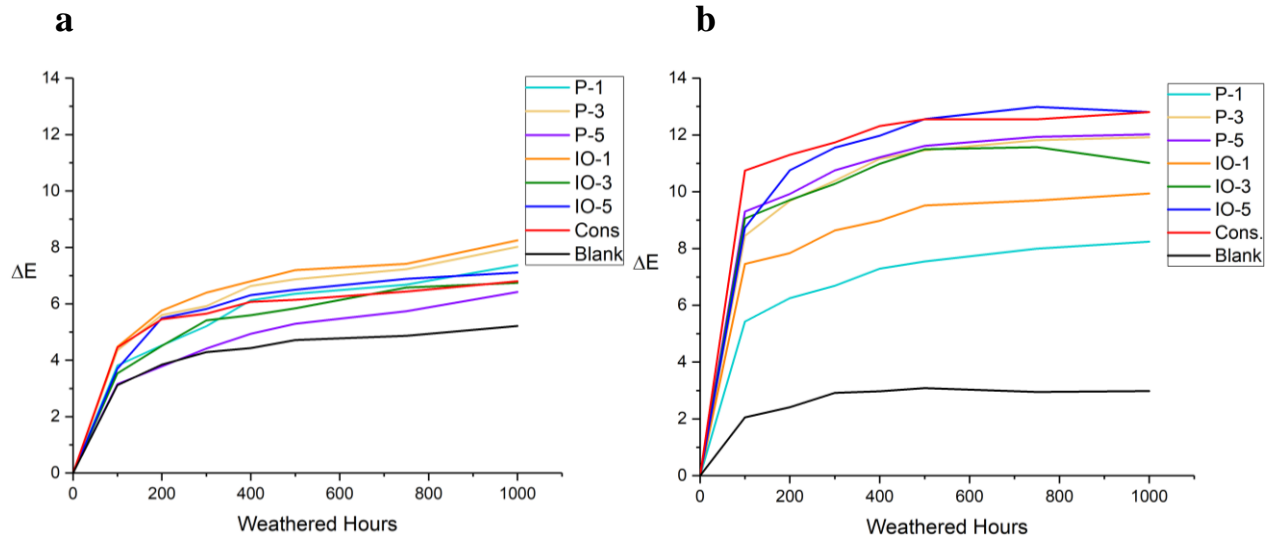


**Figure 3.28.  $\Delta E$  values of POSS consolidants over 1000 hours of accelerated weathering on a.) limestone and b.) marble**

The POSS consolidants on limestone showed lower  $\Delta E$  values compared to consolidants on the marble substrate. The large color change on marble samples is likely a result of a thicker surface film of consolidating material due to the minimal porosity of marble. Indiana limestone has porosity values ranging from 14-18%, whereas marble is significantly less porous at 1-3%.<sup>69</sup> As a result, more consolidant is absorbed into the pores of limestone via capillary force, minimizing the concentration of consolidants at the surface. Therefore, as limestone undergoes accelerated weathering, the granular surface of the stone is exposed to UV and condensation, resulting in degradation of the limestone particles at the surface. The weathering of marble, however, occurs at the consolidated film covering the surface. As a result, direct degradation of the consolidant increases the change in the  $L^*a^*b^*$  color coordinates.

From Figure 3.28 a, the consolidants on limestone indicate a steady color change increase ranging from 3 – 8  $\Delta E$ . Conservare performance falls about mid-range between the experimental samples. The unconsolidated (blank) limestone has the lowest color change, reaching 5.2  $\Delta E$  after 1000 hours of weathering. P-5 consolidant on limestone shows the least amount of color

change over 1000 hours of weathering, whereas IO-1 shows the largest color change of all the consolidants. No correlation in the data regarding POSS loading or type with  $\Delta E$  on limestone. Given that only duplicates were made for each formulation, additional replicates would be necessary for further conclusions correlating POSS type and amount with change in color.

From Figure 3.28 b, experimental consolidants on a marble substrate shows a steady color change increase ranging from 5.5 – 13  $\Delta E$ , significantly higher than color change values observed on limestone substrates. Conservare and IO-5 show the highest color change values in on marble substrates. The unconsolidated marble has the lowest color change, reaching only 3.0  $\Delta E$  at 1000 hours of weathering. P-1 indicates the best consolidant performance with regards to the least amount of color change over 1000 hours of weathering. There appears to be no correlations in the data regarding POSS loading or POSS type, in addition to no correlation between color change on limestone vs marble when measuring the same consolidant. As a result, it may be concluded that the optimal consolidant for minimal color change will depend on the substrate, however more replicates may aid in understanding further the effect of POSS loading and type.

Investigation into the  $\Delta E$  values was broken down further into the  $\Delta L$ ,  $\Delta a$  and  $\Delta b$  values (Figure 3.29) to understand the way in which color change occurred due to weathering of the consolidated stones. The  $\Delta a$  and  $\Delta b$  slightly decrease with weathering, however the most significant change occurs with the increase of  $\Delta L$ . The large increase in  $\Delta L$  values on both limestone and marble indicates lightening of the stone material, either through granular erosion of the surface (limestone) or consolidants degradation (marble).



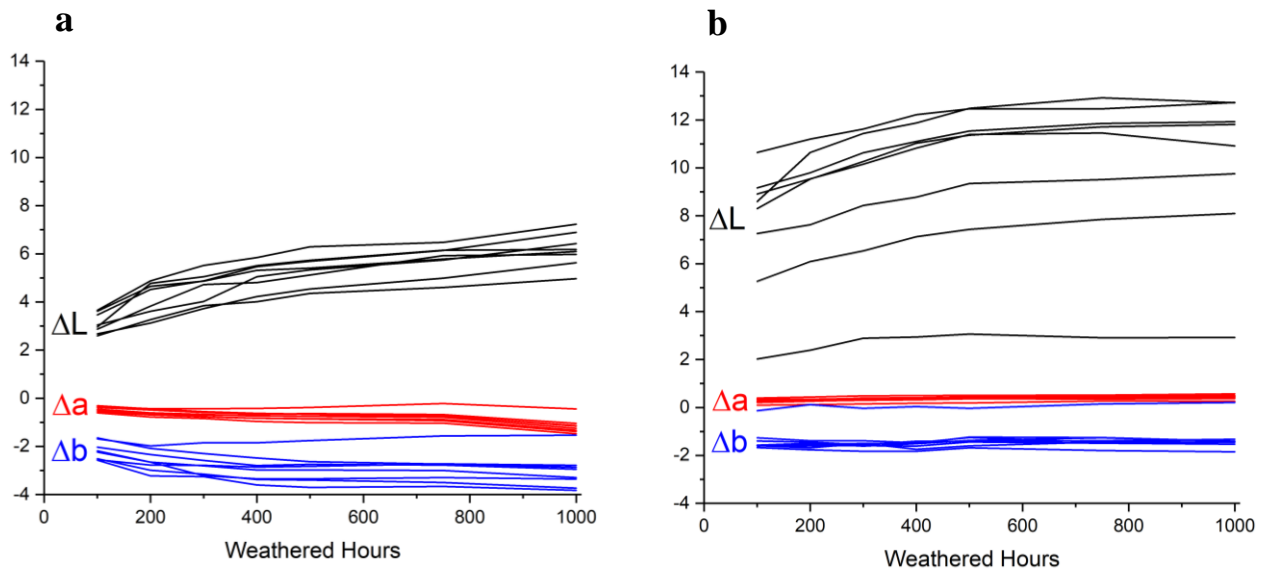


**Figure 3.29.  $\Delta L$ ,  $\Delta a$ ,  $\Delta b$  values of POSS consolidants over 1000 hours of accelerated weathering on a.) limestone and b.) marble**

Water absorption values measured using the Rilem Test Method<sup>68</sup> are shown in Figure 3.30). Due to the high porosity of limestone, water absorption values were significantly higher for consolidated limestone than those of consolidated marble. However, relative comparisons between experimental and commercial consolidants can be made for each type of stone. Figure 3.30 a shows experimental consolidants having lower water absorption values compared to Conservare with the exception of P-1. IO-5 shows the lowest water absorption at 0.25 mL H<sub>2</sub>O, followed by P-3 at 0.85 mL after 1000 hours of weathering. One interesting point to note is the minimal efficacy of Conservare on limestone compared to an unconsolidated limestone. Given the brittle nature of the commercial consolidant, water is capable of entering into the stone's porous structure in-between the cracks of the broken consolidants. As a result, Conservare is

insufficient to prevent water from penetrating into the stone, allowing for further internal degradation of the stone.

All marble samples showed significantly low rates of water absorption due to the low porosity of the stone. Unconsolidated weathered marble absorbed ~0.15 mL of H<sub>2</sub>O. All consolidants showed slightly lower water absorption values between 0-0.1 mL of H<sub>2</sub>O, and therefore differentiation between consolidants and performance is insignificant for marble substrates. Additionally, correlations between POSS loading and type was inconclusive based on the water absorption data.

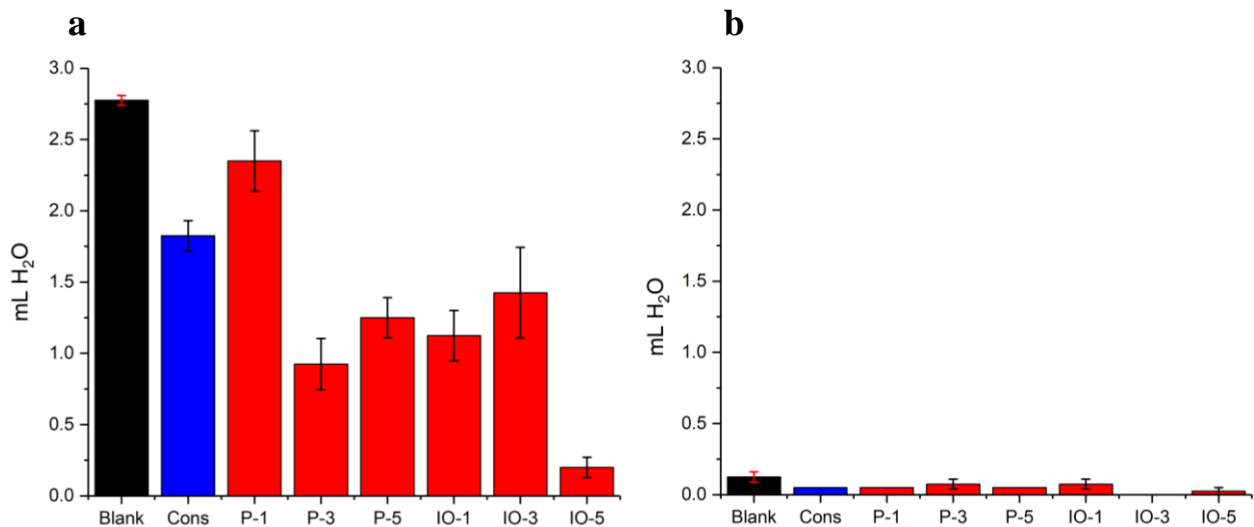


**Figure 3.30. Water absorption of POSS consolidants over 1000 hours of accelerated weathering on a.) limestone and b.) marble**

From the accelerated weathering performance, it was determined that no clear correlation between phenyl POSS and isooctyl POSS at 1%, 3% and 5% loading was made. Water absorption on limestone suggests that IO-5 and P-3 are the most promising options. IO-POSS as a high-viscosity liquid is relatively difficult to work with. As a result, P-POSS at 3% loading is

sufficient for use in the final formulations due to ease of use and a lower loading compared to IO-5.

### **3.4. Conclusions**

Solvent-free alkoxy silane stone consolidants formulations were explored and optimized resulting in identification of formulations having significantly improved performance compared to commercial consolidants Conservare OH100 and Silres BS OH 100. MTEOS and MTMOS were both found to have higher rates of hydrolysis and condensation relative to TEOS, resulting in rapid gelation within the vial prior to application. TEOS was therefore determined to be the primary alkoxy silane of choice. Colloidal silica drastically increased opacity and gelation and was therefore removed from future formulations. Ethanol was found to provide no beneficial properties to the overall consolidants, as hydrolysis of alkoxy silanes produced sufficient solvent to provide miscibility between water and alkoxy silanes. Final formulations contained GPTMS, PDMS, OTES, TEOS and DBTDL. Optimized experimental formulations exhibited improved appearance with no cracks, higher contact angle that is maintained over time, greater consolidation depth, higher % solids, significantly lower water absorption upon weathering, and an optimal water vapor transmission rate. Overall, Exp 2 and Exp 4 show promising potential for long term durability, increased flexibility, and improved breathability.

### **3.5. References**

1. Kotlik, P.; Justa, P.; Zelinger, J., The Application of Epoxy Resins for the Consolidation of Porous Stone. *Studies in Conservation* **1983**, 28 (2), 75-79.
2. Ginell, W. S.; Kotlik, P.; Selwitz, C. M.; Wheeler, G. S., Recent developments in the use of epoxy resins for stone consolidation. *Mater. Res. Soc. Symp. Proc.* **1995**, 352 (Materials Issues in Art and Archaeology 4), 823-9.

3. Selwitz, C. M. C., The Use of Epoxy Resins for Stone Consolidation. *MRS Proceedings* **1990**, 185, 181.
4. Selwitz, C., The Use of Epoxy Resins for the Stabilization of Deteriorated Masonry. *APT Bulletin* **1995**, 26 (4), 27-34.
5. Ginell, W. S.; Coffman, R., Epoxy Resin-Consolidated Stone: Appearance Change on Aging. *Studies in Conservation* **1998**, 43 (4), 242-248.
6. El-Gohary, M. m. a. y. c.; El-Magd, M. A., Influence of acrylic coatings and nanomaterials on the interfacial, physical, and mechanical properties of limestone-based monuments. Case study of "Amenemhat II Temple". *International Journal of Conservation Science* **2018**, 9 (2), 219-234.
7. Wheeler, G. S.; Shearer, G. L.; Fleming, S.; Kelts, L. W.; Vega, A.; Koestler, R. J., Toward a better understanding of B72 acrylic resin/methyltrimethoxysilane stone consolidants. *Mater. Res. Soc. Symp. Proc.* **1991**, 185 (Mater. Issues Art Archaeol. 2), 209-26.
8. Villegas, R.; Vale, J. F.; Alcalde, M., Study of water-repellent treatments applied on limestone from Andalusian cathedrals. *Mater. Constr. (Madrid)* **1991**, 41 (223), 19-27.
9. Pinna, D.; Salvadori, B.; Galeotti, M., Monitoring the performance of innovative and traditional biocides mixed with consolidants and water repellents for the prevention of biological growth on stone. *Sci. Total Environ.* **2012**, 423, 132-141.
10. Ginell, W. S.; Kumar, R.; Doehne, E., Conservation studies on limestone from the Maya site at Xunantunich, Belize. *Mater. Res. Soc. Symp. Proc.* **1995**, 352 (Materials Issues in Art and Archaeology 4), 813-21.

11. Cappitelli, F.; Principi, P.; Pedrazzani, R.; Toniolo, L.; Sorlini, C., Bacterial and fungal deterioration of the Milan Cathedral marble treated with protective synthetic resins. *Sci. Total Environ.* **2007**, *385* (1-3), 172-181.
12. Cavalletti, R., *A new type of epoxy resin for the structural consolidation of badly decayed stones*. Presses polytechniques romandes: Lausanne, **1985**; p 769.
13. Online, C. a. A. M. E. Paraloid B-72. [http://cameo.mfa.org/wiki/Paraloid\\_B-72](http://cameo.mfa.org/wiki/Paraloid_B-72).
14. Wheeler, G., *Alkoxysilanes and the Consolidation of Stone*. Getty Publications: Los Angeles, **2005**.
15. Snethlage, R.; Wendler, E., Chemical Conservation of Stone Structures. *Ullmann's Encyclopedia of Industrial Chemistry* **2000**.
16. Scherer, G. W.; Wheeler, G. S., Silicate consolidants for stone. *Key Eng. Mater.* **2009**, *391* (Progress in Sol-Gel Production), 1-25.
17. Wright, J. D.; Sommerdijk, N. A. J. M., *Sol-Gel Materials: Chemistry and Applications*. Gordon and Breach Science Publishers: Amsterdam, **2001**.
18. Smith, A. L., *Analysis of silicones*. R.E. Krieger: Malabar, Fla., **1983**.
19. Illescas, J. F.; Mosquera, M. J., Surfactant-Synthesized PDMS/Silica Nanomaterials Improve Robustness and Stain Resistance of Carbonate Stone. *J. Phys. Chem. C* **2011**, *115* (30), 14624-14634.
20. Illescas, J. F.; Mosquera, M. J., Producing Surfactant-Synthesized Nanomaterials In Situ on a Building Substrate, without Volatile Organic Compounds. *ACS Appl. Mater. Interfaces* **2012**, *4* (8), 4259-4269.

21. Xu, F.; Li, D.; Zhang, Q.; Zhang, H.; Xu, J., Effects of addition of colloidal silica particles on TEOS-based stone protection using n-octylamine as a catalyst. *Prog. Org. Coat.* **2012**, *75* (4), 429-434.
22. Li, D.; Xu, F.; Liu, Z.; Zhu, J.; Zhang, Q.; Shao, L., The effect of adding PDMS-OH and silica nanoparticles on sol-gel properties and effectiveness in stone protection. *Appl. Surf. Sci.* **2013**, *266*, 368-374.
23. Xu, F.; Li, D., Effect of the addition of hydroxyl-terminated polydimethylsiloxane to TEOS-based stone protective materials. *J. Sol-Gel Sci. Technol.* **2013**, *65* (2), 212-219.
24. Xu, F.; Liu, H.; Li, D., Synthesis of PDMS-SiO<sub>2</sub> hybrids using different templates. *J. Porous Mater.* **2016**, *23* (5), 1133-1141.
25. Xu, F.; Wang, C.; Li, D.; Wang, M.; Xu, F.; Deng, X., Preparation of modified epoxy-SiO<sub>2</sub> hybrid materials and their application in the stone protection. *Prog. Org. Coat.* **2015**, *81*, 58-65.
26. Salazar-Hernandez, C.; Alquiza, M. J. P.; Salgado, P.; Cervantes, J., TEOS-colloidal silica-PDMS-OH hybrid formulation used for stone consolidation. *Appl. Organomet. Chem.* **2010**, *24* (6), 481-488.
27. Liu, Y.; Liu, J., Synthesis of TEOS/PDMS-OH/CTAB composite coating material as a new stone consolidant formulation. *Constr. Build. Mater.* **2016**, *122*, 90-94.
28. Liu, Y.; Liu, J., Fabrication of TEOS/PDMS/F127 hybrid coating materials for conservation of historic stone sculptures. *Appl. Phys. A: Mater. Sci. Process.* **2016**, *122* (8), 1-7.

29. Liu, R.; Han, X.; Huang, X.; Li, W.; Luo, H., Preparation of three-component TEOS-based composites for stone conservation by sol-gel process. *J. Sol-Gel Sci. Technol.* **2013**, *68* (1), 19-30.
30. Facio, D. S.; Mosquera, M. J., Simple Strategy for Producing Superhydrophobic Nanocomposite Coatings In Situ on a Building Substrate. *ACS Appl. Mater. Interfaces* **2013**, *5* (15), 7517-7526.
31. Miliani, C.; Velo-Simpson, M. L.; Scherer, G. W., Particle-modified consolidants: A study on the effect of particles on sol-gel properties and consolidation effectiveness. *Journal of Cultural Heritage* **2007**, *8* (1), 1-6.
32. Ksinopoulou, E.; Bakolas, A.; Moropoulou, A., Modifying Si-based consolidants through the addition of colloidal nano-particles. *Appl. Phys. A: Mater. Sci. Process.* **2016**, *122* (4), 1-10.
33. Salazar-Hernandez, C.; Zarraga, R.; Alonso, S.; Sugita, S.; Calixto, S.; Cervantes, J., Effect of solvent type on polycondensation of TEOS catalyzed by DBTL as used for stone consolidation. *J. Sol-Gel Sci. Technol.* **2009**, *49* (3), 301-310.
34. Mosquera, M. J.; de los Santos, D. M.; Montes, A., Producing new stone consolidants for the conservation of monumental stones. *Mater. Res. Soc. Symp. Proc.* **2005**, *852* (Materials Issues in Art and Archaeology VII), 81-87.
35. Kim, E. K.; Won, J.; Do, J.-y.; Kim, S. D.; Kang, Y. S., Effects of silica nanoparticle and GPTMS addition on TEOS-based stone consolidants. *Journal of Cultural Heritage* **2009**, *10* (2), 214-221.
36. Cardiano, P., Hydrophobic properties of new epoxy-silica hybrids. *J. Appl. Polym. Sci.* **2008**, *108* (5), 3380-3387.

37. Son, S.; Won, J.; Kim, J.-J.; Jang, Y. D.; Kang, Y. S.; Kim, S. D., Organic-Inorganic Hybrid Compounds Containing Polyhedral Oligomeric Silsesquioxane for Conservation of Stone Heritage. *ACS Appl. Mater. Interfaces* **2009**, *1* (2), 393-401.
38. Mosquera, M. J.; Bejarano, M.; de la Rosa-Fox, N.; Esquivias, L., Producing Crack-Free Colloid-Polymer Hybrid Gels by Tailoring Porosity. *Langmuir* **2003**, *19* (3), 951-957.
39. Han, X.; Rong, B.; Huang, X.; Luo, H., Bridged siloxanes as novel potential hybrid consolidants for ancient Qin terracotta. *Prog. Org. Coat.* **2016**, *101*, 416-422.
40. Hasan, A.; Pandey, L. M., Kinetic studies of attachment and re-orientation of octyltriethoxysilane for formation of self-assembled monolayer on a silica substrate. *Mater. Sci. Eng., C* **2016**, *68*, 423-429.
41. Commission, R.; 25-PEM, Measurement of Water Absorption Under Low Pressure - Rilem Test Method - Test No. 11.4. Bagnex, France, **1986**.
42. Division, K. I. H. R. Carbonates. <https://kocurekindustries.com/carbonates-cores>.



## CHAPTER 4. BIOBASED EPOXY THERMOSETS DERIVED FROM VANILLIN

### 4.1. Introduction

Epoxy materials are widely used in the coatings industry, construction, composites, adhesives, and electronics as a result of their excellent thermal and mechanical properties, solvent resistance, adhesion, low shrinkage, and flexibility.<sup>70, 71</sup> Biobased epoxy resins have been investigated as alternatives to diglycidyl ether of bisphenol A (DGEBA) due to the growing concerns of bisphenol A (BPA) on human health.<sup>72-76</sup> As a known endocrine disruptor, BPA use has been limited or banned from many countries, including Canada, China, Malaysia, and the European Union. While the health effects of BPA have been debated for years,<sup>77</sup> a variety of renewable materials have been investigated as alternatives to petrochemical-derived epoxy resins.<sup>71, 78, 79</sup> These include compounds such as cardanol,<sup>80-88</sup> eugenol,<sup>89-94</sup> tannins,<sup>95-98</sup> vegetable oils,<sup>99-107</sup> furan,<sup>108-110</sup> rosin,<sup>111-113</sup> itaconic acid,<sup>114-117</sup> and lignin<sup>118-121</sup> to name a few. Given the aromatic nature of BPA, renewable aromatic compounds such as lignin and lignin-derivatives have been investigated as potential replacements. The oxidative depolymerization of lignin results in small molecular weight compounds such as vanillin, syringaldehyde, guaiacol, p-hydroxybenzaldehyde, vanillic acid, syringic acid, acetovanillone, and acetosyringone.<sup>122</sup> While the mixture of products will vary as a result of depolymerization method, wood source and geographical climate, vanillin remains one of the most abundant small molecular weight compounds produced from oxidative lignin depolymerization.<sup>123, 124</sup> Manufactured on an industrial scale, vanillin from biomass shows great potential as a biobased crosslinker given the aromatic nature, unique functionality, non-toxicity and pleasant aroma.

Vanillin-epoxy monomers were previously synthesized by Koike et al., in which vanillin and pentaerythritol underwent acetalization to form a divanillin-spiroacetal compound.<sup>125</sup> The

phenolic groups were glycidylated, forming a diepoxy compound with an epoxy equivalent weight of 270 g/equivalent. However, acetals are easily broken under aqueous acidic conditions, and therefore the stability of the divanillin-spiroacetal compound is questionable.<sup>126</sup> Nikafshar et al. developed an epoxy resin from vanillin by first oxidizing vanillin to methoxyhydroquinone followed by glycidylation to form a diepoxy vanillin compound. Crosslinking with Epikure F 205 (insert type of curing agent here) and a calcium nitrate solution as an accelerator showed increased tensile and impact strength compared to a traditional DGEBA system.<sup>127</sup>

Boutevin et al. described the synthesis of three novel diepoxy monomers from vanillin.<sup>128</sup> For the first monomer, oxidation of vanillin via the Dakin reaction resulted in 2-methoxyhydroquinone. Sodium percarbonate dissolution creates a hydroperoxide anion that attacks the aromatic aldehyde of vanillin. The solution was acidified to convert the phenolate ions into phenols for easier extraction. The resulting 2-methoxyhydroquinone was collected at 97% yield. Further glycidylation of this compound using a phase transfer catalyst (TEBAC) and sodium hydroxide resulted in a diepoxy of methoxyhydroquinone at 87% yield. For the second monomer, oxidation of vanillin results in vanillic acid. The glycidylation of both the alcohol and carboxylic acid using TEBAC and NaOH resulted in the diepoxy of vanillic acid at 97% yield. For the third monomer, the reduction of vanillin produces vanillyl alcohol. Glycidylation of vanillyl alcohol was complicated by the fact that benzyl alcohol is less acidic than phenol, and therefore the phase transfer catalyst does not form an ion-pair with benzyl alcohol. Rather, a biphasic transfer catalysis system consisting of an aqueous phase with TEBAC in addition to an organic phase aided in the successful glycidylation of both the phenol and benzyl alcohol with 89% yield. These three vanillin-diepoxy monomers were crosslinked with isophorone diamine (IPDA) at varying epoxy to amine ratios.<sup>129</sup> The vanillic acid diepoxy monomer with a 2:1 ratio

resulted in the highest  $T_g$  of 152°C, however all epoxies were found to be solids at room temperature, limiting their utility. Caillol et al. furthered the crosslinking of the vanillyl alcohol diepoxy monomer by crosslinking with dicyandiamide, showing excellent glass adhesion properties for food contact epoxy coatings.<sup>130</sup>

To further the use of vanillin in thermosets, in this study, vanillin was reacted with amines to produce novel vanillin-Schiff base (Van-SB) compounds. The vanillin-SB was further glycidylated through the phenolic groups of vanillin using epichlorohydrin. The epoxy was crosslinked with diamines to produce thermoset resins and compared to DGEBA-based systems. Reductive amination of the Schiff base was explored to minimize the yellowness caused from conjugation from the imine and the aromatic vanillin.

## **4.2. Experimental**

### **4.2.1. Raw materials**

Vanillin, ethylenediamine (ED), p-phenylenediamine (PD), sodium hydroxide, benzyltriethylammonium chloride (TEBAC), chloroform-d, dimethyl sulfoxide-d<sub>6</sub>, dichloromethane, butylamine, cyclohexylamine, and DER 332 (diglycidyl ether of bisphenol A) were purchased from Sigma Aldrich and used as is. Priamine 1071, 1073, and 1074 were obtained from Croda. Jeffamine T403 and Jeffamine D230 were received from Hunstman. 2-Methylpentamethylenediamine (Dytek A) was obtained from Invista. Methanol and epichlorohydrin were purchased from VWR. Vestamin IPD (isophorone diamine), Vestamin TMD (trimethyl hexamethylene diamine) and Vestamin PACM (4,4'-diaminodicyclohexylmethane) were received from Evonik.

## 4.2.2. Characterization methods

### 4.2.2.1. Product characterization

Synthesized products were analyzed by Fourier transform infrared spectroscopy using a Thermo Scientific Nicolet 8700 spectrometer. Solid products were made into pellets with potassium bromide (KBr). High viscosity resins or liquids were spread across a KBr disc. Absorbance was measured and product functional groups were identified.

Nuclear magnetic resonance spectroscopy was performed on synthesized compounds using a Jeol 400 MHz spectrometer. Reaction products were solubilized in either chloroform-d or dimethyl sulfoxide-d<sub>6</sub>. Proton NMR (<sup>1</sup>H NMR) and/or carbon NMR (<sup>13</sup>C NMR) were utilized to determine product structure. Integration using Mestrelab Mnova was utilized to quantify the products and byproducts.

A Waters Synapt G2-Si Mass Spectrometer with ESI+ was used to provide Collision Induced Dissociation (CID) fragmentation to the products of interest. Methanol was used to solubilize the product and ESI. The range of observation was between 50 – 1200 Da.

Epoxy equivalent weight was determined using ASTM D1652-11. Briefly, epoxy compound was solubilized in dichloromethane. Tetraethylammonium bromide solution in glacial acetic acid was added and the solution was titrated with perchloric acid. The end point was recorded, and the epoxy equivalent weight was calculated.

Gel permeation chromatography was utilized to determine the number-average molecular weight (M<sub>n</sub>) using EcoSEC HLC-8320GPC (Tosoh Bioscience, Japan) with a differential refractometer (DRI) detector. Product separations were carried out using two TSKgel SuperH3000 6.00 mm ID×15 cm columns set at 40°C. Samples were solubilized in tetrahydrofuran (THF) at a concentration of 1 mg per mL and filtered. 20µL of sample was

injected into the instrument at a flow rate of 0.35 mL per minute. Calibration was conducted using polystyrene standards (Agilent EasiVial PS-H 4ml).

#### **4.2.2.2. Cured epoxy characterization**

Thermogravimetric analysis was run on cured epoxy samples using a Q500 Thermogravimetric Analyzer (TA Instruments). A heating ramp of 20 °C/min up to 600 °C under continuous nitrogen flow was utilized to monitor thermoset stability and the temperature at which 5% weight loss occurs ( $T_{5\%}$ ).

Differential scanning calorimetry was run using a Q1000 Modulated DSC (TA Instruments). A heat/cool/heat cycle was used, with the first heat cycle ramping to 250 °C at 10 °C/min ensured complete curing of any unreacted material, followed by a cooling cycle down to -25 °C at 5 °C/min. Finally, the last heat cycle ramping up to 250 °C at 10 °C/min was useful in determining the overall glass transition temperature ( $T_g$ ) of the cured epoxy material.

#### **4.2.3. Vanillin epoxy thermosets**

Two synthetic routes for the development of vanillin-epoxy thermosets were explored. The first route begins by Schiff base formation by the addition of amine to vanillin. The phenols on vanillin were then glycidylated using epichlorohydrin. Finally, the epoxy groups were crosslinked with amines. The second route begins with the glycidylation of vanillin through the phenol using epichlorohydrin. Crosslinking occurs through both the epoxies and the aldehyde, forming crosslinked vanillin-SB compounds. Each route was explored and resulting thermoset properties were compared.

##### **4.2.3.1. Route A: Schiff base, glycidylation, crosslinking**

Vanillin (10 mmol) was solubilized in methanol (50% methanol by weight) at 23 °C. Once vanillin was fully dissolved, diamine (10 mmol) was slowly added to the solution dropwise

while stirring. Diamines used were Priamine 1071, PACM, Dytex A and p-phenylenediamine. The solution was stirred overnight at room temperature to ensure complete reaction. The methanol was removed using a rotary evaporator and the remaining product was placed under vacuum overnight to ensure complete removal of methanol and water. Van-SB product was characterized using FTIR and NMR.

Schiff base product (5 mmol), epichlorohydrin (50 mmol), and a phase transfer catalyst TEBAC (1 mmol) were added to a round bottom flask. The Schiff base product was soluble in epichlorohydrin, and therefore no solvent was necessary for carrying out the reaction. The mixture was heated to 80°C for an hour. After an hour, the temperature was turned off and allowed to cool to room temperature. A 5 M aqueous sodium hydroxide solution was slowly added over 30 minutes, and the solution was stirred overnight. The next day, the product was washed with ethyl acetate, deionized water, and finally a brine solution. Solvent was removed by rotary evaporator and the product was then dried under vacuum overnight to ensure complete removal of solvent. The Van-Pri1071 product was not glycidylated due to the high viscosity of the Schiff base, making it difficult to work with. Glycidylated vanillin-SB products (Gly-Van-SB) were characterized by FTIR, <sup>1</sup>H NMR, EEW and GPC.

#### **4.2.3.2. Route B: glycidylation, Schiff base/crosslinking**

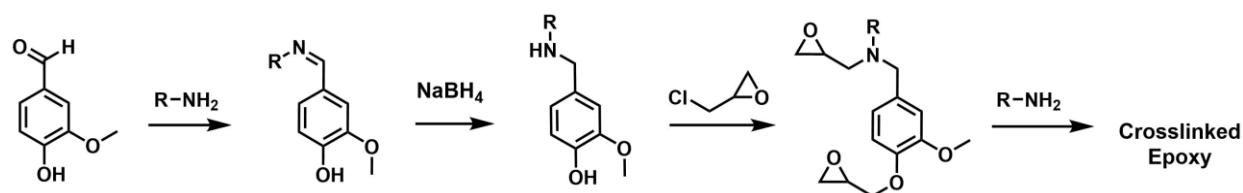
Vanillin (30 mmol), epichlorohydrin (180 mmol), and a phase transfer catalyst TEBAC (3 mmol) were added to a round bottom flask. The mixture was heated to 80°C for an hour. The temperature was turned off and allowed to cool to room temperature. Aqueous sodium hydroxide solution (5 M) was added slowly over 30 minutes, and the solution was stirred overnight. The next day, the product was washed with ethyl acetate, deionized water, and finally a brine solution. Solvent was removed by rotary evaporator and the product was dried under vacuum

overnight to ensure complete removal of solvent. Gly-Van was analyzed by FTIR,  $^1\text{H}$  NMR and EEW.

Gly-Van was crosslinked with following diamines: ethylene diamine, DytekA, IPDA, PACM, Jeffamine T403, Jeffamine D230, Priamine 1071, Priamine 1073, and Priamine 1074. Epoxy to amine ratio was formulated at 1:0.5, 1:1, and 1:2. Gly-Van was added to a 20 mL vial and melted at  $93^\circ\text{C}$  in a copper heating plate. Diamine was added to the vial using a syringe and the vial was quickly vortexed for ~5-10 seconds. The material was poured into a small aluminum pan and let sit at ambient conditions for 1 hour. The epoxy in the aluminum pans was cured in a vacuum oven at  $100^\circ\text{C}$  for 2 hours followed by  $30^\circ\text{C}$  overnight. The crosslinked epoxies were taken out of the vacuum oven and sat at room temperature for 7 days prior to testing. Cured Gly-Van epoxies were analyzed using TGA and DSC. Diglycidylether of bisphenol A (DER 332) served as a control and was formulated with Dytek A, IPDA, Jeffamine T403 and Jeffamine D230 at an epoxy to amine hydrogen ratio of 1:1.

#### 4.2.4. Reductive amination of vanillin-Schiff base compounds

Reductive amination of the imine formed during the Schiff base was investigated using sodium borohydride as the reducing agent in addition to acid co-catalysts such as boric acid and p-toluenesulfonic acid. Scheme 4.1 shows the reductive amination process for vanillin-Schiff base compounds.



**Scheme 4.1. Reductive amination of Schiff base**

Vanillin (10 mmol) was solubilized in methanol (50% methanol by weight) at 23 °C. Once vanillin was fully dissolved, cyclohexylamine (10 mmol) was slowly added to the solution dropwise while stirring. The solution was stirred overnight at room temperature to ensure complete reaction. Vanillin-cyclohexylamine Schiff base (Van-CA) was confirmed using FTIR and <sup>1</sup>H NMR. Sodium borohydride and acid activators were added to the solution according to Table 4.1. Reduced-SB compounds were characterized using FTIR, <sup>1</sup>H NMR, and HRMS.

**Table 4.1. Vanillin-cyclohexylamine reductive amination formulations**

<b>ID</b>	<b>Activator</b>	<b>Imine : NaBH<sub>4</sub> : Activator</b>
A	Boric Acid	1 : 1 : 1
B	Boric Acid	1 : 1 : 6
C	p-TSA	1 : 1 : 1
D	None	1 : 1 : 0
E	None	1 : 6 : 0

Once the preferred method for reduction was established, vanillin-butylamine (Van-BA) Schiff base was synthesized using the method described above. Reduction of Van-BA was carried out using Method D, consisting of 1:1 equivalent of imine and NaBH<sub>4</sub> with no acid activator. Red-Van-BA was confirmed using HRMS.

Red-Van-SB (30 mmol), epichlorohydrin (180 mmol), and a phase transfer catalyst TEBAC (3 mmol) were added to a round bottom flask. The reduced Schiff base compounds included Red-Van-CA and Red-Van-BA. The mixture was heated to 80°C for an hour. The temperature was turned off and allowed to cool to room temperature. Aqueous sodium hydroxide solution (5 M) was added slowly over 30 minutes, and the solution was stirred overnight. The next day, the product was washed with ethyl acetate, deionized water, and finally a brine



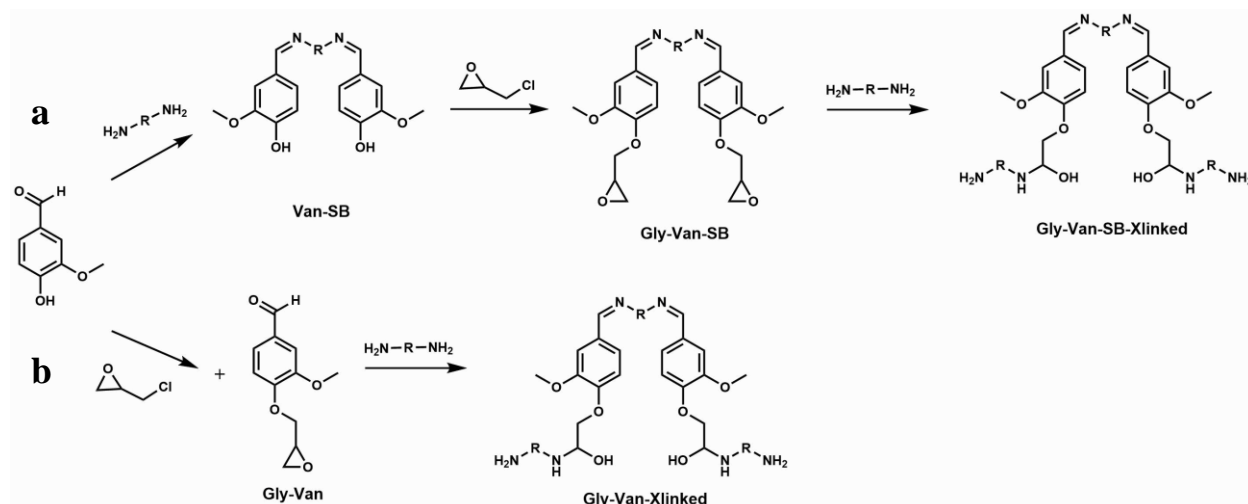
solution. Solvent was removed by rotary evaporator and the product was dried under vacuum overnight to ensure complete removal of solvent. Gly-Red-Van-SB was analyzed by FTIR, <sup>1</sup>H NMR and EEW.

Gly-Red-Van-BA and Gly-Red-Van-CA compounds were crosslinked with IPDA, PACM and TMD. Epoxy to amine ratio was formulated from 1:2, 1:1 and 1:0.5. Gly-Red-Van-SB was added to a small aluminum pan (28mm diameter), followed by the amine and stirred using a wooden applicator stick. Gly-Red-Van-BA thermosets were cured for 4 hours at 100°C, whereas the Gly-Red-Van-CA thermosets cured in 2 hours at 85°C. Cured Gly-Red-Van-SB epoxies were analyzed using TGA and DSA.

### **4.3. Results and discussion**

#### **4.3.1. Vanillin-epoxy thermosets**

Epoxy thermosets from vanillin were synthesized via two different routes. In Scheme 4.2 a, vanillin was reacted with diamines to form a vanillin-Schiff base (Van-SB) compound. Further glycidylation using epichlorohydrin resulted in glycidylated vanillin SB (Gly-Van-SB). Crosslinking through the epoxy groups with diamines or triamines produced cured epoxy thermosets in which different amines were used for the Schiff base formation and crosslinking through the epoxy. In Scheme 4.2 b, vanillin was initially glycidylated (Gly-Van) prior to reacting with amine. Formation of the Schiff base and amine crosslinking through the epoxy occurred simultaneously in the last step, limiting the amine variation within the system.



**Scheme 4.2. Crosslinked vanillin-Schiff base epoxy thermosets via a.) Vanillin-SB, glycidylation and amine crosslinking and b.) vanillin glycidylation and amine crosslinking**

#### 4.3.1.1. Route A: Schiff base, glycidylation, crosslinking

The synthesis of vanillin-SB compounds was explored using solvent to ensure full solubility of each reactant for effective contact during the reaction. Methanol was chosen as the solvent due to compatible solubility of vanillin and the chosen diamines. After removal of the methanol, all Van-SB compounds appeared as brightly colored solids. Figure 4.1 shows the FTIR and  $^1H$  NMR of the resulting Van-SB compounds.

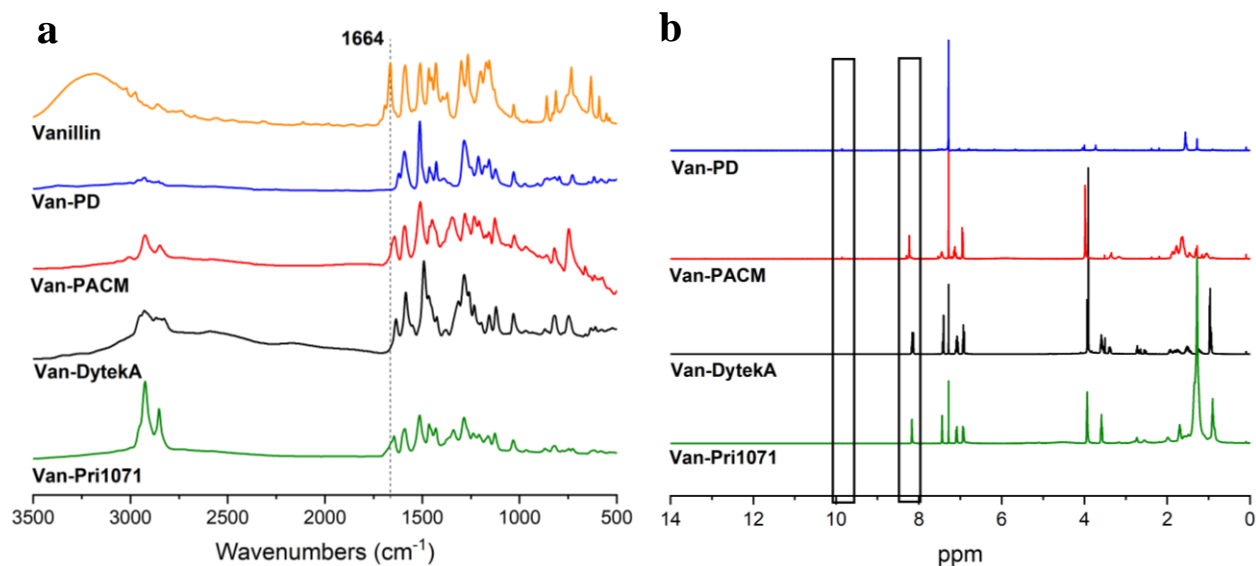


**Figure 4.1. a.) FTIR and b.) <sup>1</sup>H NMR of Van-SB products**

The FTIR for Van-SB products (Figure 4.1 a) shows challenging differentiation between the carbonyl of vanillin and the imine formation for the Schiff base between 1640-1660  $\text{cm}^{-1}$ . However, the <sup>1</sup>H NMR (Figure 4.1 b) indicates a significantly higher concentration of imine (8.2 ppm) than aldehyde (9.8 ppm). The low solubility of Van-PD in  $\text{CDCl}_3$  and  $\text{DMSO-d}_6$  resulted in inconclusive determination of product, and therefore HRMS was implemented to further characterize the Van-SB products. Table 4.2 shows the HRMS product confirmation for each Van-SB product except for Van-Pri1071 due to the high molecular weight of the Priamine.

**Table 4.2. Mass-to-charge ratio predictions vs actual values for Van-SB**

Schiff Base	Actual	Theoretical	PPM
Van-PD	377.1491	377.1501	-2.7
Van-PACM	479.2915	479.291	1.0
Van-DytekA	385.2114	384.2127	-1.3

The mass-to-charge ratios for the major products of the Van-SB reactions were all comparable to the theoretical values with less than 5 ppm, indicating conclusive identification of imine formation. As a result, Vanillin-SB compounds were successfully prepared for further glycidylation.

The Van-SB products synthesized in methanol were glycidylated using epichlorohydrin with the exception of Van-Pri1071 due to viscosity challenges. All Gly-Van-SB products became high viscosity liquids with the exception of Gly-Van-PD, which remained a solid. The colors of each product ranged from bright yellow to red.

**Table 4.3. Schiff base vs hydrolyzed product integration, EEW, and  $M_n$  values**

<b>Gly-Van-SB</b>	<b>Imine</b>	<b>Aldehyde</b>	<b>Theor. EEW</b>	<b>Actual EEW</b>	<b>Theor. <math>M_n</math></b>	<b>Actual <math>M_n</math></b>
Gly-Van-PD	84%	16%	244	-	488	-
Gly-Van-PACM	65%	35%	295	147	590	814
Gly-Van-DytekA	52%	48%	248	136	496	503

From Table 4.3, Gly-Van-PD contained the largest amount of intact imine (86%) with minimal hydrolysis compared with to Gly-Van-PACM at 65% imine and Gly-Van-DytekA at 52% imine. The conjugated aromatic amine shows greater stability to hydrolysis due to the resonance stability throughout the structure. The cycloaliphatic amine is the second most stable to hydrolysis followed by the aliphatic amine. Epoxy equivalent weight could not be performed on Gly-Van-PD due to insolubility in chloroform and dichloromethane. Gly-Van-PACM and Gly-Van-DytekA indicated EEW values of 147 and 136 respectively, significantly lower than the theoretical value of 295. Considering the high presence of hydrolyzed imine, glycidylation most likely occurred concurrently on the vanillin by-product, effectively lowering the EEW value.

Additionally, it is possible for the epichlorohydrin to glycidylate the imine hydrogen, lowering the EEW value. Gel permeation chromatography collected the  $M_n$  for all samples except for Gly-Van-PD due to insolubility in tetrahydrofuran. Gly-Van-DytekA showed comparable values between theoretical  $M_n$  and actual  $M_n$  near 500, however the Gly-Van-PACM showed a  $M_n$  of 814, significantly higher than the theoretical  $M_n$ . As the Schiff base is hydrolyzed, the resulting amines are capable of interacting with the polystyrene column of the GPC, skewing the  $M_n$  data. As a result, it is difficult to fully rely on the  $M_n$  for both compounds. Given the hydrolytic instability of the Schiff base products during the glycidylation process compounded with unreliable  $M_n$  and EEW data, further crosslinking was not explored. Route B was instead investigated in order to eliminate the potential for imine hydrolysis.

#### **4.3.1.2. Route B: glycidylation, Schiff base/crosslinking**

Previously from Route A, vanillin-Schiff base compounds were synthesized and glycidylated using epichlorohydrin, however, potential hydrolytic instability of the imine during glycidylation led to the exploration of an alternative approach. Route B began with initial glycidylation of the vanillin monomer, followed by crosslinking through both the epoxy and the aldehyde. The elimination of a separate Schiff base step in addition to minimizing imine hydrolysis makes Route B an appealing option for the production of vanillin-epoxy thermosets.

The glycidylation of vanillin produced a yellow solid material which was characterized using FTIR,  $^1\text{H}$  NMR and EEW. FTIR is shown in Figure 4.2.

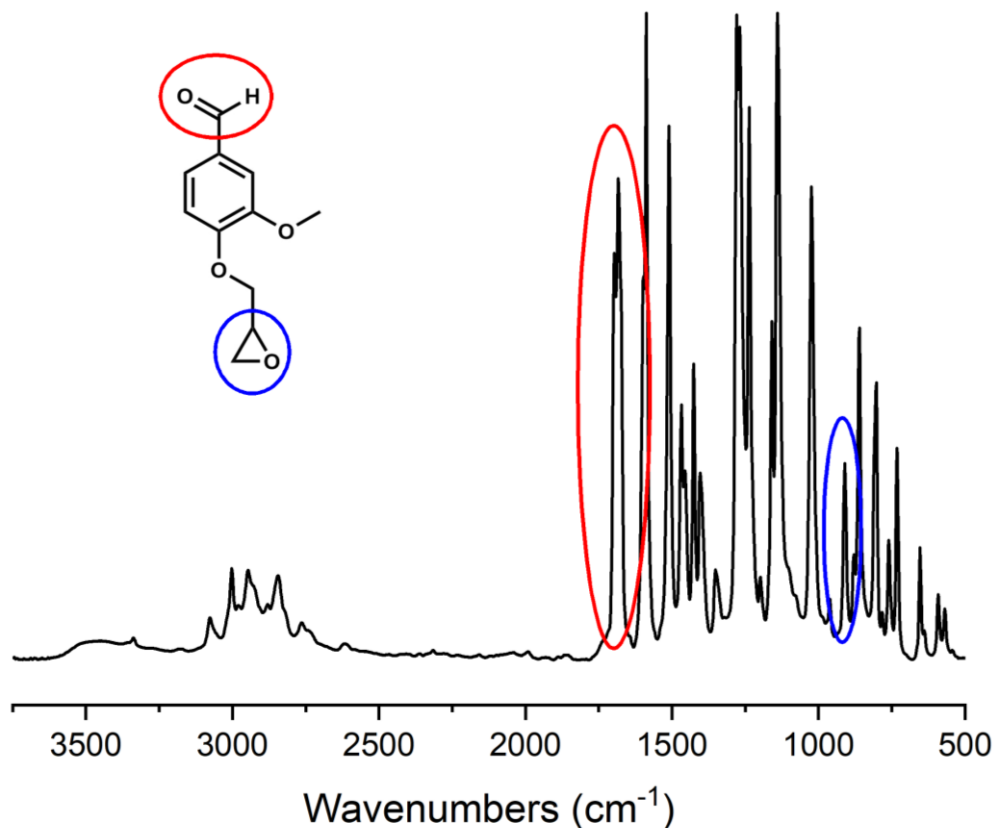


**Figure 4.2. Gly-Van FTIR**

The FTIR of glycidylated vanillin shows the strong appearance of the aldehyde at  $\sim 1680$   $\text{cm}^{-1}$  in addition to the C-O-C stretch for the epoxy at  $908$   $\text{cm}^{-1}$ . There is a slight alcohol peak near  $\sim 3500$   $\text{cm}^{-1}$ , indicating a small amount of vanillin was not epoxidized. However, the clean spectra and proper identification of the oxirane and aldehyde indicate successful synthesis of glycidylated vanillin.  $^1\text{H}$  NMR was run on Gly=Van to fully confirm the product and is shown in Figure 4.3.

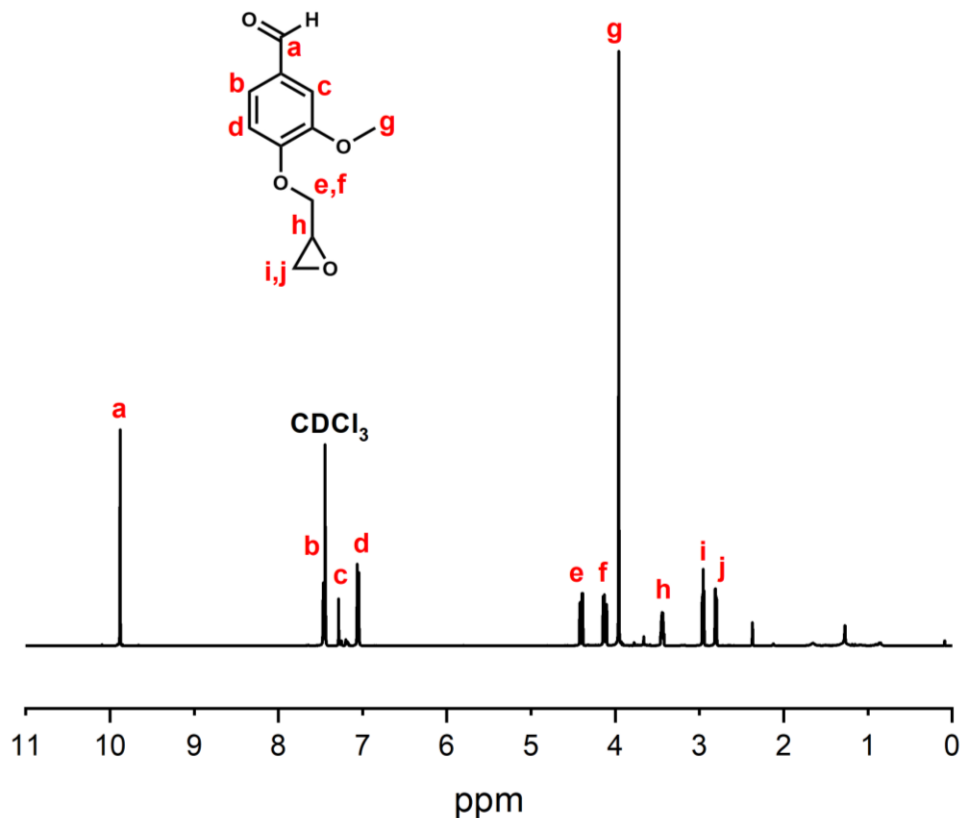


**Figure 4.3. Gly-Van  $^1\text{H}$  NMR**

From the  $^1\text{H}$  NMR spectra of Gly-Van, all peaks were correctly identified with successful glycidylation. Peaks e-f and h-j all signal the presence of an epoxy group attached to the phenolic position of vanillin. The EEW value for Gly-Van was found to be 211, comparable to the theoretical EEW of 208. From the FTIR,  $^1\text{H}$  NMR and EEW, Gly-Van was successfully synthesized using epichlorohydrin and will further be crosslinked with diamines.

Glycidylated vanillin contains both an aldehyde and epoxy that are capable of readily reacting with amines. As a result, the Gly-Van monomer serves as a biobased crosslinker for epoxy thermosets. It is suspected that the Schiff base reaction proceeds more readily than the epoxy-amine reaction, and therefore Gly-Van-SB will be produced prior to epoxy crosslinking.

Gly-Van was crosslinked using diamines such as ED, DytexA, IPDA, PACM, Pri1071, Pri1073, Pri1074 in addition to triamines Jeff T403 and Jeff D230. Epoxy to amine ratios were investigated at 1:0.5, 1:1 and 1:2. The cured materials are shown in Figure 4.4.

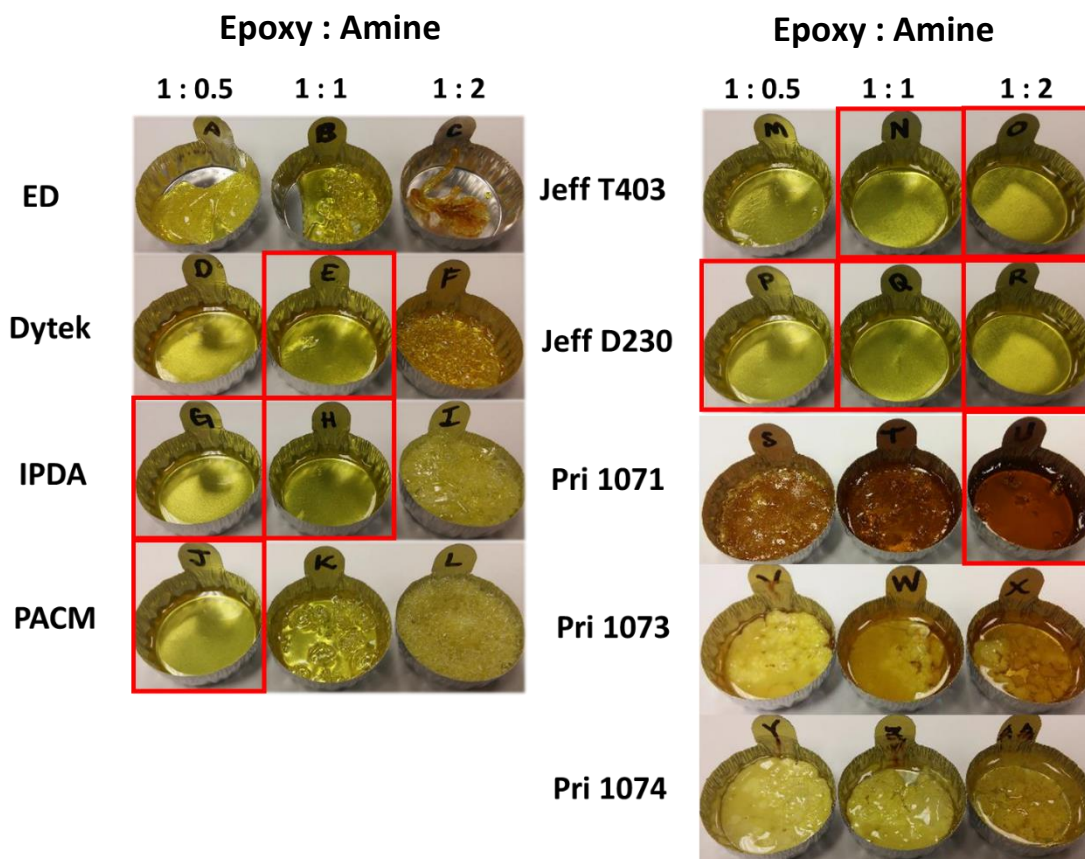


**Figure 4.4. Vanillin-epoxy thermosets**

All cured materials were transparent bright yellow to orange in color, with the Priamine thermosets containing opaque white masses within the resin. Ethylene diamine was the most reactive amine, curing within 3 minutes at ambient conditions. As a result, uniformly shaped thermosets with ED were a challenge, and further use of ED was limited. Dytex A, IPDA and PACM resins all produced significant trapped air bubbles at an epoxy to amine ratio of 1:2, a result of too rapid a cure rate. The Priamine thermosets were all tacky post-curing with the



exception of Priamine1071 at 1:2. Priamine 1071 has a slightly higher functionality at roughly 2.2 amine groups per molecule, whereas the 1073 and 1074 contain only 2 amine groups per molecule. Almost all Jeffamine materials produced uniform, cured resins with minimal air bubbles. The optimal vanillin-epoxy thermosets in regard to appearance and cure are highlighted in the red boxes in Figure 4.4. Only the cured materials without bubbles were further characterized by thermogravimetric analysis (TGA) and differential scanning calorimetry (DSC). The temperature at 5% weight loss was recorded from TGA and the glass transition temperature was recorded from DSC. Thermograms from DSC are shown in Figure 4.5 and  $T_{5\%}$  and  $T_g$  values are shown in Table 4.4.

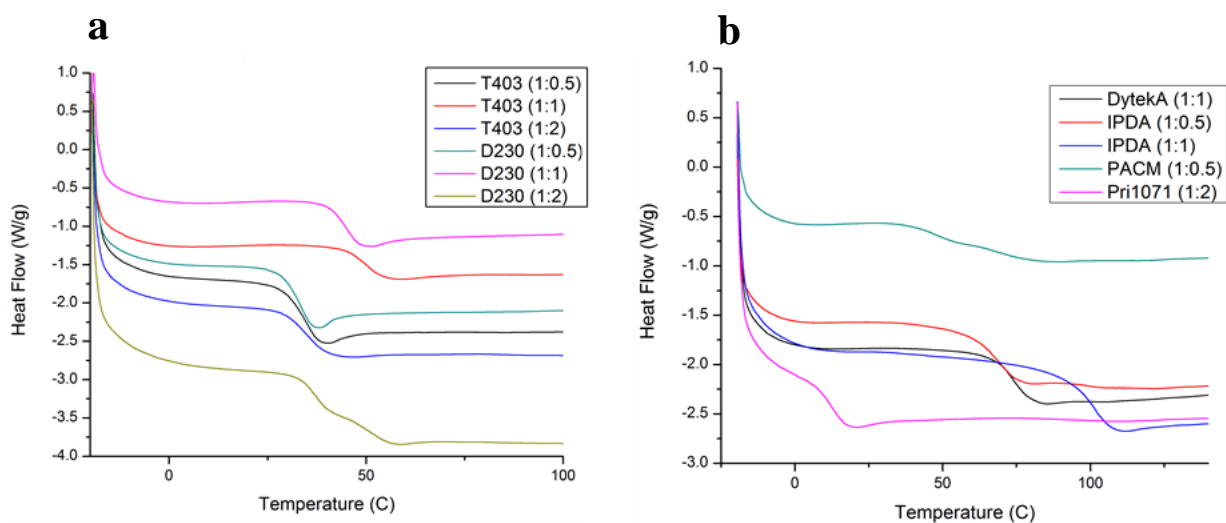


**Figure 4.5. DSC of Vanillin-epoxy thermosets for a.) triamines (Jeffamines) and b.) diamines**

**Table 4.4. Temperature at 5% weight loss ( $T_{5\%}$ ) and glass transition temperature ( $T_g$ ) of vanillin-epoxy thermosets**

Sample	$T_{5\%}$	$T_g$
Dytek A (1:1)	265.32	73.88
IPDA (1:0.5)	231.15	69.95
IPDA (1:1)	291.48	101.77
PACM (1:0.5)	205.16	47.22, 70.20
Jeff T403 (1:0.5)	-----	35.36
Jeff T403 (1:1)	284.34	50.15
Jeff T403 (1:2)	291.00	33.81
Jeff D230 (1:0.5)	230.91	33.83
Jeff D230 (1:1)	276.06	44.89
Jeff D230 (1:2)	276.49	37.61, 50.38
Pri1071 (1:2)	311.79	11.70

The temperature at 5% weight loss was measured using thermogravimetric analysis and shown in Table 4.4. Priamine 1071 thermoset shows the highest  $T_{5\%}$  at ~312 °C, whereas PACM shows the lowest  $T_{5\%}$  at 205 °C. As the epoxy to amine ratio increases from 1:0.5 to 1:1, the  $T_{5\%}$  also increases.

Glass transition temperatures for the triamines (Figure 4.5 a) range between 33 and 50 °C. Jeffamine T403 shows an increase in  $T_g$  from 0.5:1 to 1:1 epoxy to amine, followed by a decrease in  $T_g$  at 2:1 epoxy to amine. For a higher  $T_g$ , a 1:1 epoxy to amine ratio is optimal for use of the Jeffamine T403. Jeffamine D230 at 1:2 epoxy to amine appears to show two distinct glass transition temperatures, however, D230 at 1:0.5 and 1:1 only shows one  $T_g$ . It is suspected

that higher D230 content creates a separate phase within the thermoset system. To minimize multiple phases and maximize  $T_g$ , a ratio of 1:1 epoxy to amine for D230 is sufficient.

For the diamine crosslinkers, Priamine 1071 displayed the lowest  $T_g$  value of 11.7 °C due to the long, flexible aliphatic chain that increases mobility within the system. Similar to Jeffamine D230, PACM shows two distinct  $T_g$  values at 47 and 70, indicating two distinct phases within the thermoset system. The highest  $T_g$  from the Gly-Van thermosets came from IPDA at 1:1 epoxy to amine, giving a value of ~102 °C, followed by Dytek A with a  $T_g$  of ~74 °C. Generally, 1:1 epoxy to amine ratios produced higher  $T_g$  values, and therefore the control comparisons made using diglycidyl ether of bisphenol A (DGEBA) were formulated at 1:1 for Dytek A, IPDA, Jeffamine T403 and Jeffamine D230. Given the multiple  $T_g$  values within PACM in addition to the low  $T_{5\%}$  at 205 °C, the control comparison was excluded for that amine. Table 4.5 shows the DGEBA control  $T_{5\%}$  and  $T_g$  compared to the Gly-Van thermosets with the same amine and ratio. DGEBA with Jeffamine T403 at 1:1 epoxy to amine ratio did not cure, and therefore data was not collected for that sample.

**Table 4.5. Gly-Van vs DGEBA epoxy thermosets for T<sub>5%</sub> and T<sub>g</sub>**

<b>Epoxy</b>	<b>Amine</b>	<b>E : A</b>	<b>T<sub>5%</sub></b>	<b>T<sub>g</sub></b>
Gly-Van	Dytek A	1:1	265.32	73.88
DGEBA	Dytek A	1:1	328.16	60.11
Gly-Van	IPDA	1:1	291.48	101.77
DGEBA	IPDA	1:1	317.23	45.66
Gly-Van	Jeff T403	1:1	284.34	50.15
DGEBA	Jeff T403	1:1	-	-
Gly-Van	Jeff D230	1:1	276.06	44.89
DGEBA	Jeff D230	1:1	272.59	37.61

Comparing the thermal properties of traditional epoxy thermosets (DGEBA) with the synthesized biobased vanillin thermosets (Table 4.5), two interesting trends appear. First, the temperature at 5% weight loss appears to be higher for the DGEBA thermosets with the exception of Jeffamine D230. However, all Gly-Van thermosets show higher T<sub>g</sub> values compared to the corresponding DGEBA epoxies. For IPDA, vanillin-based epoxies show T<sub>g</sub> value at ~102 °C, significantly higher than the corresponding DGEBA thermoset at ~46 °C. The higher T<sub>g</sub> values for the biobased thermosets are promising, as significant challenges in replacing petrochemical materials with renewables includes the development of competing if not superior properties.

Overall, Route B has proven successful in the synthesis and crosslinking of vanillin-epoxy thermosets. One disadvantage to Route B, however, includes the limitation in diversity of amines used for the SB and epoxy crosslinking. The use of multiple amines may be possible

when considering the Schiff base will form first, and therefore stoichiometric amounts of multiple amines and the order of addition may be controlled in future studies. While thermally superior biobased epoxies were developed, the bright yellow color of the vanillin thermosets remains undesirable. Attempts at reducing the Schiff base to eliminate the bright colors were explored in the next section.

#### **4.3.2. Reductive amination and crosslinking of vanillin-Schiff base compounds**

From the previous development of biobased epoxy thermosets, the resulting materials produced brightly-colored resins due to the conjugation of the imine and the aromatic vanillin. As a result, attempts at reducing the imine via reductive amination were explored in hopes of producing a clear, transparent material. Various techniques for reductive amination have been described in literature, with the majority pertaining to the use of sodium borohydride<sup>131-144</sup> and sodium triacetoxymborohydride<sup>145-151</sup> as reducing agents. The method for reductive amination in this study focuses on the use of NaBH<sub>4</sub>.

Initial reductive amination methodology was studied on the Schiff base compound composed of vanillin and cyclohexylamine. The Schiff base was initially formed via the previously described methanol method, followed by reduction using sodium borohydride. Boric acid and p-toluenesulfonic acid were explored as activators.<sup>132</sup> See Table 4.1 (in experimental section) for formulation identification of reducing agents and acid activators. Resulting products changed from a dark orangish appearance (Schiff base) to a white powder (reduced-Schiff base) after reductive amination. The FTIR and <sup>1</sup>H NMR for each Red-Van-SB cyclohexylamine product is shown in Figure 4.6.

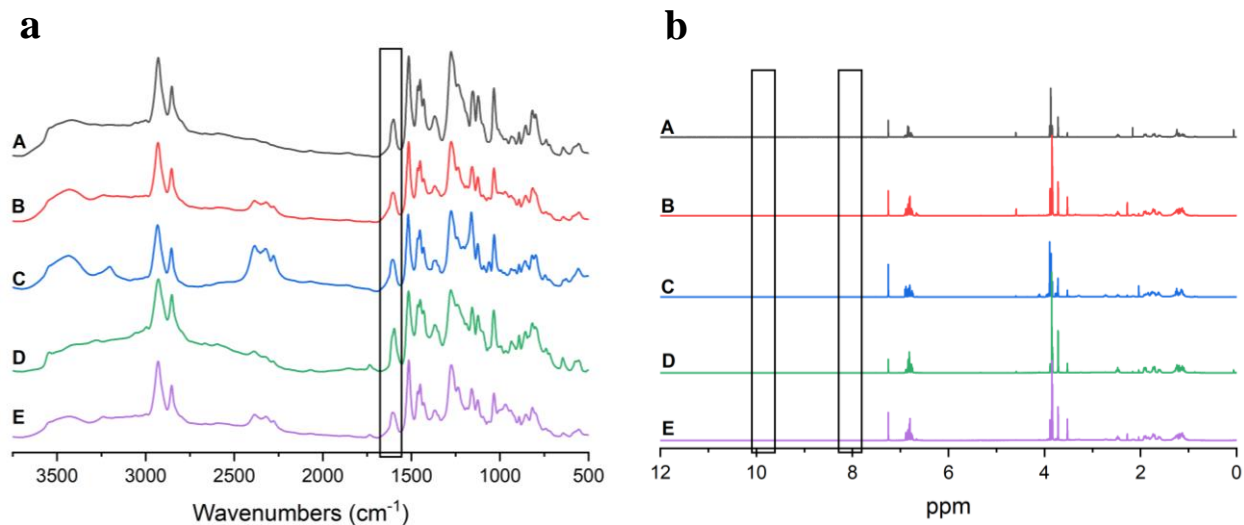


**Figure 4.6. Vanillin-cyclohexylamine reduction products a.) FTIR and b.)  $^1\text{H}$  NMR**

From the FTIR (Figure 4.6 a), all N-H peaks from the reduced imine are present at  $\sim 1600$   $\text{cm}^{-1}$ , however the sharp double peak near  $\sim 3000$   $\text{cm}^{-1}$  indicates the presence of primary amines. Successful synthesis of the Red-Van-SB would produce only secondary amines, and therefore further investigation into the final products using  $^1\text{H}$  NMR was necessary. The lack of aldehyde around  $\sim 1680$   $\text{cm}^{-1}$  in FTIR indicates that the formation of primary amine did not revert the vanillin unit back into an aldehyde. Additionally, the lack of imine near  $\sim 1640$ - $1660$   $\text{cm}^{-1}$  shows complete reduction of the Schiff base products. The  $^1\text{H}$  NMR (Figure 4.6 b) for each method A-E confirms the absence of both the aldehyde ( $\sim 9.8$  ppm) and imine ( $\sim 8.2$  ppm) peaks in each spectrum, indicating successful reductive amination of the vanillin-cyclohexylamine SB compound. However, overlapping peaks at lower ppm prove difficult for complete analysis. No significant difference in product formation between each method was observed, and therefore no acid activator was necessary for successful reduction of the vanillin-SB compounds. Simply using a 1:1 imine to  $\text{NaBH}_4$  is sufficient for complete reductive amination. Schiff base compounds consisting of vanillin-cyclohexylamine and vanillin-butylamine were synthesized

according to Method E consisting of no activator and 1 equivalent of NaBH<sub>4</sub>. Figure 4.7 shows the <sup>1</sup>H NMR spectra for the Red-Van-SB compounds of cyclohexylamine and butylamine.

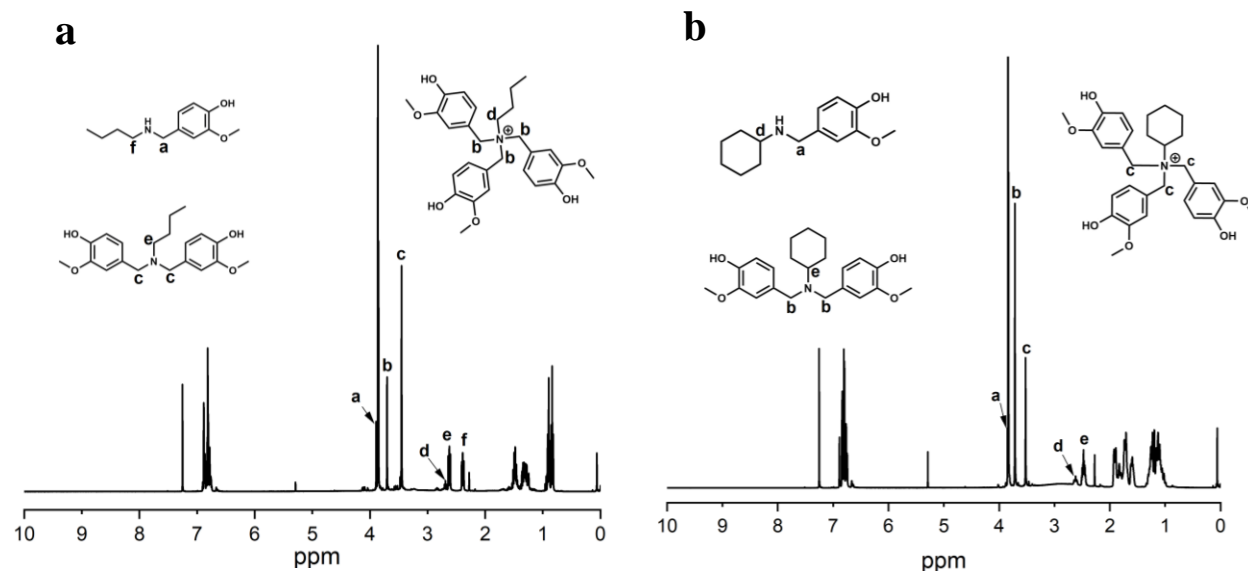


**Figure 4.7.** <sup>1</sup>H NMR for Red-Van-SB with a.) butylamine and b.) cyclohexylamine

From the <sup>1</sup>H NMR for both Red-Van-BA and Red-Van-CA, dimers and trimers of the reduced Schiff base compounds were identified, with the prominent product being the dimer. HRMS was utilized to confirm the presence of the monomer, dimer and trimer formed from Van-SB reductive amination. HRMS of the reduced products is shown in Figure 4.8 and Table 4.6.

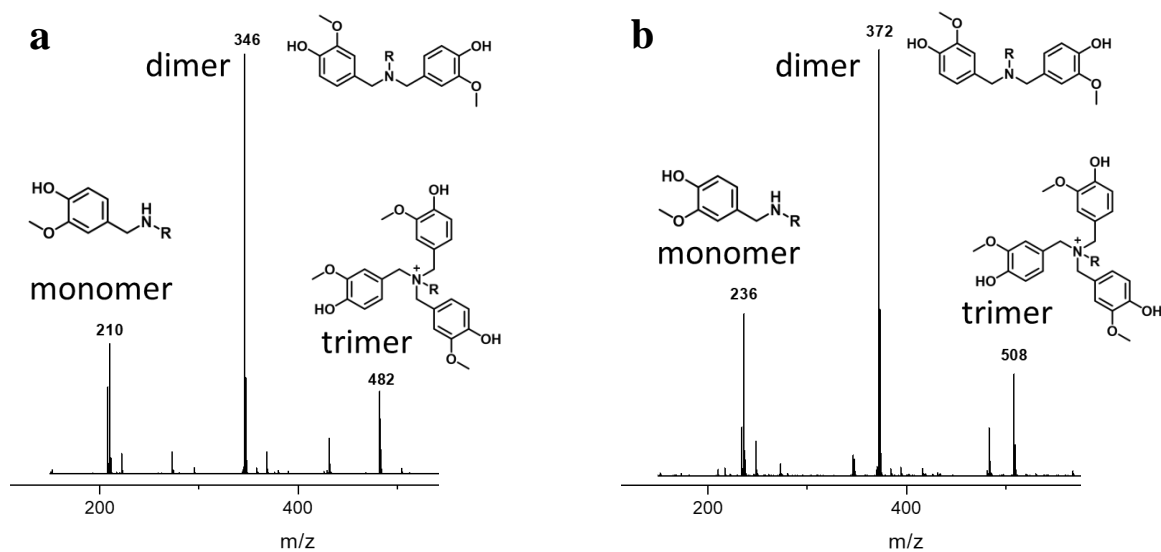


**Figure 4.8.** HRMS of a.) Van-butylamine (Van-BA) and b.) Van-cyclohexylamine (Van-CA)

**Table 4.6.** HRMS m/z values for Van-SB products

Amine	Monomer	Dimer	Trimer
Butylamine	209.28	345.43	482.59
Cyclohexylamine	235.32	371.47	508.63

From the HRMS data shown in Figure 4.8 and Table 4.6, reduced Schiff base compounds were identified and labeled as monomer. Similar to the  $^1\text{H}$  NMR data, the majority of product was found to be dimerized reduced-SB compound with a small amount of trimer present. During the reductive amination with sodium borohydride, the reactive protonated imine is more susceptible to reacting with another imine, releasing a primary amine and forming a dimer structure. This explains the distinct primary amine peak at  $\sim 3000\text{ cm}^{-1}$  shown in the FTIR spectra of the reduced SB compounds. Primary amine was removed prior to glycidylation by washing



the compound with toluene. While the product consisted mostly of dimer, glycidylation of monomers, dimers and trimers will result in di and tri-functional epoxidized compounds.

Previously synthesized Red-Van-SB compounds containing monomer, dimer and trimer were glycidylated using epichlorohydrin. Glycidylated products appeared as light yellow, high viscosity liquids (Figure 4.9) and were characterized by  $^1\text{H}$  NMR (Figure 4.9).

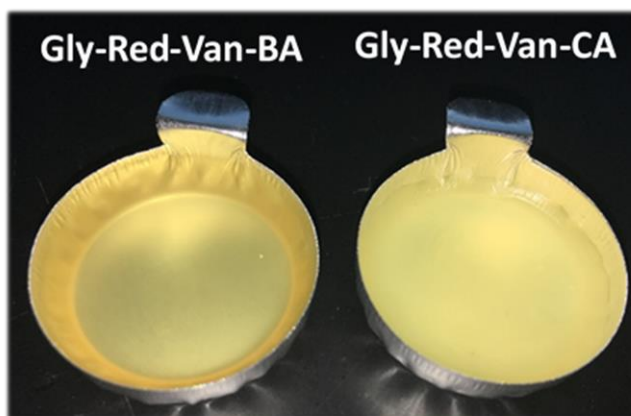


**Figure 4.9.** Gly-Red-Van-SB compounds of butylamine (left) and cyclohexylamine (right)

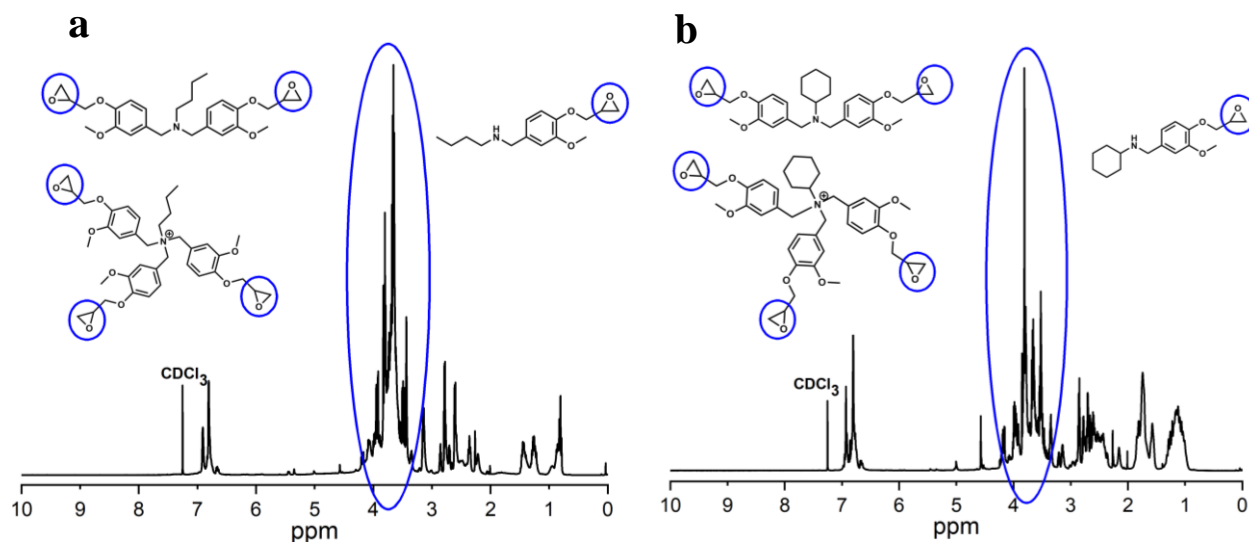


**Figure 4.10.**  $^1\text{H}$  NMR for Gly-Red-Van-SB with a.) butylamine and b.) cyclohexylamine

Characterization of Gly-Red-Van-SB compounds was done using  $^1\text{H}$  NMR for confirmation of epoxy groups. Figure 4.10 shows the spectra for both Gly-Red-Van-BA and Gly-Red-Van-CA. From both  $^1\text{H}$  NMR spectra, a large concentration of epoxy groups appears between  $\sim 3\text{-}4$  ppm, indicating the presence of glycidylated products. However, distinctions between monomer, dimer and trimer are unable to be differentiated due to overlapping peaks of the highly concentrated epoxy groups. To measure the extent of glycidylation, epoxy equivalent weight titrations were performed and compared against theoretical EEW values for monomer, dimer and trimer for each Gly-Red-Van-SB compound (Table 4.7).

**Table 4.7. Epoxy equivalent weight of Gly-Red-Van-SB products and theoretical monomer, dimer and trimer EEW values for comparison**

Product	EEW	Mono-epoxy	Di-epoxy	Dimer	Trimer
		EEW	EEW	EEW	EEW
Gly-Red-Van-BA	281.14	291.18	160.71	228.78	216.93
Gly-Red-Van-CA	180.19	265.17	173.73	241.80	225.45

Gly-Red-Van-BA shows an EEW value of  $\sim 281$ , a comparable value to the monomer with a singular epoxy attached through the phenol. From the Red-Van-SB products, the product consisted of mostly dimer, and therefore it is likely that full glycidylation did not occur. However, sufficient functionality is present within the mixture for further crosslinking with amines. For Gly-Red-Van-CA, the EEW was significantly lower, showing similar values to the di-epoxy monomer. However, considering the mixture of compounds, it is difficult to determine the extent of glycidylation for each monomer, dimer and trimer. Given the low EEW, however, it is likely that full glycidylation occurred on the monomer, dimer and trimer mixture. A separation

of products was not necessary, as sufficient functionality was present within both Gly-Red-Van-SB products for further amine crosslinking.

Crosslinking of the glycidylated compounds was performed by mixing with IPDA, PACM, and TMD at epoxy to amine ratios of 1:2, 1:1 and 1:0.5. Each of the crosslinked resins produced a solid, transparent material as shown in Figure 4.11. Although there are slight yellow tints with IPDA and PACM, the yellowness of the Gly-Red-Van-SB has significantly reduced after crosslinking with amines relative to the Schiff base compound. Cure time for the Gly-Red-Van-BA required 4 hours at 100 °C, whereas the Gly-Red-Van-CA cured within 2 hours at 85 °C. The butylamine compound required more time at higher temperatures due to the higher EEW value, whereas the cyclohexylamine compound contained more functionality, and therefore higher reactivity.

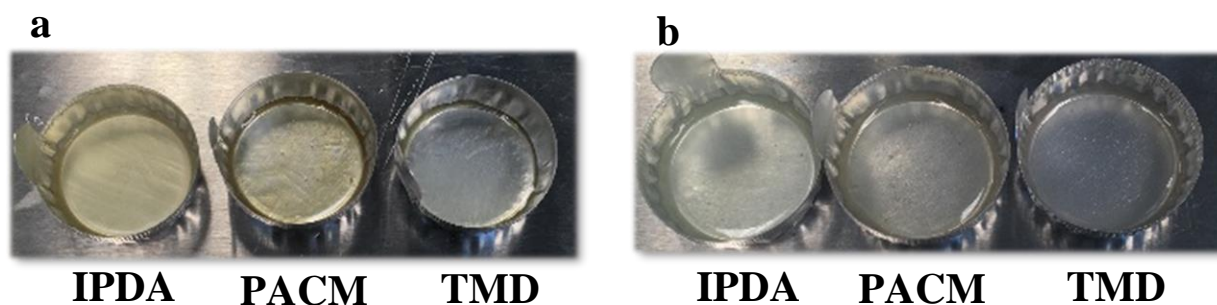


**Figure 4.11. a.) Gly-Red-Van-BA and b.) Gly-Red-Van-CA crosslinked with amines**

Thermal analysis of the cured vanillin epoxies was carried out using TGA and DSC to measure the temperature at 5% weight loss ( $T_{5\%}$ ) and the glass transition temperature ( $T_g$ ) respectively (Table 4.8). The  $T_g$  for Gly-Red-Van-BA thermosets was not observed, indicating minimal crosslinking or a  $T_g$  value below the measured temperature minimum of 0°C.

**Table 4.8. Temperature at 5% weight loss (T5%) and glass transition temperature (T<sub>g</sub>) of Gly-Red-Van-SB thermosets**

<b>Epoxy</b>	<b>Amine</b>	<b>E : A</b>	<b>T<sub>5%</sub></b>	<b>T<sub>g</sub></b>
Gly-Red-Van-BA	IPDA	1:2	246.58	-
Gly-Red-Van-BA	IPDA	1:1	234.40	-
Gly-Red-Van-BA	IPDA	1:0.5	210.17	-
Gly-Red-Van-BA	PACM	1:2	244.51	-
Gly-Red-Van-BA	PACM	1:1	238.61	-
Gly-Red-Van-BA	PACM	1:0.5	214.78	-
Gly-Red-Van-BA	TMD	1:2	237.51	-
Gly-Red-Van-BA	TMD	1:1	225.16	-
Gly-Red-Van-BA	TMD	1:0.5	206.65	-
Gly-Red-Van-CA	IPDA	1:2	245.42	77.14
Gly-Red-Van-CA	IPDA	1:1	251.99	69.76
Gly-Red-Van-CA	IPDA	1:0.5	237.93	40.68
Gly-Red-Van-CA	PACM	1:2	274.78	90.25
Gly-Red-Van-CA	PACM	1:1	259.67	80.93
Gly-Red-Van-CA	PACM	1:0.5	233.41	45.98
Gly-Red-Van-CA	TMD	1:2	250.76	57.13
Gly-Red-Van-CA	TMD	1:1	244.59	59.76
Gly-Red-Van-CA	TMD	1:0.5	221.80	29.11

From the thermal analysis data, the temperature at 5% weight loss increases as the amine content increases (epoxy to amine ratio decreases). Additionally, Gly-Red-Van-CA with PACM at 1:2 epoxy to amine shows the largest  $T_{5\%}$  at  $\sim 275^{\circ}\text{C}$ . For Gly-Red-Van-BA, however, IPDA at 1:2 epoxy to amine shows the largest  $T_{5\%}$  at  $\sim 247^{\circ}\text{C}$ . Challenges with the butylamine-based epoxy included lower reactivity as a result of decreased functionality. Therefore, the crosslink density is likely lower, a reflection in the  $T_{5\%}$  and inconclusive  $T_g$  values. The  $T_g$  values for Gly-Red-Van-CA thermosets generally increase as the amine content increases with the exception of TMD. PACM at 1:2 epoxy to amine ratio has the largest  $T_g$  of  $\sim 90^{\circ}\text{C}$ , whereas TMD at 1:0.5 ratio has the lowest  $T_g$  of  $\sim 29^{\circ}\text{C}$ . Due to the brittle nature of the thermoset materials, mechanical analysis was challenging to explore, however future crosslinking with longer aliphatic-chain amines may result in more flexible cured epoxies. Given the tunable thermal properties based on amine crosslinker and epoxy to amine ratio, Gly-Red-Van-SB compounds show promising potential as transparent, biobased epoxy thermosets. Future investigation into additional reduced vanillin-Schiff base compounds with monoamines, diamines and triamines would be beneficial in understanding more of the structure-property relationships between the Schiff base structure compounds and thermoset performance.

#### **4.4. Conclusion**

In this study, vanillin-Schiff base compounds were successfully synthesized and glycidylated with epichlorohydrin. The resulting compounds were crosslinked with amines to form biobased thermosets. Comparisons to DGEBA shows that the vanillin-epoxy thermosets have higher glass transition temperatures when formulated with the same amine at the same epoxy to amine ratio. Challenges in the bright yellow appearance caused by conjugation of the Schiff base and aromatic vanillin were overcome by reductive amination of the imine using

sodium borohydride. A successful reductive amination method was established using 1 equivalent of NaBH<sub>4</sub>. Glycidylation of the reduced vanillin-Schiff base products resulted in mostly dimerized compounds that were further crosslinked with amines, producing transparent films. Transparent, biobased epoxy thermosets from vanillin were successfully produced, and further investigation into structure-property relationships and mechanical performance of the cured resins will allow for further optimization of vanillin-derived epoxies.

#### 4.5. References

1. Kumar, S.; Samal, S. K.; Mohanty, S.; Nayak, S. K., Recent Development of Biobased Epoxy Resins: A Review. *Polym.-Plast. Technol. Eng.* **2018**, 57 (3), 133-155.
2. Kumar, S.; Krishnan, S.; Mohanty, S.; Nayak, S. K., Synthesis and characterization of petroleum and biobased epoxy resins: a review. *Polym. Int.* **2018**, 67 (7), 815-839.
3. Leranath, C.; Hajszan, T.; Szigeti-Buck, K.; Bober, J.; MacLusky, N. J., Bisphenol A prevents the synaptogenic response to estradiol in hippocampus and prefrontal cortex of ovariectomized nonhuman primates. *Proceedings of the National Academy of Sciences of the United States of America* **2008**, 105 (37), 14187-14191.
4. Sekizawa, J., Low-dose effects of bisphenol A: a serious threat to human health? (1880-3989 (Electronic)).
5. Vandenberg, L. N.; Hauser, R.; Marcus, M.; Olea, N.; Welshons, W. V., Human exposure to bisphenol A (BPA). *Reprod. Toxicol.* **2007**, 24 (2), 139-177.
6. Dekant, W.; Völkel, W., Human exposure to bisphenol A by biomonitoring: Methods, results and assessment of environmental exposures. **2008**; p 114-34.

7. Fernández, M.; Arrebola, J.; Taoufiki, J.; Navalón, A.; Ballesteros, O.; Pulgar, R.; Vílchez, J.; Olea, N., Bisphenol-A and chlorinated derivatives in adipose tissue of women. **2007**; p 259-64.
8. Vandenberg, L. N.; Maffini, M. V.; Sonnenschein, C.; Rubin, B. S.; Soto, A. M., Bisphenol-A and the great divide: a review of controversies in the field of endocrine disruption. *Endocr. Rev.* **2009**, 30 (1), 75-95.
9. Ding, C.; Matharu, A. S., Recent Developments on Biobased Curing Agents: A Review of Their Preparation and Use. *ACS Sustainable Chem. Eng.* **2014**, 2 (10), 2217-2236.
10. Auvergne, R.; Caillol, S.; David, G.; Boutevin, B.; Pascault, J.-P., Biobased thermosetting epoxy: present and future. *Chem Rev* **2014**, 114 (2), 1082-1115.
11. Unnikrishnan, K. P.; Thachil, E. T., Synthesis and characterization of cardanol-based epoxy systems. *Des. Monomers Polym.* **2008**, 11 (6), 593-607.
12. Yadav, R.; Srivastava, D., Blends of cardanol-based epoxidized novolac resin and CTBN for application in surface coating: a study on thermal, mechanical, chemical, and morphological characteristics. *J. Coat. Technol. Res.* **2010**, 7 (5), 557-568.
13. Rao, B. S.; Palanisamy, A., Synthesis of bio based low temperature curable liquid epoxy, benzoxazine monomer system from cardanol: Thermal and viscoelastic properties. *Eur. Polym. J.* **2013**, 49 (8), 2365-2376.
14. Jaillet, F.; Darroman, E.; Ratsimihety, A.; Auvergne, R.; Boutevin, B.; Caillol, S., New biobased epoxy materials from cardanol. *Eur. J. Lipid Sci. Technol.* **2014**, 116 (1), 63-73.
15. Darroman, E.; Bonnot, L.; Auvergne, R.; Boutevin, B.; Caillol, S., New aromatic amine based on cardanol giving new biobased epoxy networks with cardanol. *Eur. J. Lipid Sci. Technol.* **2015**, 117 (2), 178-189.

16. Darroman, E.; Durand, N.; Boutevin, B.; Caillol, S., New cardanol/sucrose epoxy blends for biobased coatings. *Prog. Org. Coat.* **2015**, 83, 47-54.
17. Dworakowska, S.; Cornille, A.; Bogdal, D.; Boutevin, B.; Caillol, S., Formulation of bio-based epoxy foams from epoxidized cardanol and vegetable oil amine. *Eur. J. Lipid Sci. Technol.* **2015**, 117 (11), 1893-1902.
18. Darroman, E.; Durand, N.; Boutevin, B.; Caillol, S., Improved cardanol derived epoxy coatings. *Prog. Org. Coat.* **2016**, 91, 9-16.
19. Nguyen, T. K. L.; Livi, S.; Soares, B. G.; Barra, G. M. O.; Gerard, J.-F.; Duchet-Rumeau, J., Development of Sustainable Thermosets from Cardanol-based Epoxy Prepolymer and Ionic Liquids. *ACS Sustainable Chem. Eng.* **2017**, 5 (9), 8429-8438.
20. Qin, J.; Liu, H.; Zhang, P.; Wolcott, M.; Zhang, J., Use of eugenol and rosin as feedstocks for biobased epoxy resins and study of curing and performance properties. *Polym. Int.* **2014**, 63 (4), 760-765.
21. Wan, J.; Gan, B.; Li, C.; Molina-Aldareguia, J.; Li, Z.; Wang, X.; Wang, D.-Y., A novel biobased epoxy resin with high mechanical stiffness and low flammability: synthesis, characterization and properties. *J. Mater. Chem. A* **2015**, 3 (43), 21907-21921.
22. Wan, J.; Gan, B.; Li, C.; Molina-Aldareguia, J.; Kalali, E. N.; Wang, X.; Wang, D.-Y., A sustainable, eugenol-derived epoxy resin with high biobased content, modulus, hardness and low flammability: Synthesis, curing kinetics and structure-property relationship. *Chem. Eng. J. (Amsterdam, Neth.)* **2016**, 284, 1080-1093.
23. Wan, J.; Zhao, J.; Gan, B.; Li, C.; Molina-Aldareguia, J.; Zhao, Y.; Pan, Y.-T.; Wang, D.-Y., Ultrastiff Biobased Epoxy Resin with High Tg and Low Permittivity: From Synthesis to Properties. *ACS Sustainable Chem. Eng.* **2016**, 4 (5), 2869-2880.



24. Faye, I.; Decostanzi, M.; Ecochard, Y.; Caillol, S., Eugenol bio-based epoxy thermosets: from cloves to applied materials. *Green Chem.* **2017**, 19 (21), 5236-5242.
25. Liu, T.; Hao, C.; Wang, L.; Li, Y.; Liu, W.; Xin, J.; Zhang, J., Eugenol-Derived Biobased Epoxy: Shape Memory, Repairing, and Recyclability. *Macromolecules* (Washington, DC, U. S.) **2017**, 50 (21), 8588-8597.
26. Tomita, H.; Yonezawa, K. Epoxy resin. EP95609A1, **1983**.
27. Benyahya, S.; Aouf, C.; Caillol, S.; Boutevin, B.; Pascault, J. P.; Fulcrand, H., Functionalized green tea tannins as phenolic prepolymers for bio-based epoxy resins. *Ind. Crops Prod.* **2014**, 53, 296-307.
28. Aouf, C.; Benyahya, S.; Esnouf, A.; Caillol, S.; Boutevin, B.; Fulcrand, H., Tara tannins as phenolic precursors of thermosetting epoxy resins. *Eur. Polym. J.* **2014**, 55, 186-198.
29. Shnawa, H. A.; Khalaf, M. N.; Jahani, Y., Thermal degradation, dynamic mechanical and morphological properties of PVC stabilized with natural polyphenol-based epoxy resin. *Polym. Bull. (Heidelberg, Ger.)* **2018**, 75 (8), 3473-3498.
30. Kovash, C. S., Jr.; Pavlacky, E.; Selvakumar, S.; Sibi, M. P.; Webster, D. C., Thermoset Coatings from Epoxidized Sucrose Soyate and Blocked, Bio-Based Dicarboxylic Acids. *ChemSusChem* **2014**, 7 (8), 2289-2294.
31. Shabeer, A.; Garg, A.; Sundararaman, S.; Chandrashekhara, K.; Flanigan, V.; Kapila, S., Dynamic mechanical characterization of a soy based epoxy resin system. *J. Appl. Polym. Sci.* **2005**, 98 (4), 1772-1780.
32. Omonov, T. S.; Curtis, J. M., Biobased epoxy resin from canola oil. *J. Appl. Polym. Sci.* **2014**, 131 (8), 40142/1-40142/9.

33. Park, S.-J.; Jin, F.-L.; Lee, J.-R., Effect of biodegradable epoxidized castor oil on physicochemical and mechanical properties of epoxy resins. *Macromol. Chem. Phys.* **2004**, 205 (15), 2048-2054.
34. Park, S.-J.; Jin, F.-L.; Lee, J.-R., Synthesis and thermal properties of epoxidized vegetable oil. *Macromol. Rapid Commun.* **2004**, 25 (6), 724-727.
35. Kadam, A.; Pawar, M.; Yemul, O.; Thamke, V.; Kodam, K., Biodegradable biobased epoxy resin from karanja oil. *Polymer* **2015**, 72, 82-92.
36. Manthey, N. W.; Cardona, F.; Aravinthan, T.; Cooney, T., Cure kinetics of an epoxidized hemp oil based bioresin system. *J. Appl. Polym. Sci.* **2011**, 122 (1), 444-451.
37. Wu, X.; Zhang, X.; Yang, S.; Chen, H.; Wang, D., The study of epoxidized rapeseed oil used as a potential biodegradable lubricant. *J. Am. Oil Chem. Soc.* **2000**, 77 (5), 561-563.
38. Caillol, S. In *Synthesis of biobased building blocks from vegetable oils: A chemicals platform approach for polymer synthesis*, American Chemical Society: **2016**; pp GC+E-46.
39. Cho, J. K.; Lee, J.-S.; Jeong, J.; Kim, B.; Kim, B.; Kim, S.; Shin, S.; Kim, H.-J.; Lee, S.-H., Synthesis of carbohydrate biomass-based furanic compounds bearing epoxide end group(s) and evaluation of their feasibility as adhesives. *J. Adhes. Sci. Technol.* **2013**, 27 (18-19), 2127-2138.
40. Hu, F.; La Scala, J. J.; Sadler, J. M.; Palmese, G. R., Synthesis and Characterization of Thermosetting Furan-Based Epoxy Systems. *Macromolecules* (Washington, DC, U. S.) **2014**, 47 (10), 3332-3342.

41. Nameer, S.; Larsen, D. B.; Duus, J. O.; Daugaard, A. E.; Johansson, M., Biobased Cationically Polymerizable Epoxy Thermosets from Furan and Fatty Acid Derivatives. *ACS Sustainable Chem. Eng.* **2018**, 6 (7), 9442-9450.
42. Mantzaridis, C.; Brocas, A.-L.; Llevot, A.; Cendejas, G.; Auvergne, R.; Caillol, S.; Carlotti, S.; Cramail, H., Rosin acid oligomers as precursors of DGEBA-free epoxy resins. *Green Chem.* **2013**, 15 (11), 3091-3098.
43. Brocas, A.-L.; Llevot, A.; Mantzaridis, C.; Cendejas, G.; Auvergne, R.; Caillol, S.; Carlotti, S.; Cramail, H., Epoxidized rosin acids as co-precursors for epoxy resins. *Des. Monomers Polym.* **2014**, 17 (4), 301-310.
44. El-Ghazawy, R. A.; El-Saeed, A. M.; Al-Shafey, H. I.; Abdul-Raheim, A.-R. M.; El-Sockary, M. A., Rosin based epoxy coating: Synthesis, identification and characterization. *Eur. Polym. J.* **2015**, 69, 403-415.
45. Liu, X. Z., Jin; Ma, S. Itaconic acid diglycidyl ester, its preparation method and application. CN 102731440 A. **2012**.
46. Ma, S.; Liu, X.; Jiang, Y.; Tang, Z.; Zhang, C.; Zhu, J., Bio-based epoxy resin from itaconic acid and its thermosets cured with anhydride and comonomers. *Green Chemistry* **2013**, 15 (1), 245-254.
47. Xiong, Z.; Ma, S.; Fan, L.; Tang, Z.; Zhang, R.; Na, H.; Zhu, J., Surface hydrophobic modification of starch with bio-based epoxy resins to fabricate high-performance polylactide composite materials. *Compos. Sci. Technol.* **2014**, 94, 16-22.
48. Kumar, S.; Samal, S. K.; Mohanty, S.; Nayak, S. K., Synthesis and characterization of itaconic-based epoxy resins. *Polym. Adv. Technol.* **2018**, 29 (1), 160-170.

49. Hofmann, K.; Glasser, W. G., Engineering plastics from lignin. 21. Synthesis and properties of epoxidized lignin-poly(propylene oxide) copolymers. *J. Wood Chem. Technol.* **1993**, 13 (1), 73-95.
50. Liu, W.; Zhou, R.; Goh, H. L. S.; Huang, S.; Lu, X., From Waste to Functional Additive: Toughening Epoxy Resin with Lignin. *ACS Appl. Mater. Interfaces* **2014**, 6 (8), 5810-5817.
51. Ding, J.; Gu, L.; Dong, W.; Yu, H., Epoxidation modification of renewable lignin to improve the corrosion performance of epoxy coating. *Int. J. Electrochem. Sci.* **2016**, 11 (7), 6256-6265.
52. Zhao, S.; Abu-Omar, M. M., Synthesis of Renewable Thermoset Polymers through Successive Lignin Modification Using Lignin-Derived Phenols. *ACS Sustainable Chem. Eng.* **2017**, 5 (6), 5059-5066.
53. Fache, M.; Boutevin, B.; Caillol, S., Vanillin Production from Lignin and Its Use as a Renewable Chemical. *ACS Sustainable Chem. Eng.* **2016**, 4 (1), 35-46.
54. Xu, C.; Arancon, R. A. D.; Labidi, J.; Luque, R., Lignin depolymerisation strategies: towards valuable chemicals and fuels. *Chemical Society Reviews* **2014**, 43 (22), 7485-7500.
55. Pandey, M. P.; Kim, C. S., Lignin Depolymerization and Conversion: A Review of Thermochemical Methods. *Chemical Engineering & Technology* **2011**, 34 (1), 29-41.
56. Koike, T., Progress in development of epoxy resin systems based on wood biomass in Japan. *Polym. Eng. Sci.* **2012**, 52 (4), 701-717.
57. Fache, M.; Boutevin, B.; Caillol, S., Vanillin, a key-intermediate of biobased polymers. *Eur. Polym. J.* **2015**, 68, 488-502.

58. Nikafshar, S.; Zabihi, O.; Hamidi, S.; Moradi, Y.; Barzegar, S.; Ahmadi, M.; Naebe, M., A renewable bio-based epoxy resin with improved mechanical performance that can compete with DGEBA. *RSC Advances* **2017**, 7 (14), 8694-8701.
59. Fache, M.; Darroman, E.; Besse, V.; Auvergne, R.; Caillol, S.; Boutevin, B., Vanillin, a promising biobased building-block for monomer synthesis. *Green Chemistry* **2014**, 16 (4), 1987-1998.
60. Fache, M.; Augergne, R.; Boutevin, B.; Caillol, S., New vanillin-derived diepoxy monomers for the synthesis of biobased thermosets. *European Polymer Journal* **2014**.
61. Ng, F.; Bonnet, L.; David, G.; Caillol, S., Novel biobased and food contact epoxy coatings for glass toughening applications. *Prog. Org. Coat.* **2017**, 109, 1-8.
62. Panfilov, A. V.; Markovich, Y. D.; Ivashev, I. P.; Zhironov, A. A.; Eleev, A. F.; Kurochkin, V. K.; Kirsanov, A. T.; Nazarov, G. V., Sodium borohydride in reductive amination reactions. *Pharm. Chem. J.* **2000**, 34 (2), 76-78.
63. Cho, B. T.; Kang, S. K., Direct and indirect reductive amination of aldehydes and ketones with solid acid-activated sodium borohydride under solvent-free conditions. *Tetrahedron* **2005**, 61 (24), 5725-5734.
64. Alinezhad, H.; Tajbakhsh, M.; Ahangar, R. E., Reductive amination of aldehydes and ketones in a heterogeneous system in THF and under solvent-free conditions using sodium borohydride-silica phosphoric acid. *Monatsh. Chem.* **2008**, 139 (1), 21-25.
65. Alinezhad, H.; Tajbakhsh, M.; Hamidi, N., Direct reductive amination of carbonyl compounds using sodium borohydride-silica chloride. *Turk. J. Chem.* **2010**, 34 (2), 307-312.

66. Alinezhad, H.; Tajbakhsh, M.; Hamidi, N., Reductive amination of aldehydes and ketones using sodium borohydride in the presence of silica chloride under solvent-free conditions. *Chin. Chem. Lett.* **2010**, 21 (1), 47-50.
67. Alinezhad, H.; Tajbakhsh, M.; Mahdavi, N., One-pot reductive amination of carbonyl compounds using sodium borohydride-Amberlyst 15. *Synth. Commun.* **2010**, 40 (7), 951-956.
68. Alinezhad, H.; Tollabian, Z., One-pot reductive amination of carbonyl compounds using sodium borohydride-cellulose sulfuric acid. *Bull. Korean Chem. Soc.* **2010**, 31 (7), 1927-1930.
69. Tajbakhsh, M.; Hosseinzadeh, R.; Alinezhad, H.; Ghahari, S.; Heydari, A.; Khaksar, S., Catalyst-free one-pot reductive alkylation of primary and secondary amines and N,N-dimethylation of amino acids using sodium borohydride in 2,2,2-trifluoroethanol. *Synthesis* **2011**, (3), 490-496.
70. Lee, R.; Lee, S. B.; Lee, J. C. In Direct reductive amination of aldehydes and ketones with sodium borohydride and polyethyleneglycol 200 under solvent-free conditions, American Chemical Society: **2012**; pp SERM-313.
71. Revathi, H.; Thirumalaikumar, M., Reductive amination of aldehydes with sodium borohydride-silica gel system. *Chem. Sci. Trans.* **2013**, 2 (S1), S43-S46, 4 pp.
72. Arefi, H.; Setamdideh, D., Reductive amination of aldehydes by NaBH<sub>4</sub> in the presence of NaH<sub>2</sub>PO<sub>4</sub>.H<sub>2</sub>O. *Orient. J. Chem.* **2014**, 30 (1), 299-302.
73. Gilmore, K.; Vukelic, S.; McQuade, D. T.; Koksche, B.; Seeberger, P. H., Continuous Reductions and Reductive Aminations Using Solid NaBH<sub>4</sub>. *Org. Process Res. Dev.* **2014**, 18 (12), 1771-1776.

74. Hasanloie, S. T.; Setamdideh, D., NaBH<sub>4</sub>/C: A convenient system for reductive amination of aldehydes. *Orient. J. Chem.* **2014**, 30 (1), 341-344.
75. Saberi, D.; Akbari, J.; Mahdudi, S.; Heydari, A., Reductive amination of aldehydes and ketones catalyzed by deep eutectic solvent using sodium borohydride as a reducing agent. *J. Mol. Liq.* **2014**, 196, 208-210.
76. Abdel-Magid, A. F.; Maryanoff, C. A., Reductive amination of aldehydes and ketones with weakly basic anilines using sodium triacetoxyborohydride. *Synlett* **1990**, (9), 537-9.
77. Abdel-Magid, A. F.; Carson, K. G.; Harris, B. D.; Maryanoff, C. A.; Shah, R. D., Reductive Amination of Aldehydes and Ketones with Sodium Triacetoxyborohydride. Studies on Direct and Indirect Reductive Amination Procedures. *J. Org. Chem.* **1996**, 61 (11), 3849-3862.
78. Abdel-Magid, A. F.; Maryanoff, C. A., Use of sodium triacetoxyborohydride in reductive amination of ketones and aldehydes. *ACS Symp. Ser.* **1996**, 641 (Reductions in Organic Synthesis), 201-216.
79. Labadie, J.; Rana, S.; Lindberg, T.; Gooding, O. W.; Bhattacharyya, S. In Polymer-supported borohydride, cyanoborohydride, and triacetoxyborohydride: Scope and selectivity in reduction and reductive amination, American Chemical Society: **2001**; pp ORGN-517.
80. Bhattacharyya, S.; Rana, S.; Gooding, O. W.; Labadie, J., Polymer-supported triacetoxyborohydride: a novel reagent of choice for reductive amination. *Tetrahedron Lett.* **2003**, 44 (27), 4957-4960.

81. Abdel-Magid, A. F.; Mehrman, S. J., A Review on the Use of Sodium Triacetoxyborohydride in the Reductive Amination of Ketones and Aldehydes. *Org. Process Res. Dev.* **2006**, 10 (5), 971-1031.
82. Huang, Y.; Li, M.; Yu, X.; Yuan, Z., Application of sodium triacetoxyborohydride (STAB-H) in reductive amination. *Zhongguo Yiyao Gongye Zazhi* **2008**, 39 (9), 695-701.



## CHAPTER 5. BIOBASED MELAMINE-FORMALDEHYDE COATINGS FROM VANILLIN

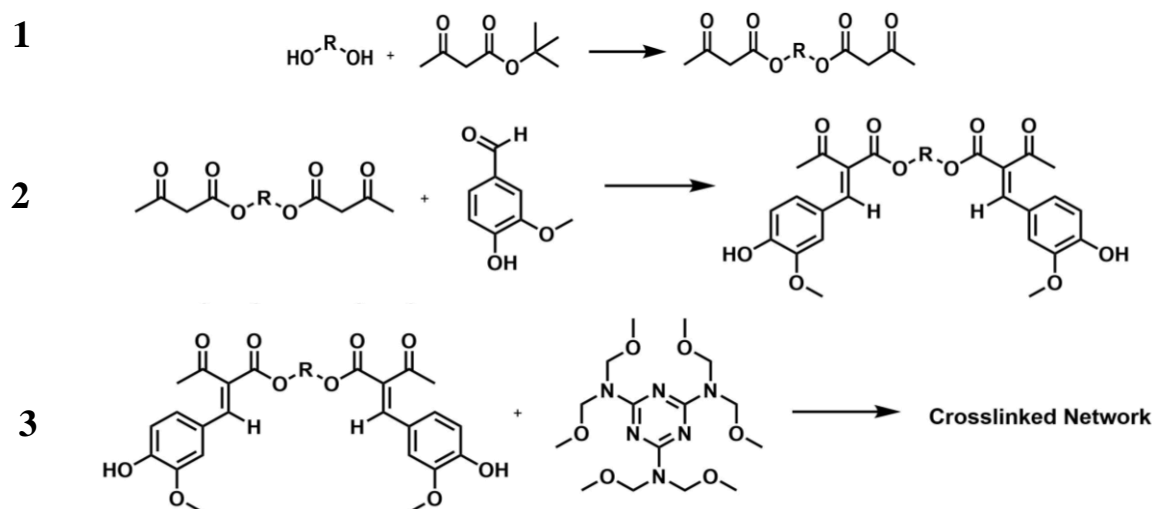
### 5.1. Introduction

Melamine-formaldehyde (MF) resins are widely used in laminate flooring, countertops, cabinetry, surface coatings, textile finishes and paper processing due to their hardness and chemical resistance.<sup>152</sup> MF resins are capable of crosslinking with hydroxyls, urethanes, carboxylic acids and amides, the most common being hydroxyls.<sup>153</sup> Acrylic polyols and polyester/alkyd polyols are the primary crosslinking agents for melamine-formaldehyde coatings depending on the application. Acrylic-MF systems offer properties such as hardness and chemical resistance, whereas polyester/alkyd-MF coatings offer enhanced adhesion, flexibility, and toughness. Hydroxyl groups react with melamine-formaldehyde resins by undergoing transesterification with the activated alkoxymethyl group or etherification of methylol groups in the presence of an acid catalyst. Self-condensation of the MF resin may also occur, however, etherification proceeds more rapidly than self-condensation.<sup>154</sup>

Given the global demand for reducing oil dependence, biobased materials have been explored as alternatives to petrochemicals in thermoset coating systems such as epoxies,<sup>70, 78, 155</sup> polyurethanes,<sup>156-160</sup> and polyesters.<sup>161-163</sup> However, very little investigation into biobased melamine-formaldehyde coatings have been explored. Kohlmayr et al. additionally investigated the use of biobased polyols such as starch, sucrose, and glycerol for modifying MF resins.<sup>164</sup> Starch and sucrose were found insufficient, as the high viscosity prevented any covalent linkage to the MF resin. Glycerol, however, was found to covalently bond to the MF resins, however, no substantial improvements were made between the modified and unmodified MF resin. Chai et al. studied bark extractives from the mountain pine beetle as a partial replacement for 30% w/w

melamine within a MF resin.<sup>165</sup> During the synthesis of melamine with formaldehyde, the tannins and degraded lignin from bark extractive were found to react with formaldehyde. The resulting resins showed higher viscosity than traditional MF resins, however, further investigation into crosslinking the produced MF resins is necessary. Bin et al. developed biobased soybean oil phosphate ester polyols and reacted with MF resin to produce coatings with improved impact resistance and adhesion, indicating the potential for biobased polyols from vegetable oils.<sup>166</sup> Nelson et al. incorporated biobased polyols of sucrose ester with melamine-formaldehyde resin and compared to polyester polyol.<sup>167</sup> While adhesion, impact resistance, and flexibility were lower than the commercial polyester polyol, hardness values were found to be comparable in addition to lower VOC generation from polyol synthesis, showing potential for improvements for biobased polyols within MF coating systems.

The current research is therefore focused at incorporating biobased materials into MF coating systems. Lignin-derived vanillin offers unique functionality consisting of an aromatic aldehyde and phenol, capable of crosslinking with MF resins. In this study, a unique synthetic approach (Scheme 5.1) was explored for incorporating vanillin into melamine-formaldehyde coatings. First, a variety of polyols, 1,3-propanediol (1,3-PD), 1,4-butanediol (1,4-BD), 1,5-pentanediol (1,5-PD), 1,6-hexane-diol (1,6-HD), and glycerol, were acetoacetylated using tert-butylacetoacetate (TBAA). Next, vanillin was added to the acetoacetylated diols, forming an enone (Knoevenagel condensation). Simultaneously, a melamine-formaldehyde resin (Cymel 301) was also incorporated in a one-pot synthesis with vanillin and acetoacetylated polyols, reacting with the phenolic groups on vanillin. The MF system was coated on steel panels and cured at 160°C for 20 minutes. The coatings were characterized and compared to acrylic polyol Joncryl-MF coatings.



**Scheme 5.1. 1.) Acetoacetylation of polyols 2.) Knoevenagel condensation of vanillin and 3.) MF crosslinking**

## 5.2. Experimental

### 5.2.1. Raw materials

All polyols (1,3-propanediol; 1,4-butanediol; 1,5-pentanediol; 1,6-hexane-diol; glycerol) were purchased from Sigma Aldrich and used as is. Tert-butyl acetoacetate (TBAA) was provided by Eastman Chemical Company. Vanillin (99%) and piperidine were supplied from Alfa Aesar. Cymel 301 was obtained from Cytec (Allnex). Methanol was purchased from BDH. BYK-370 was obtained from BYK. Joncryl 500, Joncryl 504, and Joncryl 507 were supplied by BASF. All Joncryl resins have a hydroxyl number of 140

### 5.2.2. Methods

#### 5.2.2.1. Pre-polymer characterization

Nuclear magnetic resonance spectroscopy using a Jeol 400 MHz spectrometer was performed on synthesized compounds. Reaction products were solubilized in either chloroform-d or dimethyl sulfoxide-d<sub>6</sub>. Proton NMR (<sup>1</sup>H NMR) was utilized to determine product structure.

Integration using Mestrelab Mnova was utilized to characterize and quantify the products and byproducts.

Viscosity of the synthesized acetoacetylated polyols was determined using an Ares Rheometer (TA Instruments) and measured at 25°C. The parameters operated from 0.1 rad/s to 500 rad/s with 0.1% strain, and rheology was measured in Pa/s.

#### **5.2.2.2. Coating characterization**

Byko-test 8500 coating thickness gauge from BYK Additives was used to measure the dry film thickness of each coating on steel (Fe-probe) and glass (NFe-probe). The average of ten film thickness measurements was reported for each coated panel with standard deviations.

MEK double rubs were performed according to ASTM D5402 to measure the solvent resistance of each coating. Briefly, cheesecloth saturated with methyl ethyl ketone was rubbed up and down the coating surface in the same location, with one forward and backward motion equaling one double rub. Every 25 double rubs, the cloth was re-soaked with MEK. The reported number relates to the number of MEK double rubs performed on the coating before any sign of failure was observed (cracks, coating removal, etc.).

Impact resistance of each coating was measured on steel panels according to ASTM D2794. Briefly, a 4-pound weight on top of an indenter was dropped onto the coating at various heights to determine the height at which the indenter could be dropped onto the coating without resulting cracks. The value is written as inches x pounds, which indicates the height in inches multiplied by the 4-pound weight.

Pencil hardness was measured according to ASTM D3363. Briefly, pencils of various hardness (6B – 6H) were pushed across the coatings at a 45° angle in ¼ inch strokes. The value recorded includes the highest pencil hardness value that does not scratch the coating.

König pendulum hardness was measured according to ASTM D4366. Briefly, a coated steel panel was placed in a König pendulum apparatus, where the hardness was determined by the oscillation damping of the pendulum. The reported hardness value was measured in seconds.

Crosshatch adhesion testing was performed according to ASTM D3359. Briefly, a lattice pattern cut is made on a coated steel panel. Pressure sensitive adhesive tape is placed over the scribed area and a rubber eraser from a pencil smooths over the tape to ensure complete contact with the coated substrate. Evaluation of the area upon removal of the tape determines the amount of coated material left at the surface of the cross-cut section. The percent area of coating removed is reported, ranging from 0B (> 65% coating removal) to 5B (0% coating removal).

Corrosion of the steel panels was measured according to the salt spray method, ASTM B117. Coated steel panels were scribed with an X and exposed to a salt fog chamber with continuous 5% NaCl spray for 112 hours. Coated panels were pulled after 16 hours, 40 hours, and 112 hours. Corrosion observations were made for each coating.

### **5.2.3. Acetoacetylation of polyols**

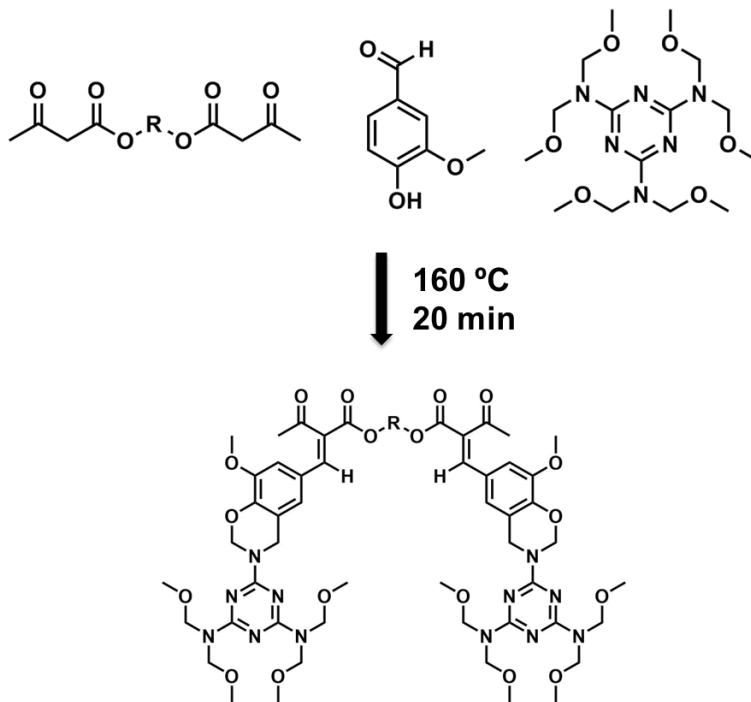
Polyol (0.1 mol) was mixed with TBAA (0.3 mol) in a round bottom flask connected to a dean stark trap. The reaction was run at 150°C for 4 hours using a silicone oil bath, and tert-butanol was collected as the reaction proceeded. Reaction completion was determined by <sup>1</sup>H NMR. Any excess TBAA and tert-butanol was removed under vacuum. Each polyol was separately acetoacetylated using the same procedure.

Acetoacetylated polyols were characterized by nuclear magnetic resonance spectroscopy using a Jeol 400 MHz spectrometer. Reaction products were solubilized in either chloroform-d or dimethyl sulfoxide-d<sub>6</sub>. Proton NMR (<sup>1</sup>H NMR) was utilized to determine product structure. Additionally, product viscosity was determined using an Ares Rheometer (TA Instruments).

## **5.2.4. Knoevenagel condensation and MF crosslinking**

### **5.2.4.1. MF coating formulation**

Attempts at combining the Knoevenagel condensation and MF crosslinking were explored through a 1 pot synthesis (Scheme 5.2). Polyols were explored at varying amounts of melamine formaldehyde content (5-30% by weight). First, a 60% solution of vanillin in methanol was heated to 60°C and mixed until full solubilization of vanillin. Acetoacetylated polyol (0.02 mol), Cymel 301 (5%, 10%, 15%, 20%, 25% and 30% by weight), BYK-370 and piperidine (1% by weight) were added to a 40 mL glass vial and mixed for 1 hour. The vanillin solution (0.06 mol of vanillin) and 1% pTSA (40% in methanol) were added to the vial and mixed for 10 minutes. Coatings were made on phosphorylated steel panels (Bondrite) and glass panels using an 8-mil drawdown bar and cured at 160°C for 20 minutes. Cured coatings were left at ambient conditions for 7 days prior to testing. Control coatings were made from Joncryl 500, Joncryl 504, and Joncryl 507. MF content varied from 20%, 30% and 40% for each Joncryl control. Coatings were made on phosphorylated steel panels (Bondrite) and cured at 160°C for 20 minutes.



**Scheme 5.2. One- Pot synthesis of Knoevenagel condensation and MF crosslinking**

#### 5.2.4.2. MF coating characterization

Melamine-formaldehyde coatings were characterized by dry film thickness, MEK double rubs, impact resistance, pencil hardness, König pendulum hardness, and crosshatch adhesion. The two best vanillin-MF systems were chosen for further testing addition to one Joncryl-MF formulation for comparison. A correlation between wet film thickness and dry film thickness was made for each system. Corrosion testing (salt spray) was performed on the three chosen MF coatings.

### 5.3. Results and discussion

#### 5.3.1. Acetoacetylated polyols

Acetoacetylation of glycerol, 1,3-propanediol, 1,4-butanediol, 1,5-pentanediol and 1,6-hexanediol was carried out at  $150^{\circ}\text{C}$  for 4 hours and collecting the t-butanol using a dean stark trap. Confirmation of each product was carried out using  $^1\text{H}$  NMR, shown in Figures 5.1-5.5.

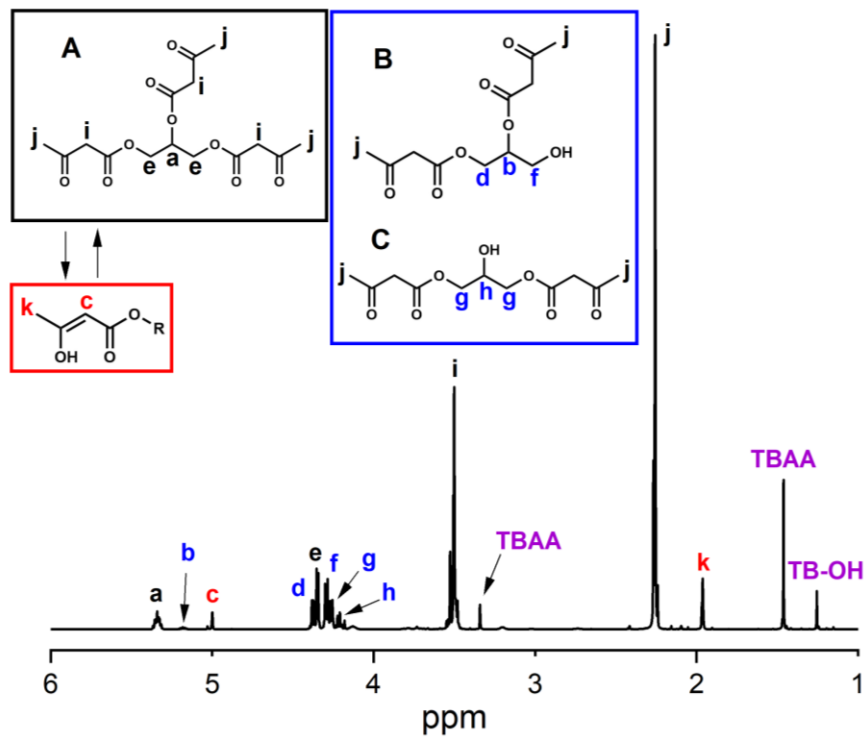


Figure 5.1.  $^1\text{H}$  NMR of acetoacetylated glycerol

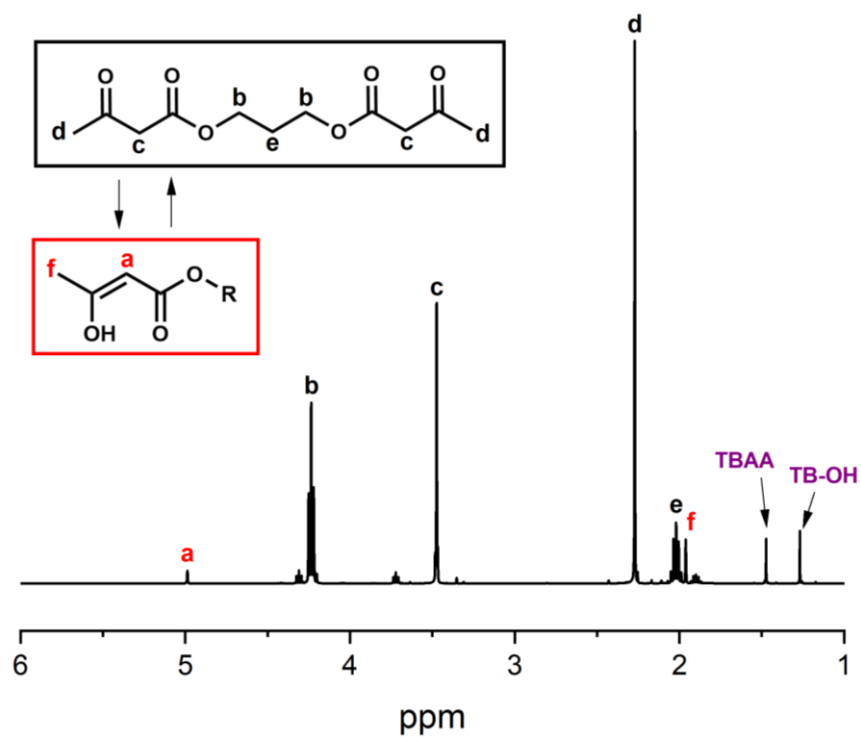


Figure 5.2.  $^1\text{H}$  NMR of acetoacetylated 1,3-propanediol



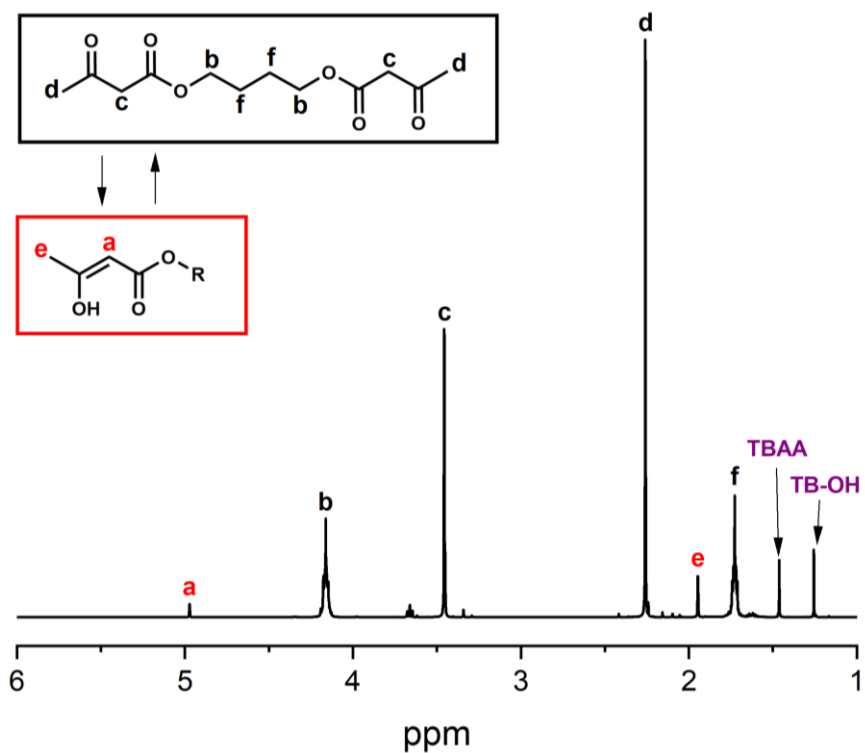


Figure 5.3.  $^1\text{H}$  NMR of acetoacetylated 1,4-butanediol

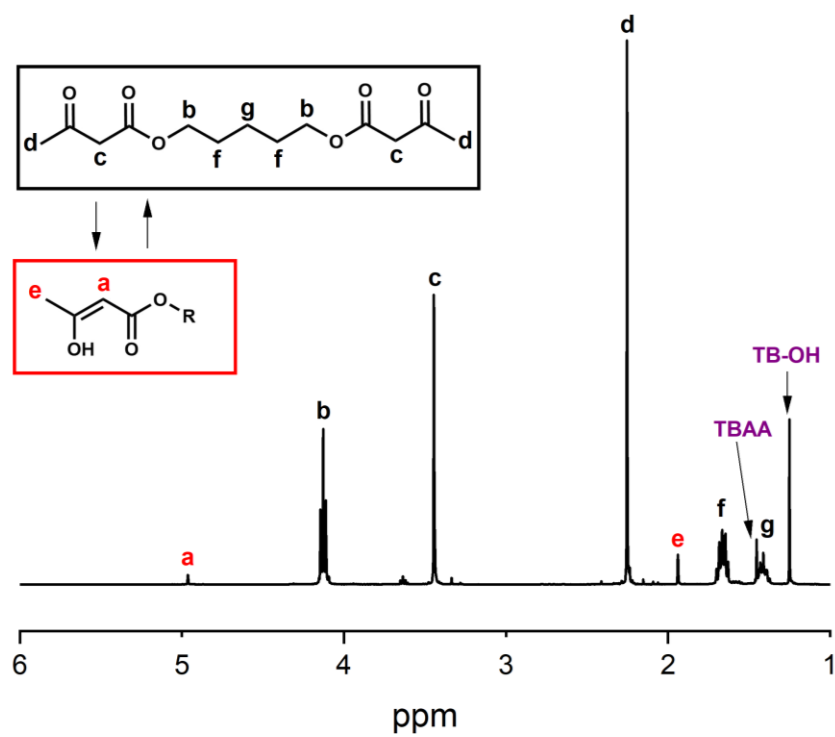
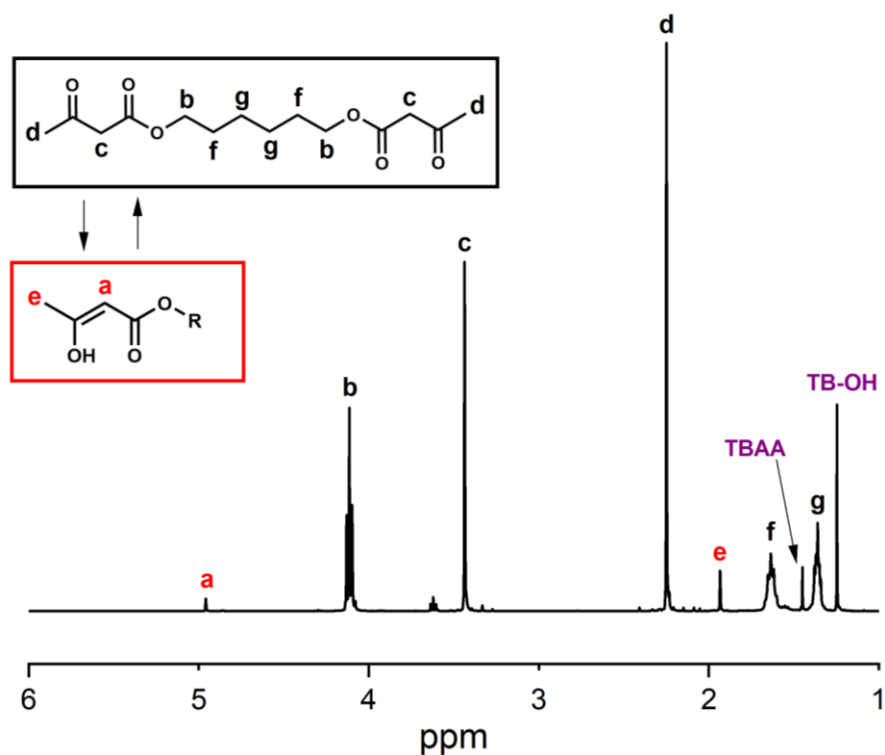
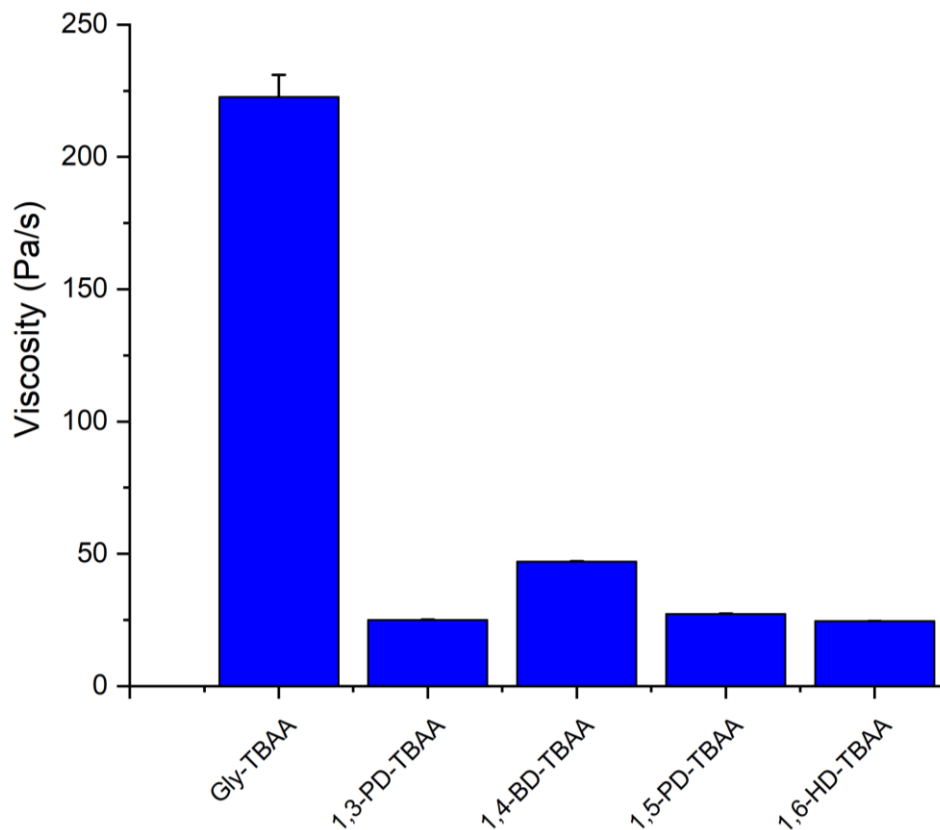


Figure 5.4.  $^1\text{H}$  NMR of acetoacetylated 1,5-pentanediol



**Figure 5.5.**  $^1\text{H}$  NMR of acetoacetylated 1,6-hexanediol

From the  $^1\text{H}$  NMR of acetoacetylated glycerol (Figure 5.1), the majority product was fully acetoacetylated glycerol (structure A) with trace amounts of diacetoacetylated glycerol with a primary hydroxyl free (structure B) and a larger amount of diacetoacetylated glycerol with the secondary alcohol free (structure C). While overlapping peaks prevents the integration of Structure C, it is evident that the formation of Structure C is more likely to occur than Structure B due to the secondary hydroxyl being less reactive than the primary hydroxyl. In  $^1\text{H}$  NMR spectra, trace amounts of TBAA starting material and tert-butanol were identified. Additionally, the enol-tautomerization of the acetoacetate was identified in each  $^1\text{H}$  NMR spectrum. Overall, the acetoacetylation of each polyol was successful and each product was confirmed by spectroscopy.



**Figure 5.6. Viscosity of acetoacetylated polyols**

From the rheology data in Figure 5.6, acetoacetylated glycerol shows a significantly high viscosity (223 Pa/s) relative to the other polyols. As glycerol contains both the highest functionality and shortest alkyl chain, mobility and flexibility are limited compared to the longer chain polyols. For the di-functional polyols, there was no observable trend between the chain length and viscosity. 1,3-propanediol and 1,6-hexanediol both showed the lowest viscosity at ~25 Pa/s, however, all polyols had workable viscosities.

### 5.3.2. Knoevenagel/MF crosslinking

A reduction in processing steps was achieved by combining the Knoevenagel condensation reaction and MF crosslinking together. The reaction of the aromatic aldehyde on vanillin with acetoacetate was uncompetitive with the crosslinking of MF and the phenol on

vanillin. Initial attempts and coating formulation were limited to acetoacetylated glycerol and 1,3-propanediol in order to optimize the melamine formaldehyde content for remaining acetoacetylated polyols. BYK-370 was added for improved wettability onto the steel and glass substrates. Cymel 301, a highly methylated melamine crosslinker, was used at 5, 10, 15, 20, 25 and 30%. Coatings formulated at 5% MF content remained uncured after 20 minutes at 160°C. However, coatings over 20% MF content showed wrinkling on the surface (Figure 5.7), a result of too fast of a cure rate. As a result, 10-15% MF content was deemed optimal for appearance. All coatings produced a yellow-orange appearance, a result of the conjugation with the enone formation from the Knoevenagel condensation

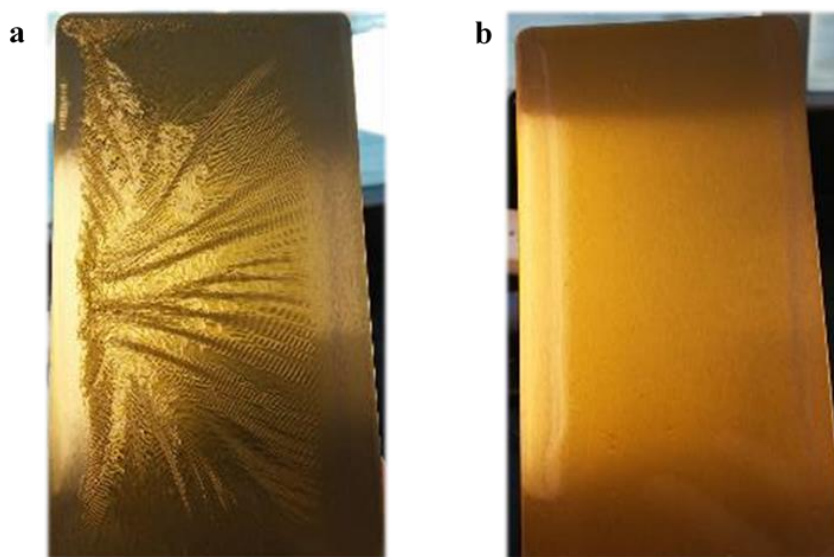


**Figure 5.7. a.) Wrinkling effect from MF content between 20-30% and b.) smooth coatings from MF content of 10-15%**

All acetoacetylated polyols were formulated at 10% and 15% MF content for optimal appearance. However, 1,4-BD-TBAA, 1,5-PD-TBAA and 1,6-HD-TBAA all displayed the “wrinkling” effect at 15% MF content, and therefore 10% was found to be optimal for higher

alkyl chain polyols. Experimental vanillin-MF coatings were compared to MF coatings made from Joncryl 500, Joncryl 504, and Joncryl 507 with Cymel 301 ranging from 20%, 30% and 40% by weight. Joncryl 500 is a high solids acrylic polyol used in melamine formaldehyde coatings containing methyl n-amyl ketone as the solvent, with a viscosity of 2,400 – 5,200 cP. Joncryl 504 is the xylene version of Joncryl 500 with a viscosity of 5,500 – 10,000 cP, and Joncryl 507 is the n-butyl acetate version of Joncryl 500 with a viscosity of 2,500 – 5,500 cP. All Joncryl resins contain 80% solids with a hydroxyl value of 140

**Table 5.1. Coating characterization of Vanillin-MF and Joncryl coatings**

AA-Polyol	% MF	DFT (μm)	MEK DR's	Impact (in-lb.)	Pencil	König (s)	X-Hatch
Gly-TBAA	10	28	32	> 160	HB	36	5B
	15	33	> 400	20	7H	219	5B
1,3PD-TBAA	10	19	> 400	> 160	2H	59	5B
	15	20	> 400	60	5H	151	5B
1,4BD-TBAA	10	22	78	> 160	3B	36	5B
1,5PD-TBAA	10	18	83	> 160	3B	35	5B
1,6HD-TBAA	10	21	60	> 160	< 8B	40	5B
Joncryl 500	20	34	> 400	24	H	172	0B
	30	38	> 400	16	2H	177	0B
	40	35	> 400	16	2H	177	1B
Joncryl 504	20	37	> 400	24	H	158	2B
	30	37	> 400	8	H	178	0B
	40	37	> 400	12	2H	185	0B
Joncryl 507	20	36	> 400	16	2H	174	0B
	30	34	> 400	12	2H	180	0B
	40	32	> 400	8	3H	186	0B

From Table 5.1, all Joncryl-MF coatings had slightly higher dry film thickness values compared to the vanillin-MF coatings. Gly-TBAA had the largest coating thickness of the experimental MF coatings, likely a result of the higher viscosity of Gly-TBAA compared to the longer alkyl chain polyols. The Joncryl-MF coatings all exhibited MEK double rub values greater than 400, indicating significant solvent resistance. For the vanillin-MF coatings, only Gly-TBAA at 15% MF and 1,3-PD-TBAA at 10% and 15% MF showed comparable solvent resistance to the Joncryl-MF coatings. Increasing the MF content allows for higher crosslink density with the acetoacetylated polyols. Although some tri-functional Gly-TBAA was present, a large amount of the product consisted of di-acetoacetylated glycerol, and therefore crosslinking required higher MF content for better solvent resistance. For impact resistance, the experimental MF coatings at 10% MF all displayed impact resistance greater than 160-inch pounds, significantly higher than the Joncryl coatings ranging from 8-24-inch pounds. Hardness values were measured using both pencil hardness and König pendulum hardness. For all coatings, as the MF content increases, the hardness values also increase. Pencil hardness values for the Joncryl-MF coatings range from H to 3H, whereas the vanillin-MF coatings ranged between 8B and 7H. As the alkyl chain of the polyol grows, the pencil hardness decreases, with 1,6-HD-TBAA showing the lowest pencil hardness of 8B. The largest pencil hardness values for experimental MF coatings included the Gly-TBAA at 15% MF and 1,3-PD-TBAA at 15% MF, displaying pencil hardness values of 7H and 5H respectively. However, the increased hardness of these two experimental formulations also correlates with lower impact resistance values, a tradeoff between hardness and flexibility. König pendulum hardness values correlate with the pencil hardness values, increasing with MF content and decreasing with alkyl chain length. Joncryl-MF coatings all display König hardness values between 158-186 seconds, whereas the vanillin-MF

coatings range from 35-219 seconds based on MF content and polyol chain length. Crosshatch adhesion resulted in 5B for all vanillin-MF coatings, whereas the Joncryl-MF coatings indicated mostly 0B.

A comprehensive overview of the coating properties indicates that the vanillin-MF systems are capable of competing with Joncryl-MF coatings in solvent resistance and hardness, while outperforming the Joncryl systems in impact resistance and adhesion. Gly-TBAA at 15% MF content and 1,3-PD-TBAA at 10% MF were chosen for further corrosion testing as the optimal experimental MF coatings due to excellent solvent resistance, impact resistance and hardness value. Joncryl 504 at 20% MF was chosen as the control based on higher impact resistance and adhesion values for all the Joncryl formulations. Given the higher dry film thickness values for the Joncryl coatings, a correlation between the wet film thickness (WFT) and dry film thickness (DFT) of the chosen coated formulations was made. (Figure 5.8).

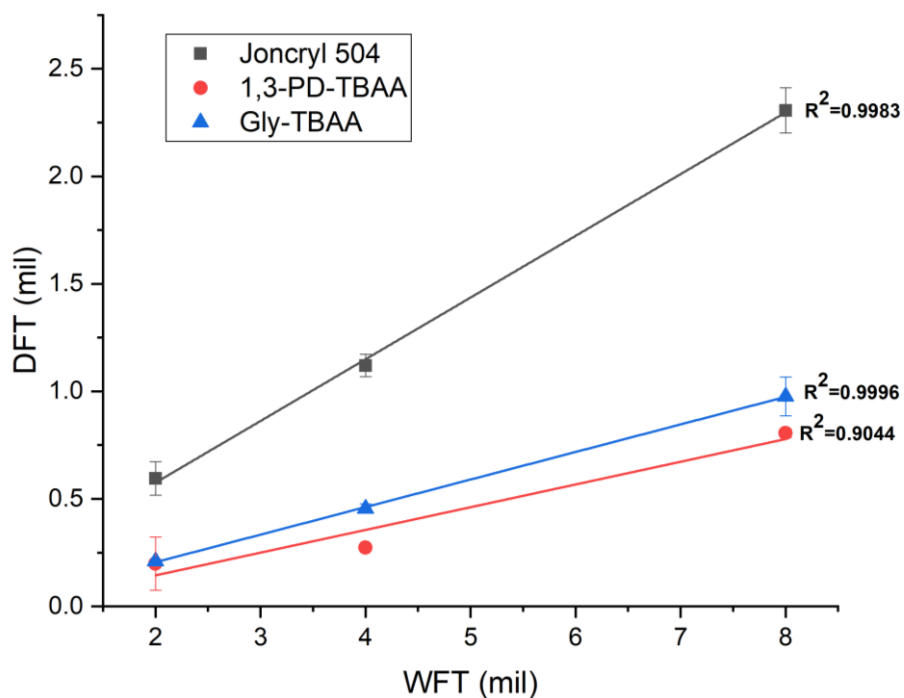


**Figure 5.8. Wet film thickness vs dry film thickness of Joncryl 504 MF, 1,3-PD-TBAA MF, and Gly-TBAA MF**

Thickness correlations were relatively linear for wet film thickness and dry film thickness. Joncryl 504 MF coating shows a significantly higher DFT compared to the vanillin-MF coatings. Gly-TBAA had slightly higher DFT values compared to 1,3-PD-TBAA. To achieve a DFT for the vanillin-MF coatings, exploration into minimizing the methanol content could potentially be explored. However, 4 mil WFT produced sufficient DFT values for salt spray evaluation.

Corrosion testing was performed on the three chosen MF formulations according to ASTM B117 and observations were made after 16 hours, 40 hours, and 112 hours of continuous salt spray exposure. Figure 5.9 shows the panels after 0, 16, 40 and 112 hours of salt spray exposure. Prior to B117 testing, the Joncryl coatings appeared transparent with a slight yellow tint. The vanillin-MF coatings displayed a deeper yellow shade than the Joncryl coatings, however all formulations produced smooth, even films on steel substrates. After 16 hours of salt spray exposure, the 1,3-PD-TBAA began to show darkening around the scribe, whereas Joncryl and Gly-TBAA appeared relatively unchanged. Corrosion of the Joncryl-MF coatings became apparent at the 40-hour check, showing patches of corroded substrate around the scribe. The 1,3-PD-TBAA also indicated more corrosion and darkening around the scribe, however, Gly-TBAA appeared relatively intact, showing slight traces of corrosion around the scribe. After the final 112-hour check, the Joncryl-MF coated panels were almost entirely corroded. The vanillin-MF coatings showed significant localized corrosion near the site of the scribe, however, darkening on the coating extended generally throughout the panel with the exception of 1,3-PD-TBAA. The darkening effect is likely a result of water penetrating the interface between the coating and the substrate, effectively lowering the adhesion and overall performance of the coating. While 1,3-PD-TBAA showed early signs of corrosion and darkening near the scribe, it outperformed both



Joncryl 504 and Gly-TBAA regarding localized darkening and overall corrosion. The experimental vanillin-MF coatings showed better overall appearance at half the DFT values of the Joncryl-MF coatings.

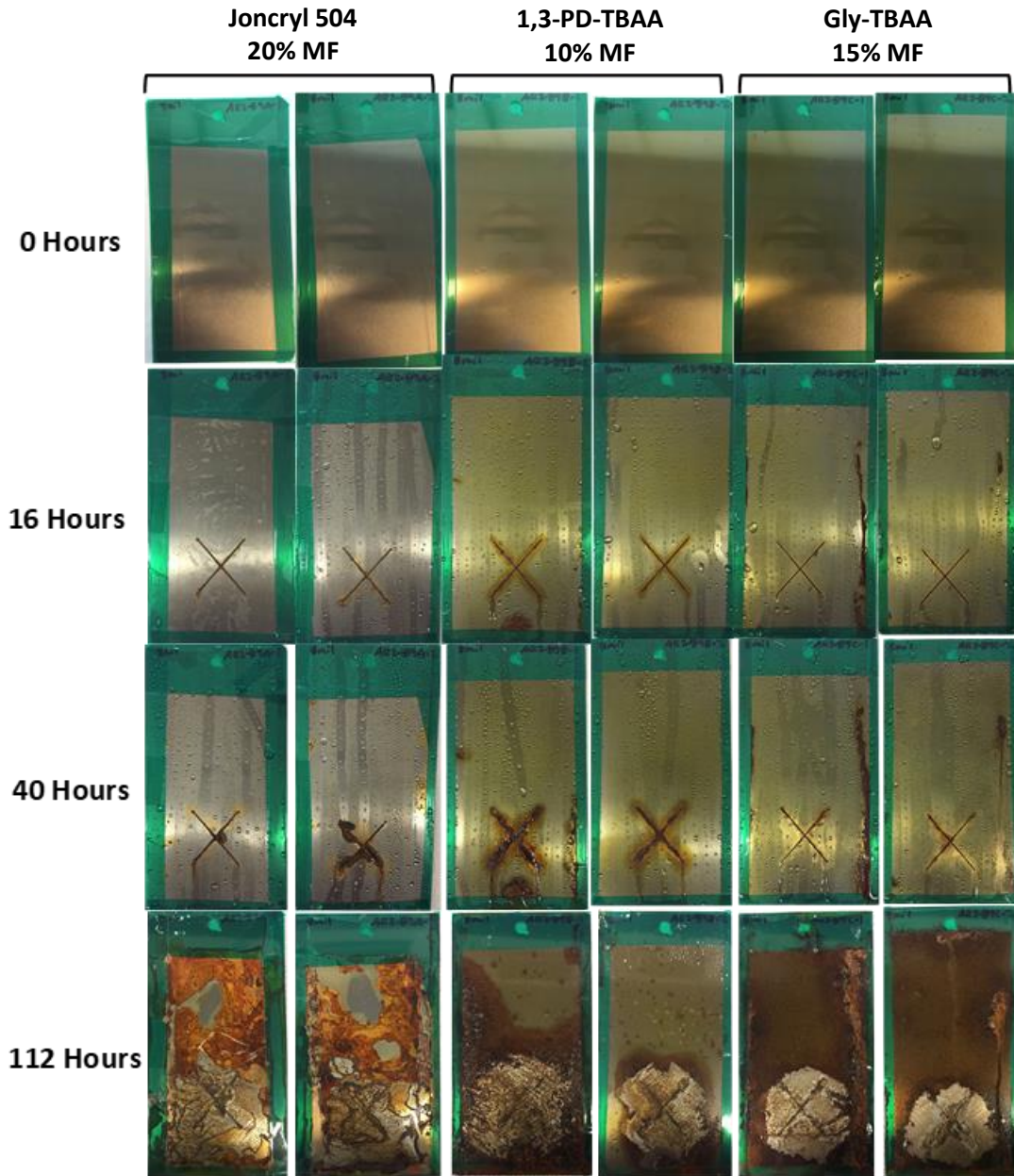


Figure 5.9. Corrosion of MF coated panels from salt spray exposure

#### 5.4. Conclusion

In this study, polyols were successfully acetoacetylated using tert-butyl acetoacetate and characterized using  $^1\text{H}$  NMR. A reduction in synthetic steps was achieved by combining the Knoevenagel condensation and the MF crosslinking, resulting in vanillin-MF coatings with various acetoacetylated polyols. MF content was varied from 5-30%, with an optimal range between 10-15% for the prevention of wrinkling on the surface. Coating performance was compared against Joncryl-MF coating systems. The vanillin-MF coatings containing glycerol and 1,3-propanediol showed superior performance in regard to impact resistance, hardness, and adhesion, in addition to comparable solvent resistance (>400 MEK double rubs). Corrosion analysis using ASTM B117 salt spray indicates localized corrosion around the scribe, outperforming the Joncryl control. The vanillin-MF coatings show promising potential to compete with acrylic polyol MF coating systems, offering a biobased alternative to petrochemical systems.

## 5.5. References

1. Hexion Melamine Formaldehyde (MF) Resins. (accessed February 8).
2. Wicks, J. Z. W.; Jones, F. N.; Pappas, S. P.; Wicks, D. A., *Organic Coatings, 3rd ed.* Wiley: Hoboken, NJ, **2007**.
3. Jones, F. N., Overview of acrylic/melamine resin and polyester/melamine resin higher-solids baking enamels. *Polym. Mater. Sci. Eng.* **1986**, *55*, 222-8.
4. Auvergne, R.; Caillol, S.; David, G.; Boutevin, B.; Pascault, J.-P., Biobased Thermosetting Epoxy: Present and Future. *Chem. Rev. (Washington, DC, U. S.)* **2014**, *114* (2), 1082-1115.
5. Ding, C.; Matharu, A. S., Recent Developments on Biobased Curing Agents: A Review of Their Preparation and Use. *ACS Sustainable Chem. Eng.* **2014**, *2* (10), 2217-2236.
6. Kumar, S.; Samal, S. K.; Mohanty, S.; Nayak, S. K., Recent Development of Biobased Epoxy Resins: A Review. *Polym.-Plast. Technol. Eng.* **2018**, *57* (3), 133-155.
7. Yu, A. Z.; Setien, R. A.; Sahouani, J. M.; Docken, J. J.; Webster, D. C., Catalyzed non-isocyanate polyurethane (NIPU) coatings from bio-based poly(cyclic carbonates). *J. Coat. Technol. Res.* **2018**, Ahead of Print.
8. Webster, D. C.; Crain, A. L., Synthesis and applications of cyclic carbonate functional polymers in thermosetting coatings. *Prog. Org. Coat.* **2000**, *40* (1-4), 275-282.
9. Desroches, M.; Escouvois, M.; Auvergne, R.; Caillol, S.; Boutevin, B., From Vegetable Oils to Polyurethanes: Synthetic Routes to Polyols and Main Industrial Products. *Polym. Rev. (Philadelphia, PA, U. S.)* **2012**, *52* (1), 38-79.
10. Pan, X.; Webster, D. C., New Biobased High Functionality Polyols and Their Use in Polyurethane Coatings. *ChemSusChem* **2012**, *5* (2), 419-429.

11. Caillol, S. In New biobased and sustainable epoxy and polyurethane materials and foams from vegetable and microalgal oil, American Chemical Society: **2017**; pp CELL-261.
12. Noordover, B. A. J.; Duchateau, R.; van Benthem, R. A. T. M.; Ming, W.; Koning, C. E., Enhancing the Functionality of Biobased Polyester Coating Resins through Modification with Citric Acid. *Biomacromolecules* **2007**, *8* (12), 3860-3870.
13. Sousa, A. F.; Matos, M.; Freire, C. S. R.; Silvestre, A. J. D.; Coelho, J. F. J., New copolyesters derived from terephthalic and 2,5-furandicarboxylic acids: A step forward in the development of biobased polyesters. *Polymer* **2013**, *54* (2), 513-519.
14. Jiang, Y.; Loos, K., Enzymatic synthesis of biobased polyesters and polyamides. *Polymers (Basel, Switz.)* **2016**, *8* (7), 243/1-243/53.
15. Martin, K., Modification of melamine-formaldehyde resins by substances from renewable resources. *Journal of applied polymer science* **2012**, *124* (6), 4416.
16. Chai, Y.; Zhao, Y.; Yan, N., Synthesis and Characterization of Biobased Melamine Formaldehyde Resins from Bark Extractives. *Ind. Eng. Chem. Res.* **2014**, *53* (28), 11228-11238.
17. Bin, Z., Novel coatings from soybean oil phosphate ester polyols. *JCT, Journal of coatings technology* **2001**, *73* (915), 53.
18. Nelson, T. J.; Masaki, B.; Morseth, Z.; Webster, D. C., Highly functional biobased polyols and their use in melamine-formaldehyde coatings. *J. Coat. Technol. Res.* **2013**, *10* (6), 757-767.

## CHAPTER 6. OVERALL CONCLUSIONS

### 6.1. Hydrolytic stability of the silanol-isocyanate

The silanol-isocyanate reaction was explored using silanol-terminated PDMS and phenyl isocyanate, cyclohexyl isocyanate, and hexyl isocyanate. Comparisons were made by reacting the monoisocyanates to carbinol-terminated PDMS. Characterization of the silanol-NCO reaction products using spectroscopic techniques indicated 85-90% amine with 10-15% of urea present. No silyl carbamate linkage was found from silanol-NCO reaction products. Given the large presence of amine, the formation of silyl-carbamate likely occurs, however rapid hydrolysis and decomposition results in amine by-product. The formation of urea, however, may not be concluded as to whether isocyanate reagent reacts with water, or amine-byproduct from the silyl-carbamate reacts with isocyanate. All carbinol-terminated PDMS-NCO reaction products indicated 100% carbamate. Computational calculations of the Wiberg Bond Index values, natural charges on atoms, and dipole moment agree with the experimental observations, indicating hydrolytic instability at the silicon-oxygen bond of the silyl-carbamate linkage. Overall, the use of the silanol-isocyanate reaction in polyurethane systems should be avoided.

### 6.2. Alkoxysilane stone consolidants

Novel solvent-free alkoxysilane stone consolidants were developed using tetraethylorthosilicate as the major alkoxysilane. Substantial improvements in flexibility from commercial consolidants were achieved by the incorporation of polydimethylsiloxane, octyltriethoxysilane, and 3-glycidyloxypropyltrimethoxysilane. Polyhedral oligomeric silsesquioxane was incorporated for enhanced breathability, allowing for the transport of trapped moisture within the stone to permeate out of the consolidant. Water vapor permeability tests indicate that commercial consolidants promote the transport of water throughout the consolidant

as a result of the more hydrophilic nature, preventing discrimination of water vapor into or out of the stone. Experimental consolidants, however, showed greater hydrophobicity while maintaining a level of water permeability. Additionally, experimental consolidants showed greater penetration depths, higher solids content, and significantly lower water absorption values after 1000 hours of weathering on limestone.

### **6.3. Vanillin-epoxy thermosets**

Biobased epoxy thermosets from vanillin were successfully developed. Vanillin was initially reacted with amine, forming a vanillin-Schiff base compound. Then, the phenol group on vanillin was glycidylated using epichlorohydrin. One of the challenges with this route included the hydrolysis of the Schiff base during the glycidylation procedure. As a result, vanillin was glycidylated first, followed by a one-pot crosslinking through the aldehyde and epoxy using various amine crosslinkers. Thermosets from Jeffamines and IPDA indicated higher  $T_g$  values compared to DGEBA controls. However, the bright yellow appearance from the conjugation between the imine and the aromatic vanillin are less-than-ideal for applications where clear, transparent thermosets are desired. Therefore, efforts into reducing the Schiff base were explored through the use of sodium borohydride. The resulting materials consisted of mostly dimerized vanillin compound with trace amounts of monomer and trimer. Further glycidylation resulted in light yellow, high viscosity liquids, which were crosslinked to form transparent epoxy thermosets.

### **6.4. Vanillin-MF coatings**

Melamine-formaldehyde coatings from vanillin were developed by first acetoacetylated polyols using tert-butyl acetoacetate. A reduction in synthetic steps was achieved by combining the Knoevenagel condensation and the MF crosslinking, resulting in vanillin-MF coatings with

various acetoacetylated polyols. The optimal MF content was between 10-15%, with higher MF contents resulting in a “wrinkling” effect on the surface of the coating. The vanillin-MF coatings were compared against commercial acrylic polyols, Joncryl 500, 504 and 507. MF coatings containing glycerol and 1,3-propanediol exhibited excellent impact resistance, hardness, adhesion, and solvent resistance. Corrosion testing using continuous 5% NaCl spray showed superior performance from the vanillin-MF coatings compared to a commercial Joncryl system. The vanillin-MF coatings show promising potential to compete with acrylic polyol MF coating systems, offering a biobased alternative to petrochemical systems.

## **CHAPTER 7. FUTURE WORK**

### **7.1. Hydrolytic stability of the silanol-isocyanate**

The silanol-isocyanate reaction as shown to form a hydrolytically unstable silyl-carbamate linkage. Current research investigated the use of mono-isocyanates, however, diisocyanates may also be of interest in more complex coating systems. Various stability factors may come into play depending on chemical composition of polymeric system, isocyanate structure, molecular weight of PDMS, temperature, and solvent. Additionally, experimental data on rate of hydrolysis and decomposition would aid in understanding the mechanism of urea formation.

### **7.2. Alkoxysilane stone consolidants**

Successful solvent-free alkoxysilane stone consolidants were developed and optimized, showing improved performance from commercial consolidants. Further development of the optimized consolidant formulations includes natural weathering testing to measure outdoor performance in comparison to commercial consolidants. Spray or brush application to weathered gravestones at multiple national cemeteries throughout the United States should be explored, preferably in regions with different climates for a range of weathering performance. After application of the consolidants, measurements in water absorption and color change will be measured as an indication of consolidant performance

### **7.3. Vanillin-epoxy thermosets**

Further investigation into the developed vanillin-epoxy thermosets includes exploration into the mechanical properties. A major challenge of the developed epoxies included samples that were too brittle for mechanical property testing. As a result, further research into structure-property relationship of the vanillin-epoxy thermosets is necessary for mechanical property



testing. The use of multiple amines with glycidylated vanillin should be explored for tunability of properties. For example, the addition of PACM for forming the vanillin-SB, followed by the addition of Jeffamine T403 for crosslinking with the epoxy will add structural diversity for tunable performance.

Additionally, cured epoxy thermosets from reductive amination showed potential in thermal properties. Additional diamines for crosslinking should be explored, such as Dytex A, Jeffamine D230, and Jeffamine T403. For potential elimination of dimers and trimers during the reductive amination process, sodium triacetoxyborohydride should be explored given the lower reactivity compared to sodium borohydride.

#### **7.4. Vanillin-MF coatings**

Future work into the vanillin-MF coating systems includes increasing the MF content by incorporating a tailing solvent such as ethyl 3-ethoxypropionate (EEP). Increased MF content may improve the coating performance in the systems with longer chain polyols. Additionally, comparisons between a commercial polyester polyol such as Polymac 575776 AS10 should be explored.